Brendan Albert Beeming
BSc(Eng)

Synthesis and Characterisation of Carbon supported Gold Catalysts prepared by Ion-Exchange

A Thesis submitted in the

Department of Chemical Engineering

Centre for Catalysis Research

University of Cape Town

In partial fulfilment of the requirements of the degree of

Master of Science in Engineering

Supervised by: Prof Eric van Steen and A/Prof Jenni Case

2008

Synopsis

Gold has been previously overlooked as a catalyst, mainly because the metal has been regarded as catalytically inert, and was tested as large aggregates, and not as nano-crystallites. Large crystallites of gold do not exhibit significant catalytic activity, and if they do, their activity is small compared with platinum group metals. The recent interest in gold as a catalyst has been fuelled by the development of processes to deposit gold on a catalyst support as nano-crystallites (Prati and Martra, 1999).

Gold catalysts with nano-crystallites on selected supports have been shown to exhibit high activity for mainly redox reactions (Gluhoi, 2005; Hutchings, 2005). These catalysts have recently been attracting attention as they can be used at near ambient conditions, which allows for cheaper and more environmentally friendly processes.

Glucose yielding gluconic acid is an industrially important reaction (Biella *et al.*, 2002). Gluconic acid and its salts are used as water-soluble cleansing agents or as additives in food and beverages which makes these products important in industrial applications (Kirk-Othmer, 1995). Industrially, the aerobic oxidation of glucose is an enzyme catalysed process. However, due to the low productivity of the glucose fermentation process, the development of a chemical route is of interest. Gold catalysis provides a promising alternative route which can be applied at mild conditions.

Very little work has been done on gold catalysts prepared by ion-exchange, although this method is well established for other supported metal catalysts. The potential advantage of ion-exchange is that the average gold particle size on the support might be smaller compared to that which can be achieved by the other preparation methods such as deposition precipitation and co-precipitation. Many preparation methods in gold catalysis use chloride containing precursors mainly $HAuCl_4$. Therefore ion-exchange using a tetramminegold (III) nitrate ($Au(NH_3)_4(NO_3)_3$) precursor can offer a further advantage in that there is no chloride present during catalyst preparation.

Two different carbon supports were used in this project: carbon nanotubes and activated carbon. The catalysts were prepared using tetramminegold (III) nitrate at pH

4 and 2 and $HAuCl_4$ at pH 0.8. Carbon nanotubes were boiled in nitric acid for 6 and 48 hours to introduce functional groups onto the surface as carbon nanotubes are relatively inert.

The crystallite sizes obtained varied widely. The crystallite size distributions on the carbon nanotubes were relatively wide with mean crystallite sizes ranging from 4nm to 15nm. The smallest crystallites on each support were obtained using the tetramminegold (III) nitrate precursor at a preparation pH of 4. A narrow crystallite size distribution was obtained on the 6 hour acid treated carbon nanotubes with a mean crystallite size of about 4nm. The largest crystallites were obtained using the tetramminegold (III) nitrate precursor at pH 2 and the $HAuCl_4$ precursor with mean crystallite sizes between 10nm and 15nm.

The catalysts were active for glucose oxidation and for the most part, almost 100% selective towards gluconic acid. However, smaller crystallites below 10nm in size showed lower activity and there appears to be an optimum crystallite size of between 10nm and 15nm.

"I know the meaning of plagiarism and declare that all the work in the document, save for that which is properly acknowledged, is my own".

MR BRENDAN BEEMING

Signed by candidate

Contents

List of Figures

List of Tables

Glossary

Active Site	A site onto which a molecule adsorbs and reacts to yield products which then desorb (Heterogeneous catalysis)
Activity	A measure of how well the catalyst works for a given reaction.
Agglomeration	Joining of crystallites to form a collection of crystallites
Deactivation	The process whereby the catalyst loses catalytic activity
Dispersion	Number of atoms at the surface of a metal crystallite divided by the number of atoms in the crystal.
Iso-electric point	The point at which the net surface charge of a solid in an aqueous solution is zero.
Leaching	Process to remove the active metal species from the surface of a catalyst support.
Macropores	Pores in the size range >50nm
Mesopores	Pores in the size range 2-50nm
Micropores	Pores in the size range <2nm
Precursor	The substance from which the catalytically active metal species is produced.
Sintering	Joining of crystallites to form a single larger crystallite.
Support	The substance onto which metal crystallites are deposited.

Acknowledgements

Support and Assistance

I wish to thank the following for their support:

Academic

Prof Eric van Steen

A/Prof Jenni Case

Technical

Dr Mohamed Jaffer

Sean Carriem

Marc Wüst

Helen Divey

Susana Vasic

Kerry Horne

Bill Randall

Stephen Roberts

Financial

Mintek Pty Ltd / Project Autek

University of Cape Town post graduate funding office

Centre for Catalysis Research, Department of Chemical Engineering, University of Cape Town

To the undergraduate students Tshepo Mashile and Lynsey McEwan for producing the catalysts. Also to Glassmen Retreat for keeping some of their glass off cuts so I could make my baffles. And lastly to the Parish of St Andrew for their kindness and understanding throughout the duration of this project, especially when I miss Parish Council meetings!

1 Literature review

1.1 Properties of gold

1.1.1 Physical properties

Bulk gold is a bright yellow metal. Thin sheets of gold appear to be green or blue in light. The colour of colloidal gold changes with crystallite size due to surface plasmon absorption (coherent motion of the conduction band electrons caused by interaction with an electromagnetic field) (Burda *et al.*, 2005; Link and El-Sayed, 2000; Link and El-Sayed, 1999). Colloidal gold may appear red for crystallites of about 100nm in size and purple for crystallites of about 10nm in size (Burda *et al.*, 2005; Link and El-Sayed, 2000; Link and El-Sayed, 1999). Bulk metallic gold is one of the most ductile and malleable of metals. It is also one of the densest metals with a density of 19.3 g/cm^3. Only rhenium, platinum, iridium and osmium have a higher density. Bulk metallic gold melts at 1064°C and boils at 2808°C.

Gold has only one naturally occurring isotope, ^{197}Au. Gold has the electronic configuration: [Xe] $4f^{14}$ $5d^{10}$ $6s^1$. Due to relatavistic effects, gold has an atomic radius of 135pm which is slightly smaller than silver with a radius of 160pm (Gorin and Toste, 2007; Schmidbaur et al., 2005; Bond and Thompson, 1999; Bartlett, 1998; Bayler et al., 1996). Compared to silver, gold has larger nuclear charge (Z=47 for Ag compared to 79 for Au). The increased nuclear charge results in higher velocity of the s-electrons (Bartlett, 1998). One consequence of relativity is that the mass increases as the velocity approaches the speed of light (Gorin and Toste, 2007; Schmidbaur *et al.*, 2005; Bartlett, 1998). This causes the s electrons and to a lesser extent the p electrons to occupy smaller orbitals. The 6s orbital in a gold is therefore contracted hence the smaller atomic radius. As the s electrons are more strongly bound, they shield the nuclear charge from other electrons, consequently the d- and f-electrons are less bound to the nucleus and occupy larger orbitals than if these effects were absent (Bartlett, 1998).

The only stable crystal structure of metallic gold is face centred cubic and has a lattice constant of 4.0781Å (Bond and Thompson, 1999; Bailar *et al.*, 1973).

1.1.2 Chemical properties

Gold is the most electronegative metal and will not easily react with other electronegative elements such as oxygen which explains its resistance to corrosion at ambient conditions (Lagowski, 1983; Bond and Thompson, 1999). Another consequence of this high electronegativity is the formation of anionic gold as in CsAu. Both gold oxides Au_2O and Au_2O_3 decompose on heating at 205°C and 160°C respectively (Bailar et al., 1973) to form metallic gold as a further consequence of the high electronegativity of gold. All salts of gold are unstable and decompose easily on heating.

Gold has a higher electron affinity than oxygen. It readily forms alloys with other metals (Bond and Thompson, 1999). Gold is also not affected by sulphuric, nitric or hydrochloric acid and nearly all organic acids up to its boiling point. Gold will only dissolve in a solution with an oxidising agent such as nitric acid, and a hydrohalic acid, such as aqua regia. Gold also dissolves in alkali metal cyanides in the presence of oxygen and in sodium thiosulphate solutions in the presence of oxygen.

Gold has lower second and third ionisation energies than the group 1A metals and can therefore have oxidation states higher than 1 (Bond and Thompson, 1999). The +1 and +3 oxidation states are the most common. The +5 oxidation state exists in $[AuF_6]^-$ (Bond and Thompson, 1999). Organogold compounds are also known, mainly for the oxidation states +1 and +3 (Parish, 1997). These include ethene, propene, butadiene and CO complexes (Bond and Thompson, 1999).

1.1.3 Catalytic activity of gold

Gold has long been regarded as catalytically inert as it was regarded as an unreactive noble metal. Reactive molecules such as CO and H_2 do not adsorb on the surface of bulk gold (Wolf and Schüth, 2002; Haruta, 1997). Only HCOOH, H_2S and thiol can adsorb on the surface of bulk gold (Haruta 1997). Haruta *et al.* (1989) discovered that gold deposited as nanosized crystallites on selected supports exhibited high activity for CO oxidation. Gold nano-crystallites display different properties to bulk gold: they have a lower melting point and can adsorb CO, H_2 and O_2 (Choudhary and Goodman, 2002). Recent interest in gold as a catalyst has been fuelled by the development of processes to deposit gold as nano-particles on selected supports.

1.1.3.1 Activation energies

A significant property of gold catalysts is their low apparent activation energies for CO oxidation (Haruta, 2004). The apparent activation energy is almost zero at temperatures above 300K. Below 300K, the obtained activation energy ranges between 20 and 40 kJ/mol. By comparison the activation energies for CO oxidation for platinum group metals range from 50 to 170 kJ/mol. Platinum is more active than gold but only at temperatures above 500K. Gold is 1 to 4 orders of magnitude more active than platinum at room temperature (Haruta, 2004).

1.1.3.2 Crystallite size

As previously mentioned, Haruta *et al.* (1989) discovered gold nano-crystallites show high activity for CO oxidation. Smaller crystallites were more active with the most active catalyst having a mean crystallite size of 4.1nm. Choudhary and Goodman (2002) also found the activity per surface gold atom (or turnover frequency) to be very sensitive to gold crystallite size (Figure 1.1). They synthesised gold on titania catalysts with mean particle diameters ranging from 2 to 6nm and found maximum turnover frequency at an average crystallite size of 3.2nm. At 6nm, the turnover frequency was significantly lower. This trend was confirmed by Wolf and Schüth (2002). Haruta (2004) observed a sharp increase in the activity for CO oxidation with decreasing crystallite size from 5nm for gold on titania. A tentative explanation for this observed size dependency was put forward by Phala and van Steen (2007). They showed using molecular modelling that the strength of CO adsorption increases with decreasing crystallite size. This may explain the observed behaviour, since weak chemisorption leads to a low surface coverage and hence a low activity and strong chemisorption may lead to inhibition.

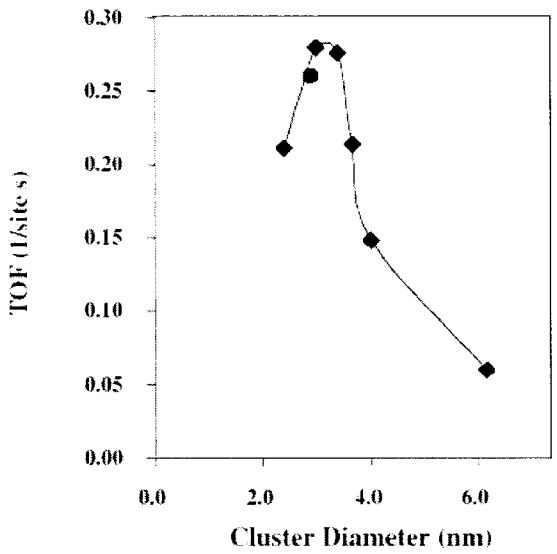

Figure 1.1: CO oxidation activity as a function of crystallite size for an $Au/TiO_2/Mo$ system (Choudhary and Goodman, 2002)

Recent work by Beeming and Bialek (2006) showed that gold crystallite size is also important for glucose oxidation. Gold on zinc oxide catalysts with gold crystallites larger than 10nm showed much lower activity than the catalysts with crystallites below 5nm.

1.1.3.3 Nature of the support

The support material plays an important role in gold catalysis (Min *et al.*, 2006; Andreeva, 2002). It has been suggested that metal oxide supports stabilise small gold crystallites (Wolf and Schüth, 2001; Bocuzzi *et al.*, 1998; Valden *et al.*, 1998; Haruta, 1997; Haruta *et al.*, 1989). For CO oxidation, it has been proposed that the reaction takes place on the interface between the gold metal oxide interface and that the metal oxide acts as a source of oxygen, with the oxygen adsorbed on vacant sites on the metal oxide surface (Haruta, 2004; Choudhary and Goodman, 2002). However, there is still no agreement on the role of the support in this reaction. It seems to be generally accepted that CO is adsorbed on the gold crystallites (Choudhary and Goodman, 2002; Bond and Thompson, 1999).

Schubert *et al.* (2001) showed that reducible transition metal oxides were more active than irreducible metal oxides such as Al_2O_3 and MgO. They attributed this difference in activity to the ability of the reducible metal oxides to adsorb molecular oxygen at relatively low temperatures. They claimed that oxygen dissociates at the gold/support

interface and reacts with the CO either on the gold particle or at the interface between the gold particle and the support.

1.1.3.4 Active sites

The location of the active sites on gold catalysts is still debated. It has been suggested that the adsorption sites on gold crystallites are edge, corner and step sites (Haruta, 2004), with the reaction zone at the gold/support interface (Haruta, 2004; Schubert *et al.*, 2001). These conclusions were reached as the decrease in the crystallite size would lead to an increase in these adsorption sites, and gold/support interface (Haruta, 2004). However, the gold surfaces cannot be discounted.

1.1.3.5 Active species

The oxidation state of gold in active gold catalysts is still unclear and may differ for various reactions. Some researchers argue that Au^{+} and Au^{3+} might be the active species (Fierro-Gonzalez and Gates, 2007; Boyd *et al.*, 2005). For the water-gas shift reaction, a few studies have been carried out whereby the metallic gold is leached off. The activity remained more or less unchanged for the water-gas shift reaction thus suggesting cationic gold as the active species for this reaction (Fu *et al.*, 2003; Fu *et al.*, 2005). However, Kim and Thompson (2006) prepared gold on ceria catalysts and reported that the unleached catalyst was significantly more active than the leached catalyst. Contamination due to the NaCN leaching process was ruled out as the sodium concentration for both the leached and unleached catalysts was very low. These results suggest that metallic gold is the active species for the water-gas shift reaction. Previous studies on the hydrochlorination of ethyne using gold catalysts have revealed a reduction in activity with reduction of Au^{3+} to metallic gold suggesting Au^{3+} is the active species for this reaction (Hutchings, 1996).

1.2 Gold catalyst preparation

Metal oxide supports are generally used in gold catalysis for CO oxidation, the hydrochlorination of ethyne and NO reduction (Haruta, 2004; Hutchings, 1996). Current applications of gold catalysts use predominantly metal oxide supports.

However, carbon is commonly used as a support for gold catalysed liquid phase oxidations of alcohols such as glycerol, glucose and propylene glycol (Beltrame *et al.*, 2006; Comotti *et al.*, 2006; Hutchings, 2005; Önal *et al.*, 2004; Biella *et al.*, 2002; Bianchi *et al.*, 2000). Metal oxide supports have also been shown to be active for the liquid phase oxidation of glucose (Baatz *et al.*, 2007). The product from glucose oxidation, gluconic acid, is used in the food and pharmaceutical industries and carbon is therefore preferred as it is harmless if ingested.

1.2.1 Carbon as a support for gold catalysts

Carbon is a common support in heterogeneous catalysis. It exhibits many of the properties required for a good support (Prinsloo, 2000; Rodríguez-Reinoso, 1998), such as:

i. Resistance to acids and bases
ii. Cheaper than conventional supports
iii. The chemical character of the surface is easy to modify
iv. Carbon can be combusted to obtain the active metal species
v. It is easy to modify its pore structure

Many different types of carbon have been used to prepare supported catalysts: graphite, carbon black, activated carbon, activated carbon fibres, carbon-covered alumina, graphite intercalation compounds, glassy carbon, pyrolytic carbon, polymer-derived carbon, fullerenes and nanotubes (Rodríguez-Reinoso, 1998). High surface area carbon materials are usually preferred in supported catalysts (Rodríguez-Reinoso, 1998).

1.2.2 Carbon nanotubes as a support

Carbon nanotubes were discovered in 1991 by Iijima. They have a unique structure and behave differently to familiar catalyst supports such as alumina and other metal oxides (Ma *et al.*, 2006; Odom *et al.*, 2000). The advantages of carbon nanotubes over other carbon materials include high mesoporous structure, mechanical strength, filterability and stability under oxidising and reducing conditions (Kleinsmidt, 2005; Prinsloo, 2000).

Single walled carbon nanotubes can be viewed as a graphene sheet rolled up to form a tube (Odom *et al.*, 2000; see Figure 1.2). They have high surface areas and mesopores as opposed to micropores. Open tubes yield a higher surface area and exhibit higher activity for certain reactions than closed tubes (Prinsloo, 2000). The mesopores reduce the transport limitations which can become a limiting factor with activated carbon. Mesopores allow the reactants and products to diffuse easily (Ma *et al.*, 2006). This is especially significant in liquid phase reactions.

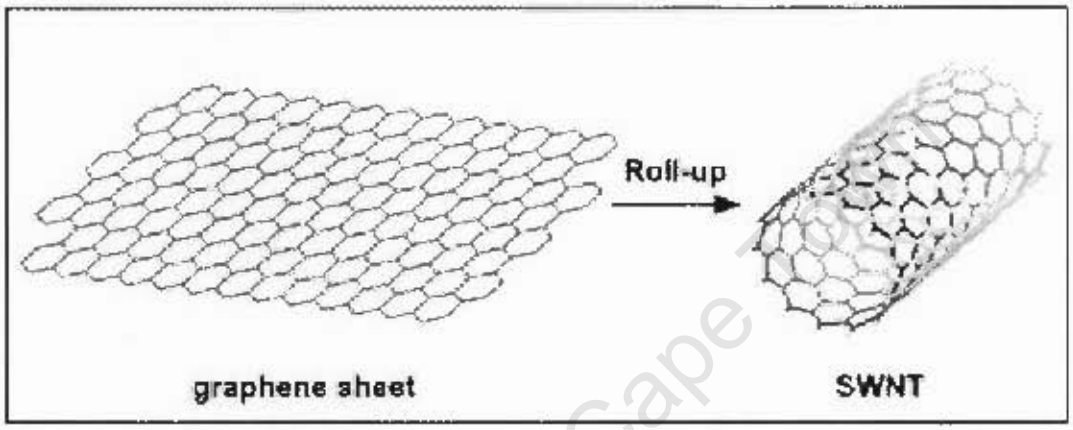

Figure 1.2: Diagram of a graphene sheet and a single walled nanotube (Odom *et al.*, 2000)

Multi-walled carbon nanotubes can be viewed as multiple sheets stacked on top of each other rolled up forming the tube walls (Kleinsmidt, 2005). Depending on the preparation method, multi-walled nanotubes can have a parallel or fishbone arrangement (Kleinsmidt, 2005; Prinsloo, 2000; see Figure 1.3).

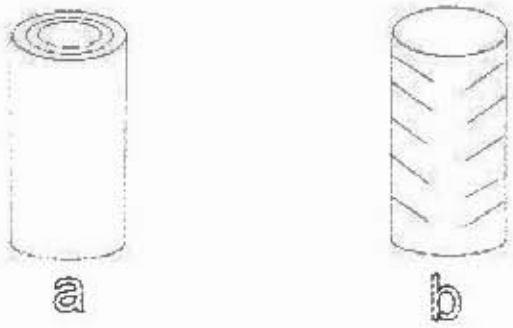

Figure 1.3: Multi-walled carbon nanotubes: (a) Parallel type and (b) Fishbone type (Hoogenraad, 1995)

Carbon nanotubes are hydrophobic and chemically inert (Ma *et al.*, 2006). A process to activate the surface is therefore needed. Treating the nanotubes with an oxidant is the most common method (Ma *et al.*, 2006).

1.2.3 Iso-electric point of the support

The iso-electric point of a solid material is the pH at which the net surface charge is zero. At a pH above this point, the surface is negatively charged. At a pH below this point, the surface is positively charged. Different carbons have different iso-electric points and may vary widely depending on the type and source of the carbon due to the presence of different surface groups (Table 1.1).

The pH of the solution is important during catalyst preparation as it influences the amount of chloride adsorbed on the support when $HAuCl_4$ is used as the precursor (Oh *et al.*, 2002). The amount of adsorbed chloride on the support depends on the iso-electric point of the support and its adsorption capacity. The amount of chloride adsorbed by Al_2O_3, which has an iso-electric point of 8, decreased rapidly as the pH approached the iso-electric point of the support (Oh *et al.*, 2002). Catalyst synthesis should therefore be carried out at pH values at or above the iso-electric points of the selected supports when a chloride containing precursor is used.

Table 1.1: Iso-electric points of different carbons

Support	Iso-electric point (pH)
Activated carbon (coal based)[1,2]	8.1
Activated carbon F400 (coal based)[1]	6.0
Carbon black (rice based)[2]	2.6
Carbon black (wheat based)[2]	3.3
Multi-walled carbon nanotubes[3]	4.0

[1] Chingombe *et al.*, 2005
[2] Qiu *et al.*, 2008
[3] Liu and Gao, 2005

1.2.4 Preparation methods

It is relatively difficult to deposit gold as nanocrystallites on metal oxide supports as gold has a lower melting point and low affinity for metal oxides compared with

platinum and palladium (Haruta, 2004). This lower melting point is significant during calcination/reduction as it may result in the sintering of gold crystallites.

The synthesis procedure has a significant effect on the size of the gold crystallites obtained. The catalytic activity for gold catalysts can change dramatically while some platinum catalysts appear to be independent of the preparation method (Haruta, 1997).

The most common methods of gold catalyst preparation are impregnation, co-precipitation and deposition precipitation (Bond & Thompson, 1999). Ion-exchange and liquid phase grafting have not been widely used for the preparation of supported gold catalysts. The non-precipitation methods (ion-exchange, impregnation and grafting) are summarised in Table 1.2.

1.2.4.1 Deposition precipitation

Deposition precipitation is currently the most commonly used method to synthesise supported gold catalysts. The gold precursor is placed in a slurry containing the support (Bond & Thompson, 1999; Ueda and Haruta, 1999). The support surface acts as a nucleating agent. The gold precursor is precipitated out of solution on the surface of the support and should lead to the majority of the precursor attaching to the support. Using $HAuCl_4$ as the precursor, by increasing the pH the partially hydrolyzed species reacts with the support to form $Au(OH)_3$ on the surface (Bond & Thompson, 1999).

It has been shown that the catalytic activity of gold on metal oxide supports is strongly dependent on the pH during preparation by deposition-precipitation and the temperature of calcination (Wolf and Schüth, 2002). Haruta (1997) prepared gold catalysts supported on TiO_2 by the deposition-precipitation method and reported that the pH of the synthesis solution has a strong effect on the resulting size of the Au particles. It was shown that catalysts with smaller Au particle sizes were prepared at higher pH values. To illustrate this, mean Au particle diameters of about 10 nm were obtained by deposition precipitation at pH 5 compared to diameters smaller than 4 nm at pH values above 6. Similar results were obtained by Wolf and Schüth (2002) for their gold on titania catalysts. Preparation at higher pH values resulted in catalysts active at temperatures as low as -50°C for CO oxidation.

NaOH and urea are typically used as precipitating agents in deposition precipitation. Zanella *et al.* (2002) achieved higher gold loadings using urea than NaOH, although the crystallite sizes obtained were more or less the same. Baatz *et al.* (2007) explained the difference in the amount of gold deposited by the fact that using urea, the method starts in an acidic medium and the pH is slowly and continuously raised allowing the adsorption of anionic species on a positively charged alumina surface. Using NaOH, the initial pH of the suspension is neutral and the support is much less positively charged (Baatz *et al.*, 2007).

Barkhuizen et al. (2006) developed an alternative deposition precipitation method whereby the precursor ($HAuCl_4$) and the precipitating agent were added simultaneously to the slurry containing the support thus keeping the pH constant. A narrower crystallite size distribution was achieved with an improved loading efficiency.

1.2.4.2 Impregnation

Impregnation is also a simple method of preparing gold catalysts. $HAuCl_4$ is the most commonly used precursor (Solsona *et al.*, 2006). The support is place in a precursor solution such that all the pores of the support are filled (Li *et al.*, 2006; Solsona *et al.*, 2006; Lee and Gavriilidis, 2002; Bond and Thompson, 1999). The slurry is agitated and left to allow for impregnation to occur. The slurry is then filtered and washed to remove any chloride ions. The resulting catalyst is then dried and calcined (Solsona *et al.*, 2006; Bond and Thompson, 1999).

Industrially, impregnation is the easiest way of producing a catalyst but the formation of large crystallites and difficulty in removing the chloride ions are problems in this method. (Li *et al.*, 2006).

Baatz and Prüße (2007) prepared gold on alumina catalysts by impregnation and deposition precipitation which exhibited similar activity and small gold crystallites. The crystallite sizes using these two preparation methods were the same at similar gold loadings. The reason for this may lie in the fact that the impregnation catalyst

they prepared was calcined in hydrogen, thus removing the chloride ions, whereas the deposition precipitation catalyst was not.

1.2.4.3 Ion-exchange

Ion-exchange is a process by which cations or anions are exchanged with other cations or anions on the surface of a support (Bond and Thompson, 1999). This method is sometimes called strong electrostatic adsorption (Miller *et al.*, 2006). This method has not been widely used in the synthesis of supported gold catalysts. One possible reason is the limited number of gold complexes available. Known complexes include gold ethylenediamine $[Au(en)_2]^{3+}$, and ammines of gold $[Au(NH_3)_2]^{+}$ and $[Au(NH_3)_4]^{3+}$ (Bond and Thompson, 1999). Another possible reason for the lack of utilisation of this method is that gold ammine complexes can form explosive fulminating gold at high pH (Skibsted and Bjerrum, 1974). For preparing gold on carbon nanotubes using tetramminegold (III) nitrate for example, the positively charged $Au(NH_3)_4^{3+}$ will exchange with a proton from a surface carboxylate group (COOH).

Ion-exchange has been used to prepare other supported metal catalysts such as Cu/SiO_2, Pd/SiO_2 and Pt/SiO_2 (Bonivardi and Baltanás, 1990; Kohler *et al.*, 1987; Kohler *et al.*, 1987;). This method produces supported metal catalysts with a high dispersion. Popp (2004) and Beeming and Bialek (2006) have prepared Au on ZnO catalysts using ion-exchange. The gold complex used as the precursor was tetramminegold (III) nitrate. The precursor was dissolved in solution and the ZnO support added. The agitated solution was then left to age for 24 hours to ensure equilibrium conditions (Popp, 2004). The slurry was then filtered, washed and dried in the ambient air for 24 hours, then calcined.

The high dispersion that can be achieved with ion-exchange can be explained by the inter-grain diffusion of the amine species (Popp 2004; Goguet, 2000). This process can occur either on the surface of the catalyst support or in the solution and can occur at very low concentration and metal loading.

Using ion-exchange to produce Au on ZnO, Popp (2004) obtained smaller mean particle diameters compared with the deposition-precipitation method (2.5nm for ion-

exchange, 3.2nm for deposition precipitation). Narrower particle size distributions were also achieved with ion-exchange. Beeming and Bialek (2006) had great difficulty in locating particles on the surface of the support during TEM analysis. From the AAS results they obtained reasonable loadings (between 0.3% and 2%). It may be possible that very small Au crystallites were present on the support that could not be seen by TEM.

1.2.4.4 Grafting

Grafting involves a gold complex in solution which reacts with the surface of the support to form the precursor (Bond and Thompson 1999). Gold phosphine complexes have been use in this method and attached to metal hydroxide supports (Yuan *et al.*, 1997).

This method can produce small gold crystallites (Yuan *et al.*, 1997). The disadvantage of this method is the dispersion obtained can be less homogeneous than other liquid phase preparation methods depending on the gold precursor and support material used.

Table 1.2: Summary of non-precipitation methods

Method	**Impregnation**	**Ion-exchange**	**Grafting**
Precursors	$HAuCl_4$ mostly used. $KAu(CN)_2$, $[Au(en)_2]Cl_3$ less common	$HAuCl_4$, $Au(NH_3)_4(NO_3)_3$	$[Au(PPh_3)]NO_3$, $[Au_9(PPh_3)_8](NO_3)_3$
Deposition Technique	Can be done by adding just enough precursor solution to fill the pores of the support, or larger volume may be used from which the solvent is removed by evaporation[1]	Support is added to a solution of the precursor, where gold containing cations or anions are exchanged with other cations or anions on the surface of the support	The gold complex in solution reacts with the surface of the support forming some other species which may then be converted to some other form using calcination/reduction[1,2]
Preparation	pH not controlled	pH of suspension	pH not controlled

pH		must be above or below the iso-electric point of the support for cationic and anionic exchange respectively	

1.2.5 Calcination and reduction

The crystallite size is affected by calcining temperature, calcining time and the reducing gas used. Increased calcination temperature leads to larger particles (Zanella and Louis, 2005; Wolf and Schüth, 2002). This sintering can occur at relatively low temperatures owing to gold's relatively low melting temperature when present as nanocrystallites (Buffat and Borel, 1976)

Zanella and Louis (2005) calcined their catalysts in both air and H_2. H_2 gave smaller particle sizes at a given temperature. They deduced that this was due to the chloride ions being removed as HCl thus preventing particle sintering. Increased calcining time is also expected to result in larger particle sizes (Zanella and Louis, 2005). The effect of calcining time and temperature is also dependent on the support material and how it interacts with the gold particles.

Gold loading is an important factor during calcination. Increased loading can lead to increased agglomeration, resulting in much larger gold crystallites (Beeming and Bialek, 2006; Wolf and Schüth, 2002). The effect of calcining time and temperature will be dependent on the support material and how it interacts with the gold crystallites.

1.3 Deactivation of gold catalysts

An unfavourable characteristic of gold catalysts is their tendency to deactivate at temperatures close to or above ambient conditions. Gold catalysts exhibit the same types of deactivation as other supported metal catalysts such as platinum, nickel and cobalt supported catalysts.

The most common gold catalyst poison is chlorine. Chloride containing gold precursors (for example $HAuCl_4$) are widely used in the preparation of these catalysts. Chlorine poisons the catalyst by electrostatic interactions, blocking an active site. Furthermore it promotes the agglomeration of Au crystallites at elevated temperatures (Broqvist *et al.*, 2004; Oh *et al.*, 2002). Work has been carried out to remove the chlorine during preparation and the use of non-chloride containing precursors has been investigated (Simakov, 2007; Beeming and Bialek, 2006; Bond and Thompson, 1999; Okumura *et al.*, 1997).

Sintering occurs on gold catalysts at relatively low temperatures as gold nano-crystallites have a relatively low melting point (Buffat and Borel, 1976). However this only appears to be a hindrance during calcining as most gold catalysed reactions take place at near ambient temperatures.

Although still debated, many studies claim that Au^0 is not active and deactivation is a result of Au^{3+} and Au^+ being reduced to Au^0.

A recent study by Lee *et al.* (2007) found that Au/TiO_2 is sensitive to light. Light as weak as that in a desk drawer with an intensity of 0.01 $\mu W/cm^2$ can cause Au/TiO_2 to slowly deactivate. Analysis of the catalysts revealed that the gold had been reduced to gold metal and this is claimed to cause the deactivation. No sintering was observed.

Gold catalysts are less susceptible to metal leaching in liquid phase alcohol oxidations compared to Pt and Pd catalysts (Mallat and Baiker, 2004; Prati and Rossi, 1998). Prati and Rossi (1998) studied the oxidation of diols on carbon supported metal catalysts and observed metal leaching with the Pt and particularly the Pd catalysts. This leaching resulted in a decline in activity and selectivity of the reaction products. They detected no leaching with the gold catalysts.

1.4 Characterisation of gold catalysts

Bulk gold chemisorbs poorly and may only chemisorb at low temperatures or at high temperature if the process is activated (Bond and Thompson, 1999). Treating the bulk

gold surface by making it rough improves chemisorption (Bond and Thompson, 1999). Nanocrystallites of gold will readily chemisorb H_2, O_2, CO and NO due to the increased presence of gold atoms with low coordination numbers (Debeila *et al.*, 2005; Franceschetti *et al.*, 2003; Berndt et al., 2003; Bond and Thompson, 1999; Shastri *et al.*, 1984; Fukushima *et al.*, 1979). CO chemisorption has been extensively studied on gold catalysts owing to the extensively studied CO oxidation over supported gold catalysts (Meyer *et al.*, 2004).

Chemisorption can be used as a means of determining the average gold crystallite size and dispersion. This has been studied using CO and O_2 (Franceschetti *et al.*, 2003; Berndt *et al.*, 2003; Shastri *et al.*, 1984; Fukushima *et al.*, 1979). The stoichiometry used to calculate the average crystallite size is significant when comparing chemisorption results to TEM and researchers have deduced the stoichiometry by comparison with the TEM results. Fukushima *et al* (1979) found that using an Au:O ratio of 2 (one oxygen chemisorbing onto 2 gold atoms) at 200°C and below corresponded well with the TEM data, but at 300°C an Au:O ratio of 1 was used in order to correspond with the TEM data. The Au:O stoichiometry of 2 at 200°C was also applied by Shastri *et al* (1984) and Berndt *et al* (2003). Both obtained results in good agreement with their TEM results.

1.5 Glucose oxidation

Glucose oxidation to gluconic acid is an industrially important reaction. Annual worldwide production of gluconic acid is estimated at 60 000 tons (Önal et al., 2004; Lichtenthaler, 2002). Gluconic acid is used as a water-soluble cleaning agent and as a food additive (Biella *et al.*, 2002). It is also applied in the pharmaceutical, paper and concrete industries (Baatz *et al.*, 2007; Önal *et al.*, 2004).

1.5.1 Biochemical production process

Industrially glucose oxidation is an enzyme catalysed process (Baatz *et al.*, 2007; Comotti *et al.*, 2006; Ramachandran *et al.*, 2006; Önal *et al.*, 2004; Biella *et al.*, 2002). The most widely used method is a fermentation process using the fungus *aspergillus niger* (Ramachandran *et al.*, 2006). The reaction takes place in an aerated glucose solution at pH 5.5 and 30°C (Ramachandran *et al.*, 2006; de Wilt, 1972).

Glucose concentrations of up to 35wt-% are used (de Wilt, 1972). Reactions take from 10 to 30 hours (de Wilt, 1972).

This method is sensitive to contamination (de Wilt, 1972). The bioconversion of glucose to gluconic acid also consumes a large quantity of oxygen compared to heterogeneous catalytic methods (Ramachandran *et al.*, 2006; Biella *et al.*, 2002; de Wilt, 1972). Higher oxygen concentrations, therefore higher air or oxygen pressures are needed for greater productivity (Ramachandran *et al.*, 2006).

1.5.2 Heterogeneous catalytic process

Glucose oxidation using Pt/C catalysts has been well studied (Dirkx and van der Baan, 1981; de Wilt, 1972). However the selectivities achieved with platinum catalysts were not as high as the industrial biological process (de Wilt, 1972).

Work done by Biella *et al.* (2002) shows promising results for glucose oxidation using carbon supported gold catalysts (Figure 1.4). Biella *et al.* (2002) prepared their Au/C catalysts and tested them at pH values of 7, 8 and 9.5. The optimum pH conditions were found to be at pH 9.5 as the Au/C catalyst was most active at pH 9.5 while maintaining high (close to 100%) selectivity towards gluconic acid. This optimum pH was confirmed by other studies on gold catalysed glucose oxidation (Baatz and Prüße, 2007; Comotti *et al.*, 2006; Önal *et al.*, 2004). If the pH is too high, alkali promoted reactions such as isomerisation, condensation, Cannizzaro and retro-Claisen are favoured. The Au/C catalyst was considerably more active than the Pt/C, Pd-Bi/C and Pt-Pd-Bi/C catalysts with the Au/C catalyst achieving 100% conversion in less than 50 minutes with selectivity close to 100% as shown in figure 1.4 (Biella *et al.*, 2002).

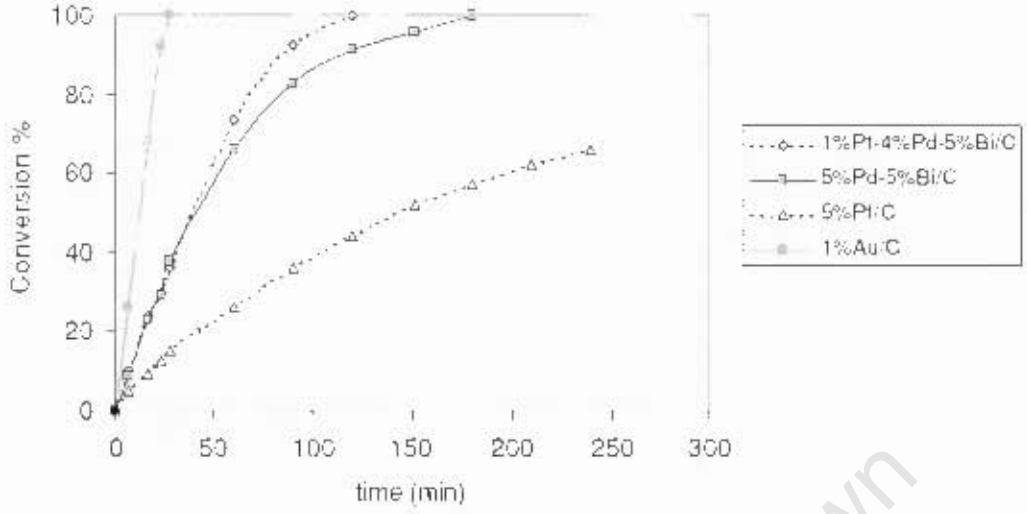

Figure 1.4: Glucose oxidation at pH 9.5, maintained by the addition of 0.3M NaOH. Reaction conditions: 4 wt% glucose, glucose/Au: 1000, O_2 flow: 20 ml/min, temperature: 50°C (Biella *et al.*, 2002)

Önal *et al.* (2004) prepared a Au/C catalyst for glucose oxidation and tested the effect of both temperature and pH. They observed a decrease in the reaction rate and selectivity with increasing temperature, owing to the formation of side products such as fructose (Figure 1.5). An analysis on the effect of gold crystallite surface area on the initial reaction rate revealed an exponential increase in the initial rate of reaction with increasing surface area with only a slight increase in the selectivity at pH 9.5.

Önal *et al.* (2004) also investigated the influence of catalyst concentration and initial glucose concentration on the reaction rate. To ensure that mass transfer at the phase boundaries could be neglected, they first examined the effects of stirring rate and airflow rate on the reaction rate at 50°C and pH 9.5 over an Au/C catalyst. They found that by intensive stirring (900 rpm) and high volumetric flow rate of air (1600 ml/min), the overall reaction rate was not limited by external mass transfer (diffusion). The intrinsic rate of gluconic acid formation was asymptotically dependent on catalyst concentration suggesting the rate limiting step is the surface reaction. The initial rate of reaction does not depend strongly on the initial glucose concentrations. If adsorption of glucose on the catalyst surface was the overall rate limiting step, an increase in the initial glucose concentration should result in a strong increase in the reaction rate. As this is not observed here, the overall reaction rate is most likely limited by the surface reaction or desorption of gluconic acid. They also

found that the selectivity towards gluconic acid decreased slightly with increasing initial glucose concentration. They concluded that this decrease in selectivity is caused by the increasing isomerisation of glucose to fructose with an increasing initial glucose concentration.

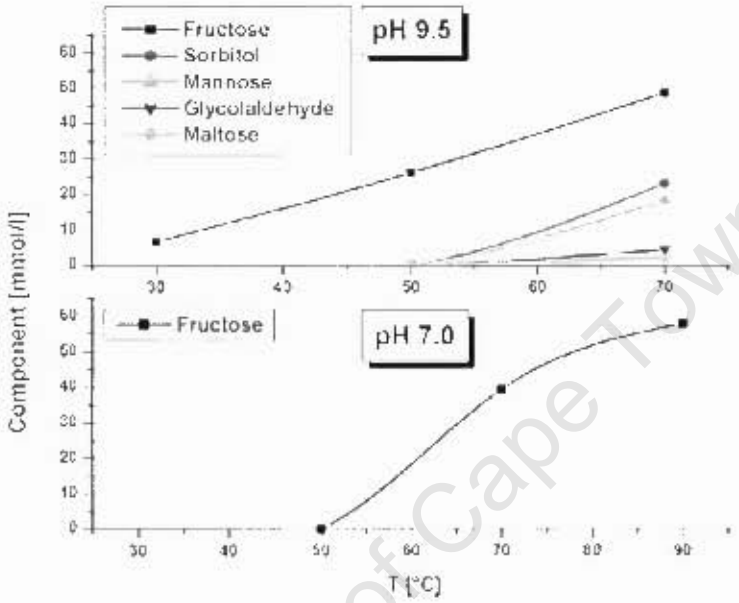

Figure 1.5: Formation of by-products in glucose oxidation at pH 7 and 9.5 as a function of temperature over a Au/C catalyst (Önal *et al.*, 2004)

Beltrame *et al.* (2006) studied the kinetics of glucose oxidation, comparing it to the biological process. They found the biological and heterogeneous catalytic process have the same stoichiometric reaction equation:

$$C_6H_{12}O_6 + O_2 + H_2O \rightarrow C_6H_{12}O_7 + H_2O_2$$

This reaction is followed by the decomposition of H_2O_2. They found the rate determining step for the biological process is the oxidation of glucose by the enzyme with the reaction order with respect to dissolved oxygen to be zero. For the gold catalyst, the rate determining step is also the oxidation of glucose, however the rate is first order with respect to dissolved oxygen.

Supported metal catalysts for glucose oxidation are susceptible to poisoning by the gluconate produced (Önal *et al.*, 2004; Biella *et al.*, 2002). This occurs to a greater

extent at lower pH as the amount of gluconate present is higher (Biella *et al.*, 2002; Abbadi and van Bekkum, 1995). The effect of this poisoning can be reduced significantly by increasing the pH of the reaction solution and reducing the amount of gluconate. As noted above, glucose oxidation with gold catalysts is therefore normally carried out at pH 9 or 9.5 (Mirescu and Prüße, 2007; Thielecke *et al.*, 2007; Önal *et al.*, 2004; Biella *et al.*, 2002). Biella et al. (2002) found that introducing a fresh glucose solution appeared to restore most of the catalytic activity. However when the catalyst was removed, washed and dried, then reused, they observed a significant loss in activity. An analysis of the catalysts revealed that some of the gold had been leached; particularly the catalysts used in the pH 7 reactions. No leaching occurred on the catalyst used in the pH 9.5 reaction but the crystallite size increased.

A recent study on gold catalysts using glucose oxidation was carried out in a flow reactor (Thielecke *et al.*, 2007). They used a CSTR to test an Au/Al_2O_3 catalyst at pH 9. The catalyst was tested over 70 days and exhibited no loss in activity or selectivity therefore making it suitable for industrial applications. However, alumina may not be suitable for food or pharmaceutical applications.

1.6 Objectives of this study and hypotheses

The aim of this study is to prepare gold catalysts on activated carbon and on carbon nanotube supports using the ion-exchange method and to test these catalysts using glucose oxidation. The experiments were designed in order to test the following hypotheses based on what has previously been noted in literature.

Gold particle sizes will be affected by the pH during preparation and the loading obtained.

Increasing the pH may result in higher loadings depending on the concentration of anchoring points for ion-exchange to take place. Higher loadings may however lead to increased particle sizes due to agglomeration.

Gold on carbon catalysts prepared by ion-exchange will be an effective catalyst for glucose oxidation.

Gold on carbon catalysts prepared by other methods such as deposition precipitation have been shown to be active for glucose oxidation. Ion-exchange has the potential to produce highly dispersed small gold crystallites on a support (Baatz *et al.*, 2007; Comotti *et al.*, 2006; Önal *et al.*, 2004; Biella *et al.*, 2001).

Gold particles below 10nm are active for glucose oxidation

Larger particles of gold are not active for glucose oxidation. Below this size, they will exhibit significant activity for glucose oxidation. Larger crystallites above 10nm in size will not be active for glucose oxidation.

2 Experimental

2.1 Preparation of gold catalysts

2.1.1 Preparation of tetramminegold (III) nitrate ($Au(NH_3)_4(NO_3)_3$)

$Au(NH_3)_4(NO_3)_3$ was prepared following the method described by Skibsted and Bjerrum (1979). A supersaturated solution of 95g NH_4NO_3 in 70ml de-ionised water was prepared. To assist the dissolution of the NH_4NO_3, the solution was agitated and heated slightly. 10 ml of a gold solution ($HAuCl_4$) containing 50g-Au/l, corresponding to 0.5g of gold, was added to the NH_4NO_3 solution and the resulting mixture was stirred at room temperature.

The glass beaker was then immersed in a bucket of ice until the temperature of the solution registered 0°C (Figure 2.1). A pH probe was inserted and an aqueous, 2.5wt-% NH_3 solution was added drop-wise to the ice-cooled mixture, with simultaneous stirring. The dark yellow solution began to turn light yellow and a small amount of a white precipitate started to form at about pH 5. The pH was adjusted until the pH of the solution registered 7. The following reaction occurs:

$$HAuCl_4 + 3\ NH_4NO_3 + 4\ NH_3 \rightarrow Au(NH_3)_4(NO_3)_3 + HCl + 3\ NH_4Cl$$

Beaker was covered with laboratory film (Parafilm) and aged for 24 hours at room temperature to allow for further precipitate to form.

The adjustment of the pH during the preparation of $Au(NH_3)_4(NO_3)_3$ needed to be exercised with caution as the tetramminegold (III) ion ($Au(NH_3)_4^{3+}$) hydrolyzes rapidly in alkaline solution which results in the formation of fulminating gold (Skibsted and Bjerrum, 1974). Fulminating gold is orange-brown, amorphous, highly explosive and shock sensitive. In the event of a fulminate forming, acid (such as HNO_3) can be added to dissolve it as the tetramminegold (III) ion is stabilized in acid solution and the hydrolysis is slow.

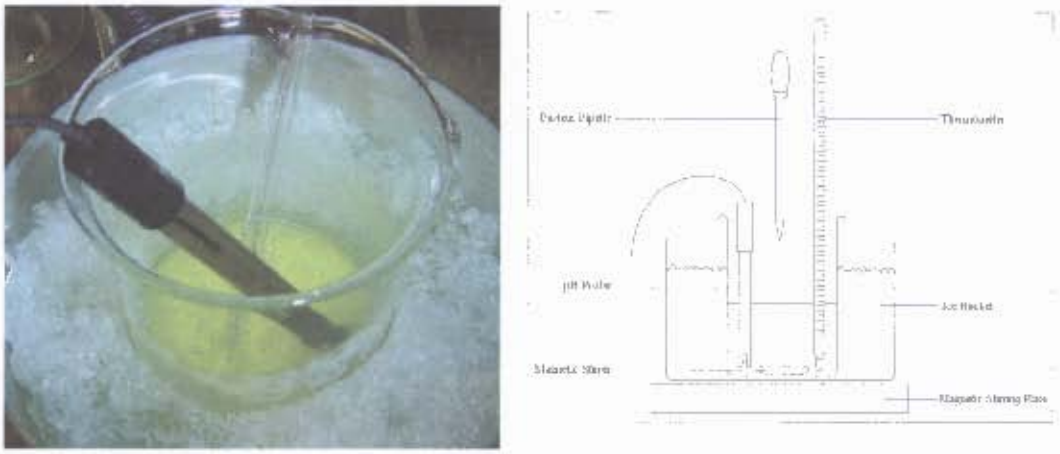

Figure 2.1: Preparation of tetrammingold (III) nitrate (Beeming and Bialek, 2006)

After 24 hours, the white precipitate was filtered through a Buchner flask. High quality Advantec No.2 (40301074) filter paper was used to ensure good filtration and to minimise the accumulation of filter paper in the dry product at a later stage. About 20ml of chilled ethanol (99.9%) was used as the washing fluid. The product was dried overnight at room temperature. The salt was subsequently analysed with atomic adsorption spectroscopy (AAS) to determine its gold content.

2.1.2 Activation of the fishbone carbon nanotube support

The fishbone carbon nanotubes supplied by Sasol were boiled in nitric acid in order to activate the surface by introducing functional groups. 2.5g of carbon nanotubes were added to 300ml 55wt-% nitric acid in a 500ml conical flask. A condenser was fitted into the neck of the flask. The slurry was boiled under continuous stirring (300rpm) for 6 hours or 48 hours. Subsequently the nanotubes were filtered off and dried in an oven at 150°C overnight. The mass of the boiled sample was recorded and compared to the initial mass.

2.1.3 Preparation of gold on carbon nanotubes and activated carbon

508ml of a 1mmol/l tetramminegold (III) nitrate solution is prepared in a conical flask. 2g of carbon nanotubes or activated carbon (Norit) are added to the solution and the pH adjusted. The solution was stirred for 24 hours and subsequently filtered and washed with de-ionised water. The pH of the tetramminegold (III) nitrate solutions and $HAuCl_4$ solutions was chosen based on the zeta potential measurements carried out on the support and the iso-electric point obtained. The catalysts prepared using

tetramminegold (III) nitrate were prepared at pH 2, 4 and 6. The catalysts prepared using the aurochloric acid precursor were prepared at pH 0.8.

Some of the catalysts produced were initially calcined in air at 200°C for 2 hours. These catalysts were later reduced in hydrogen at 200°C for 6 hours, with a 1 hour ramp up from 25°C and 1 hour ramp down to 25°C. Other catalysts produced were all reduced in hydrogen at 200°C for 6 hours.

2.2 Characterisation of materials

2.2.1 Atomic adsorption spectroscopy (AAS)

2.2.1.1 AAS analysis on tetramminegold (III) nitrate

The gold-containing tetramminegold (III) nitrate product was digested in acid to allow for elemental analysis. 10 ml of concentrated HCl was added to about 0.1 g of the solid product in a 100 ml conical flask. 10 ml of concentrated HNO_3 was subsequently added. The flask was agitated until the dissolution of the gold particles was complete. 25 ml of de-ionised water was added and the flask was gently heated and agitated until vapours were observed. The contents were filtered through a Buchner flask to remove any solid impurities and the filtrate was transferred to a 50 ml volumetric flask and diluted. About 5 ml of this solution was used for Au analysis.

2.2.1.2 AAS on preparation solutions

The filtrate from the catalyst preparation was made up to 1000ml in a volumetric flask. A 10ml sample was taken for AAS analysis to determine the concentration of gold in the solution in order to obtain a gold mass balance for the catalyst preparation. The loading on the catalyst was determined from the gold uptake from the solution.

2.2.2 Zeta potential

The zeta potential of the treated and untreated fishbone carbon nanotubes and activated carbon was measured using a Malvern Zeta-Sizer Nano ZS on a 1M KCl background. 1g of carbon nanotubes or activated carbon was placed in 100ml de-ionised water. pH adjustment was made using HCl and KOH solutions with concentrations of 1M, 0.1M and 0.01M, starting from low pH moving to high pH. The

equilibration time for the pH was 48 hours. The pH was remeasured prior to the zeta potential measurement. The zeta potential of activated carbon was also measured using the same procedure.

2.2.3 TEM analysis

The activated carbon, treated and untreated carbon nanotubes were analysed using a Leo 912 electron microscope. This was used to view changes in the physical structure of the nanotubes. Five images for each sample were obtained. The diameters and the wall thicknesses of the tubes were measured using the freeware ImageJ© software package.

Transmission electron microscopy (TEM) was also used to measure the size of the gold crystallites. A JEOL JEM-1200EX II electron microscope was used. With TEM, a crystallite size distribution can be measured. It also allows one to obtain information on the gold crystallite shape (Bond and Thompson, 1999).

The sizes of between 100 and 200 gold crystallites were measured to obtain a particle size distribution and a mean particle diameter. The crystallites did not appear to be spherical and were measured along the crystallite's longest axis as indicated by particle (a) and particle (b) in figure 2.2.

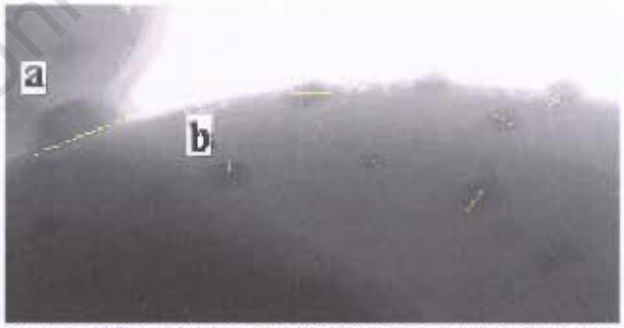

Figure 2.2: Measurement of gold crystallites from TEM images (Beeming and Bialek, 2006)

2.2.4 N_2 physisorption

N_2 physisorption was performed on the untreated and acid treated carbon nanotubes as well as the activated carbon using a Tristar 3000. A BET analysis was carried out at 77K. A BJH pore size distribution was determined from the data.

2.2.5 Hg pycnometry

The mercury pycnometry was conducted on an Autopore II 9220. About 0.3g of sample was used for each analysis. Activated carbon, untreated carbon nanotubes, 6hr and 48hr boiled carbon nanotubes were analysed. A mercury contact angle of 130° and surface tension of 485dyn/cm was assumed. The pore diameters were obtained assuming the pores are cylindrical.

2.2.6 Infrared spectra

The infrared spectra of the activated carbon, treated and untreated carbon nanotubes were recorded using a Nicolet 5700 FT-IR with the Smart-OMNI Transmission accessory. A wafer containing 0.1wt-% carbon nanotubes or activated carbon was prepared by adding about 2mg of carbon nanotubes to 2g of KBr, crushed using a marble mortar and pestle and pressed at 20 tons pressure into a tablet of 1mm in thickness. The measurement was carried out using 1000 scans at a resolution of $8cm^{-1}$ at wavelengths from 400 to $4000cm^{-1}$ under N_2 flow. An XT-KBr beamsplitter and a DTGS-TEC detector were used.

2.2.7 Raman spectra

The Raman spectra of the carbon nanotubes were obtained using a Thermo Electron NXR FT-Raman module with a HeNe laser. As with the infrared spectra, 0.1wt-% carbon nanotube KBr wafers were pressed at 20 tons pressure. The thickness of the wafers pressed for the Raman spectra are 2mm. Thinner wafers and wafers pressed with higher carbon nanotube concentration exhibited excessive heating therefore thicker wafers with lower carbon nanotube concentrations were used. All analyses were carried out using a laser power of 0.5W using an InGaAs detector and an XT-KBr beamsplitter. 1000 scans were recorded at a resolution of $16cm^{-1}$ for all analyses.

2.2.8 O_2 chemisorption on catalysts

O_2 chemisorption was performed on the catalysts on a Micromeritics ASAP 2020C. About 0.25g of sample was used for the analyses. The catalyst was subjected to flow in H_2 and heated to 200°C at a rate of 5°C/min and held at 200°C for 16 hours. The H_2 was then evacuated for 2 hours and the sample cooled to the analysis temperature. A

leak test was subsequently performed. Further evacuation is performed for another 10 minutes followed by the O_2 chemisorption analysis. Analyses were carried out at 35°C and 200°C at pressures between 0.1mmHg and 650mmHg. From this data the average crystallite size and dispersion were determined.

2.2.9 Glucose oxidation

Glucose oxidation was used as the test reaction for the catalytic activity of the catalysts. The experimental setup is illustrated in figure 2.3 and figure 2.4. A 1 litre round bottomed boiling flask was used as the reactor. The flask contains 5 necks: one large neck in the middle and 4 smaller 24/29mm necks on the sides. The large neck is required for the Heidolph RZR-1 overhead stirrer.

400ml of de-ionised water was first added to the reactor. The reactor was immersed in a water bath which was then placed on a hot plate. The water bath is agitated at 400rpm to ensure the temperature is uniform throughout the bath. The catalyst is added first and the resulting aerated slurry agitated for 3 hours. An aeration rate of 800ml/min synthetic air was used. This was followed by the addition of the glucose powder to the solution and the titration was started.

Glucose oxidation produces gluconic acid. To maintain the pH, a Schott Alpha Plus TA50 autotitrator was used. The pH probe and doser from the autotitrator are placed in the smaller necks along with the temperature probe, gas dispersion tube (porosity 2) and baffles. The autotitrator measures the pH and doses the reaction mixture with 0.05M NaOH to maintain the pH at a constant 9.5.

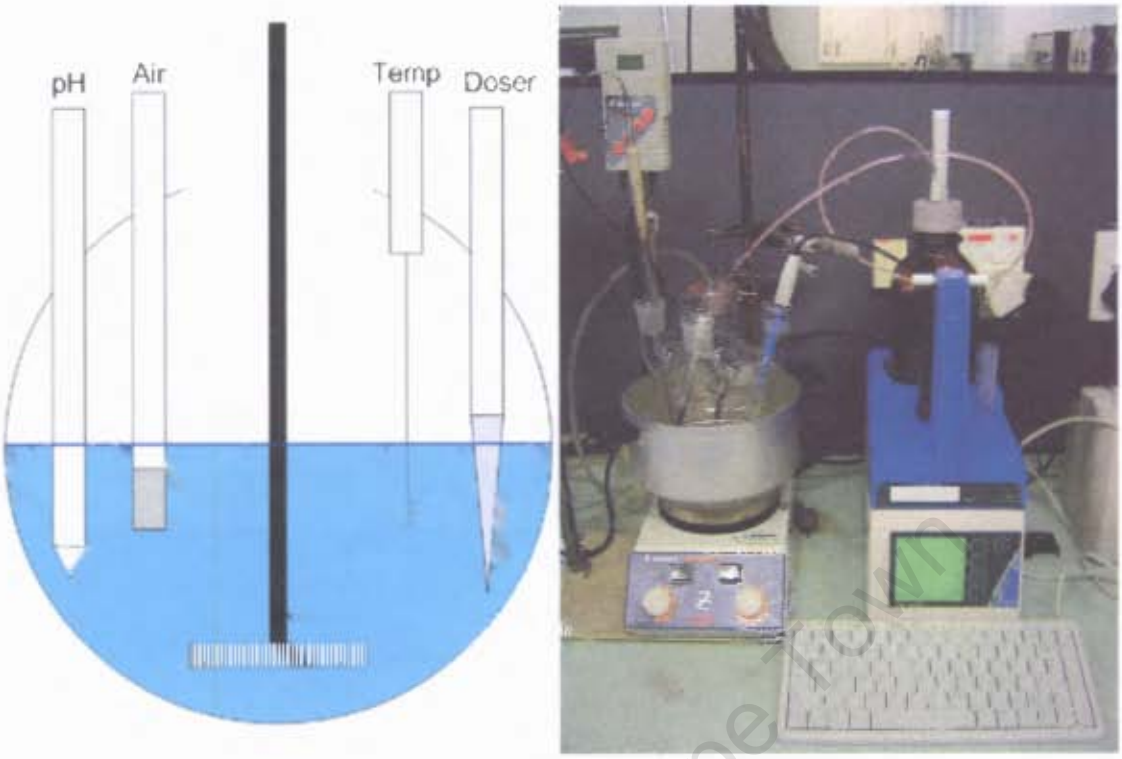

Figure 2.3: Glucose oxidation reactor

Before testing of the gold catalysts, the reaction was tested with an Engelhard 2% Pt on activated carbon catalyst. This catalyst was used to establish the presence of mass transfer limitations. The reaction was tested at agitation speeds between 600 and 2200 rpm and aeration rates between 100 and 1000ml/min. Aeration rates were controlled via a needle valve and measured using a bubble column.

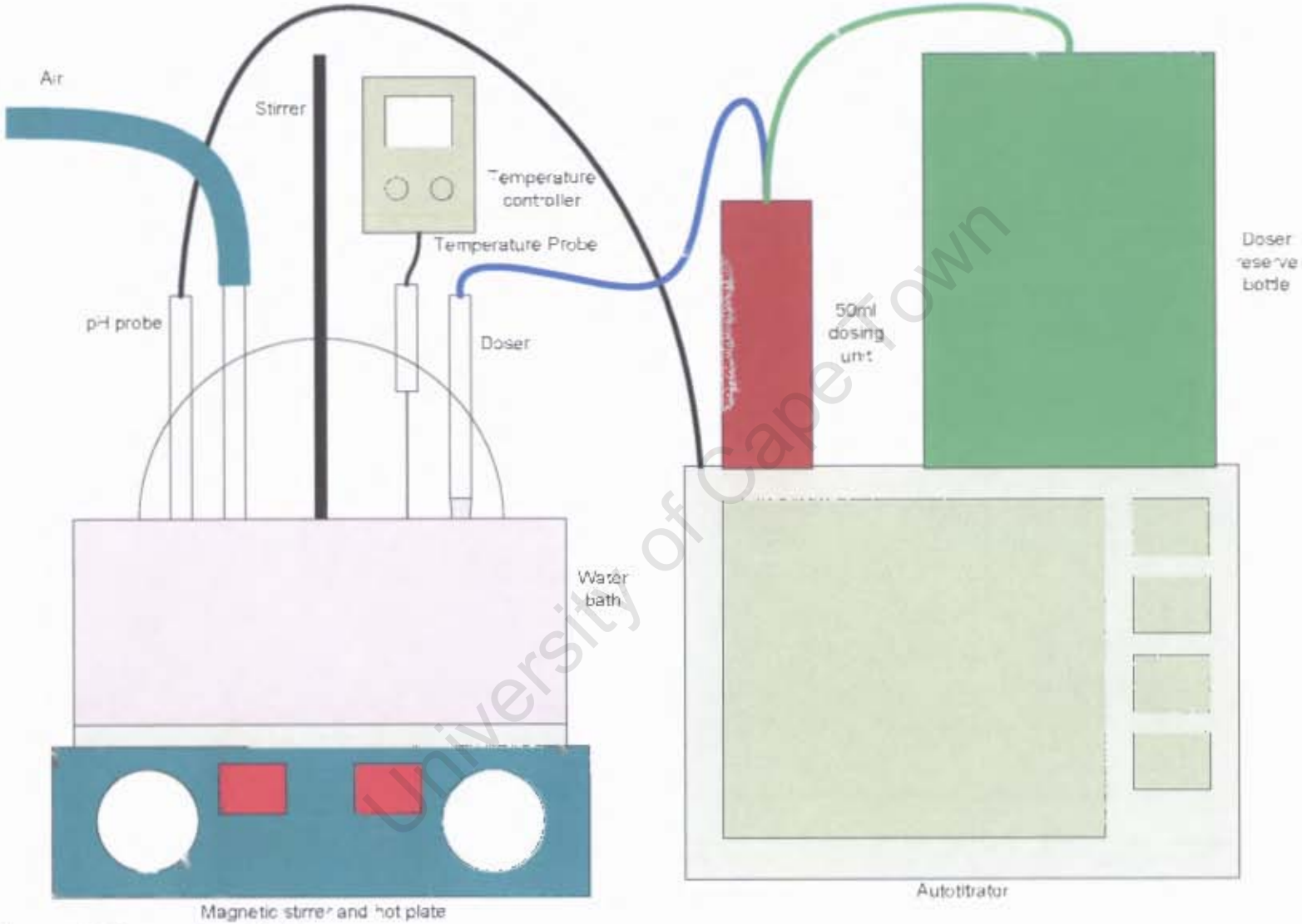

Figure 2.4: Glucose oxidation experimental setup

2.2.10 HPLC characterisation of glucose oxidation products

The reaction mixture was filtered to remove the catalyst. The filtrate was made up to 500ml in a volumetric flask and a sample taken. The samples were analysed using high performance liquid chromatography (HPLC) with a Bio-Rad Aminex® HPX-87H ion exclusion column (300mm x 7.8mm) with 9μm packing. The analysis was carried out at room temperature using a 0.01M H_2SO_4 solution as the mobile phase. Two detectors were used: ultraviolet (UV) and refractive index (RI). The UV detector is needed to detect the gluconic acid and the RI detector is required to detect all other reactants and products.

Standards of 3 known concentrations were produced. The surface areas under the peaks and retention times were evaluated and used to characterise the reaction products. Standards using the following possible reaction products were produced:

Maltose
Sorbitol
Fructose
Mannose
Sucrose
Glycoaldehyde
Oxalic Acid
Gluconic Acid
Glucose

2.3 Safety

Gold chloride, ammonia, ammonium nitrate, nitric acid, and sodium hydroxide are all used in this experiment, and all are toxic. Not much is known about tetramminegold (III) nitrate, but this was assumed to be toxic for safety reasons. Lab coat, safety glasses, and gloves must be worn when working with these materials. All experiments must take place in a fume cupboard, as the vapours of these chemicals are irritants. Skin contact with these chemicals must also be avoided.

Gold chloride is the least harmful of these materials, however caution must be taken. Gold chloride is also light sensitive, and must therefore be stored in a non-transparent container.

One of the biggest safety concerns in this experiment is the possible formation of fulminating gold. Fulminating gold is highly explosive and shock sensitive. If the pH is too high when the tetramminegold (III) nitrate is present, the fulminate will form. However, the fulminate can be dissolved just by adding an acid such as nitric acid.

The other chemicals used are mainly irritants, and their vapour must not be inhaled, and skin contact should be avoided. However, the nitric acid is a strong oxidising agent, and will burn the skin, causing 2^{nd} or 3^{rd} degree burns on short contact. In case of skin contact, one must immediately wash the affected area with water. Gloves should be worn when handling nitric acid. Ammonia is also a potentially harmful or even fatal substance. Inhalation of this gas may be fatal. It is soluble in water, and will form a corrosive solution.

3 Results

3.1 Preparation of tetramminegold (III) nitrate

Tetramminegold (III) nitrate was produced in three batches in order to prepare the catalysts (Table 3.1 and Figure 3.1). The purity achieved as measured by AAS analysis on the solid product was nearly 60% except for the third attempt where a purity of only 30% was achieved. The main impurity in the tetramminegold (III) nitrate is most likely ammonium nitrate from the preparation. The variation in purity is most likely due to the filtering stage. Ammonium nitrate is very soluble in water and has a solubility of about 190g per 100ml water at ambient conditions. During filtering, differing amounts of ammonium nitrate in the filter cake will be exposed to different amounts of water for each preparation. The tetramminegold (III) nitrate is washed with chilled ethanol in a wash bottle. Ammonium nitrate is also soluble in ethanol, but with a solubility of about 4g per 100ml ethanol. The filter cake is not washed in exactly the same way and is also used to remove precipitate from the side of the Buchner funnel therefore the amount of ethanol passing through the bulk of the filter cake may be different for the three preparations.

The gold which does not end up in the tetramminegold (III) nitrate ends up in the filtrate. This may be unreacted $HAuCl_4$ or dissolved tetramminegold (III) nitrate. The gold mass balance presented in figure 3.1 shows that not all gold could be accounted for. Some of the gold may have been lost during preparation due to spillage or to parts of the beaker wall that were not washed properly or inaccuracy in the AAS sample preparation or measurement.

Table 3.1: Tetramminegold (III) nitrate production

Preparation No.	1	2	3
Mass Au from $HAuCl_4$ (g)	0.5	0.5	0.5
Mass TAGN produced (g)	1.35	1.43	2.19
Au content of TAGN produced (%)	25.0	24.7	14.7
Au content of pure TAGN (%)	43.7	43.7	43.7
Purity of TAGN produced (%)	57.2	56.4	33.7
Au recovery from $HAuCl_4$ (%)	67.7	70.6	64.6

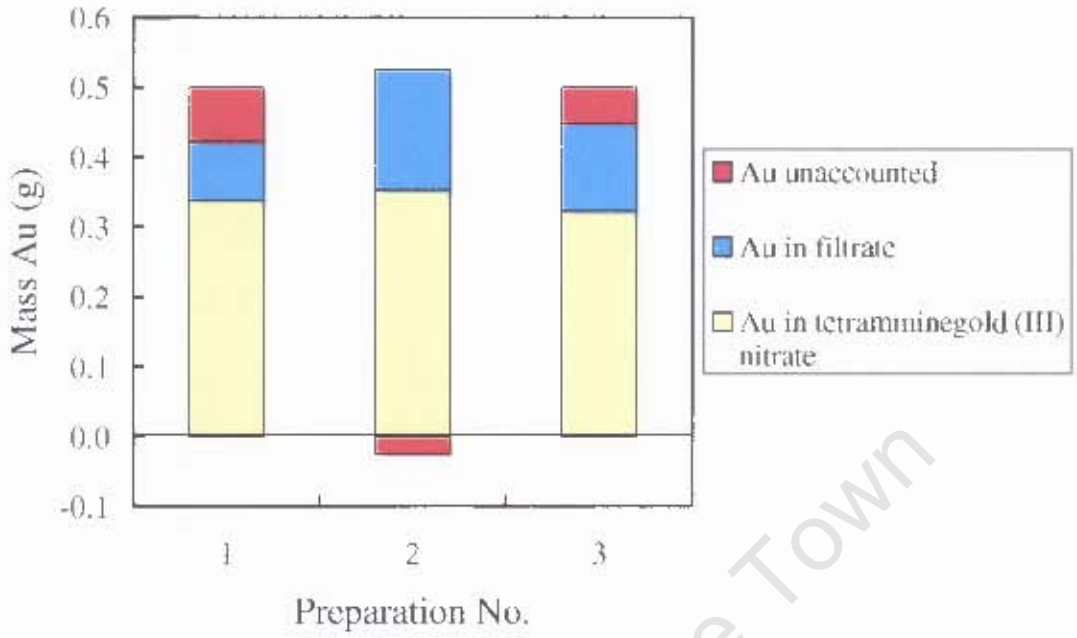

Figure 3.1: Gold mass balance for tetramminegold (III) nitrate production

3.2 Support characterisation

3.2.1 Support treatment

Carbon nanotubes are relatively inert (Rosca *et al.*, 2005). In order to activate the surface, functional groups need to be added to the surface. This can be done by treating the nanotubes in an oxidising agent. Separate batches of untreated carbon nanotubes were boiled in 55wt-% nitric acid for 6 and 48 hours. The pH of the solutions both before and after treatment was measured and was less than zero for all cases suggesting the concentration of nitric acid in the slurry remained relatively high therefore even after 48 hours the nitric acid is still oxidising the surface of the nanotubes (The pH calculated for 55wt-% nitric acid (11.7M) assuming complete dissociation is about -1).

The mass of the carbon nanotubes before and after treatment was recorded (Table 3.2). After 6 hours treatment, only a small amount of carbon was lost. After 48 hours treatment, about a quarter of the mass of carbon nanotubes was lost. The reaction of nitric acid with carbon can explain the loss of carbon as carbon dioxide which can proceed via the following 2 reactions (Parkes, 1960):

$C + 4HNO_3 \rightarrow CO_2 + 4NO_2 + 2H_2O$

$3C + 4HNO_3 \rightarrow 3CO_2 + 4NO + 2H_2O$

Table 3.2: Mass loss during treatment of carbon nanotubes in HNO_3

Sample	Initial Mass	Final Mass	Loss
	g	g	%
Blank	1.9800	1.9750	0.3
6 hours	2.5200	2.4756	1.8
48 hours	2.5177	1.9028	24

3.2.2 Transmission electron microscopy (TEM)

TEM images of the treated and untreated carbon nanotubes were obtained in order to view the physical effects of the nitric acid treatment. Untreated, 6 hour and 48 hour acid treated nanotubes, along with activated carbon were analysed.

The images clearly show the fishbone structure of the tubes for all the carbon nanotubes (Figure 3.2). Outer diameters range from 60 to 80nm. The 6 and 48 hour acid treated nanotubes appeared to have a more pronounced fishbone structure with each fishbone plate protruding out slightly more than the untreated nanotubes. There did not appear to be a significant difference in the fishbone structure of the 6 and 48 hour acid treated nanotubes.

A significant portion of the untreated nanotubes appeared to be closed (Figure 3.3). It is however unclear from the TEM images whether the nanotubes are closed on one end or both ends as the tubes are relatively long and the images show only part of a single tube in most cases. After 6 hours acid treatment a much smaller portion of the nanotubes appeared to be closed and after 48 hours acid treatment, very few nanotubes appeared to be closed. This suggests the nitric acid has removed the carbon covering the ends of the nanotubes.

A significant number of the untreated nanotubes appeared to have an outer layer of what appears to be amorphous carbon which does not form part of the structure (Figure 3.4). This extra layer is about the same thickness as the wall of the nanotubes

in the case of the untreated nanotubes. It is unclear from the images whether or not this layer covers the ends of the nanotubes. The thickness of this layer appears to be reduced with the acid treatment. After 48 hours acid treatment, this layer was not seen in the TEM images. This is most likely from the action of the nitric acid and the reaction of nitric acid with carbon removing this layer.

For a number of tubes, the diameter is not constant and many bends and deformations were seen particularly on the 48 hour acid treated nanotubes (Figure 3.5 and Figure 3.6). Figure 3.5 shows an individual fishbone plate detaching from a nanotube. A larger portion of the 48 hour acid treated nanotubes appeared to be breaking apart compared with the 6 hour acid treated nanotubes. Figure 3.6 shows an agglomeration of amorphous carbon which could be a result of the destruction of the nanotube structure from the action of the nitric acid. Agglomerations of amorphous carbon were seen in other TEM images of the 48 hour treated nanotubes. However, this was not seen in the TEM images of the 6 hour treated nanotubes. It appears that between 6 and 48 hours, the nitric acid has begun to destroy the nanotube structure.

The nanotube diameters and the wall thicknesses were measured using the TEM images. This is difficult to measure as a single nanotube is not uniform and the diameters and wall thicknesses vary across the length of the tubes. A large standard deviation is associated with the geometric mean diameters given in table 3.3. It may be difficult to draw any conclusions from this data. The treated nanotube walls were expected to be thinner however from the data this does not appear to be the case. It is possible that part of the nanotube structure is destroyed leaving only the thicker walls to be measured.

Activated carbon was also analysed (Figure 3.7). The TEM images of the activated carbon appear as a collection of sheets. This was expected as activated carbon is made up of graphene layers.

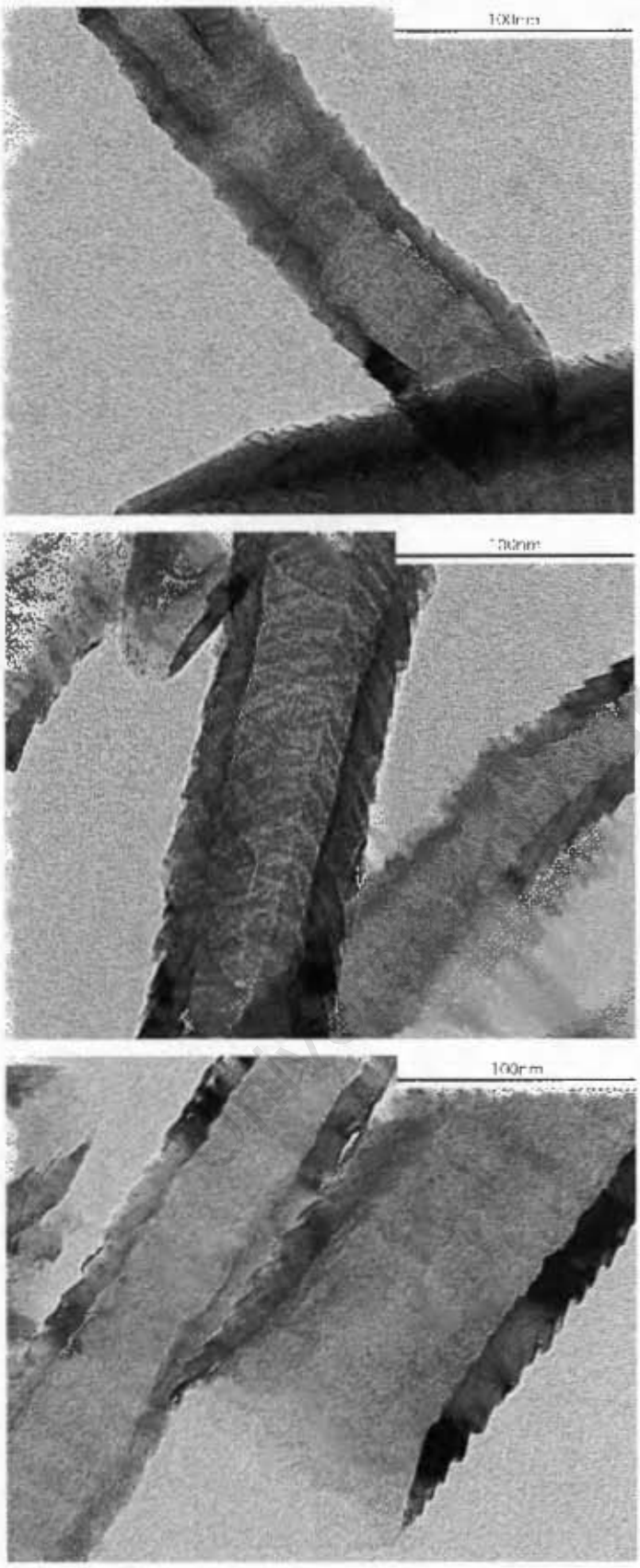

Untreated carbon nanotubes

6 hour treated carbon nanotubes

48 hour treated carbon nanotubes

Figure 3.2: TEM images of untreated and treated carbon nanotubes

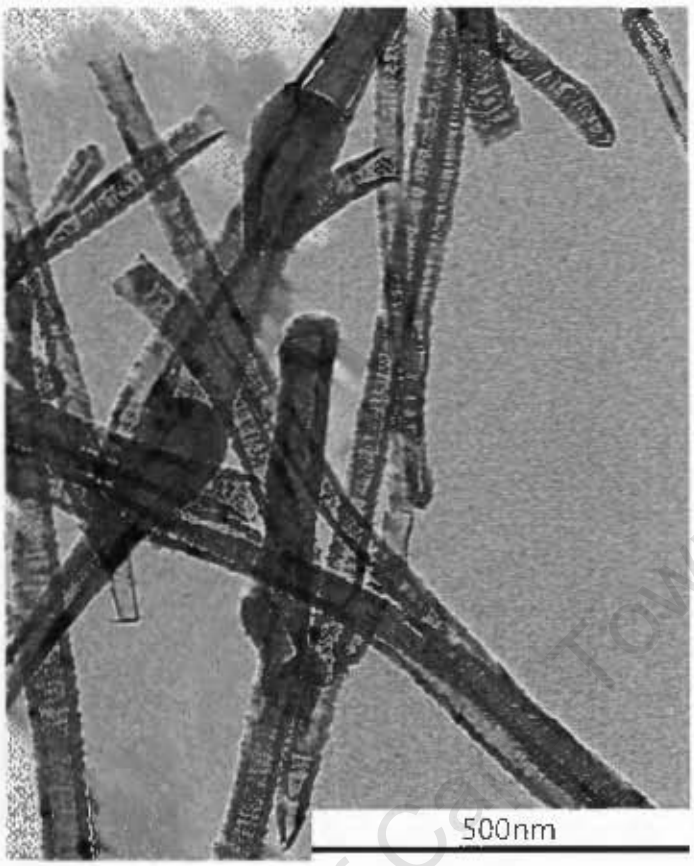

Figure 3.3: TEM image of untreated carbon nanotubes showing closed and open tubes

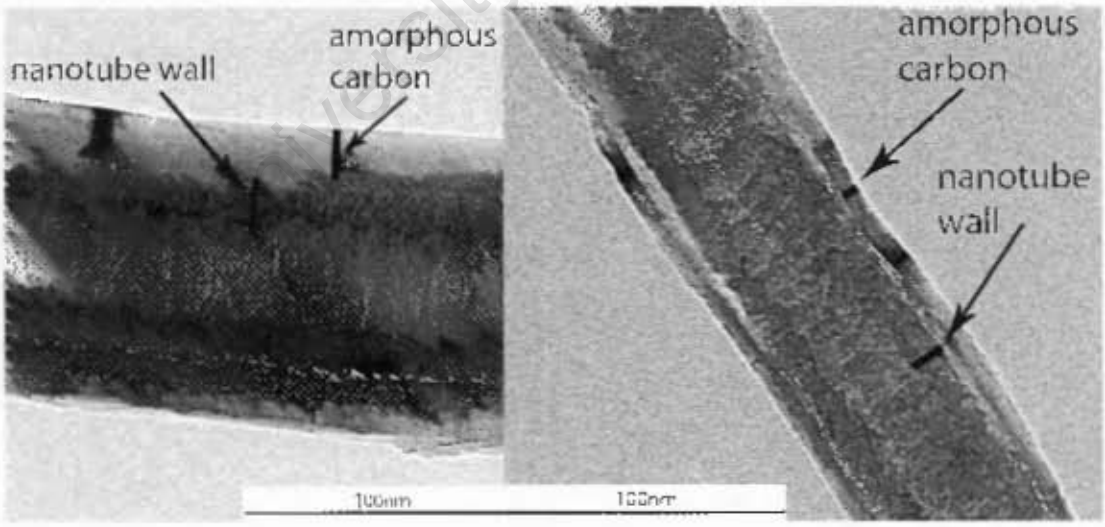

(a) **(b)**

Figure 3.4: TEM images of (a): untreated nanotubes and (b): 6 hour treated nanotubes showing an extra layer covering the surface of the nanotubes

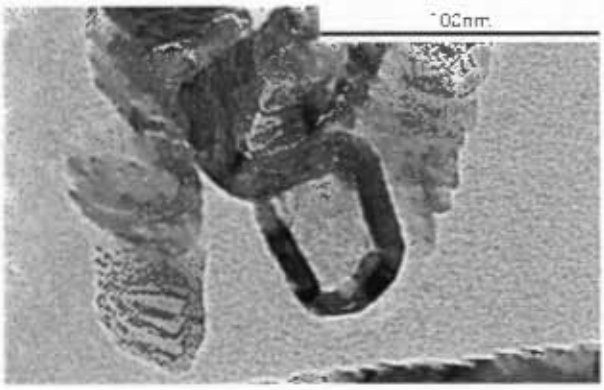

Figure 3.5: TEM image of 48 hour treated nanotubes showing the destruction of the nanotube structure

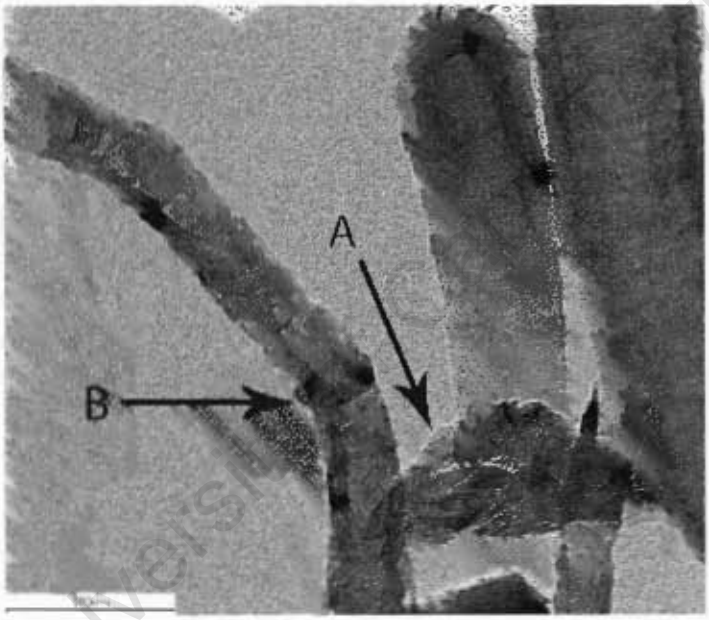

Figure 3.6: TEM image of 48 hour treated nanotubes showing the formation of amorphous carbon (A) and kinks in the nanotubes (B)

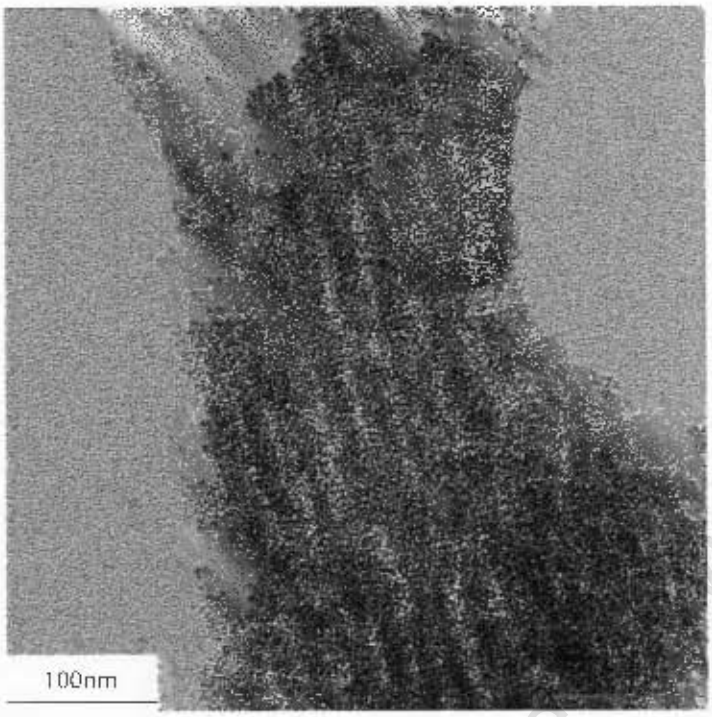

Figure 3.7: TEM image of activated carbon

Table 3.3: Carbon nanotube diameters and wall thickness

	Mean outer diameter		No of tubes measured	Mean inner diameter		No of tubes measured	Mean wall thickness	
	nm	σ nm		nm	σ nm		nm	σ nm
Untreated	58	24	34	27	15	55	32	20
6 hour acid treated	50	18	19	28	12	18	22	15
48 hour acid treated	64	22	28	33	17	31	31	19

3.2.3 Hg pycnometry

Pore diameters from 3nm to 18000nm were analysed. The untreated carbon nanotubes showed the lowest total pore area of $34m^2/g$ and the largest average pore diameter of 373nm. The 6hr treated nanotubes have a total pore area of $242m^2/g$ with an average pore diameter of 134nm, about one third of the pore diameter of the untreated nanotubes. The porosities of the nanotubes were between 70 and 80% with the 6 hour acid treated nanotubes yielding the highest porosity of 80%.

The 48 hour boiled nanotubes contained a smaller pore area of $96m^2/g$. The average pore diameter according to this analysis is smaller than the 6 hour nanotubes, but the porosity is significantly lower than the 6 hour nanotubes at 72%. The skeletal density of the 48 hour nanotubes is $1.56g/cm^3$, higher than the 6 hour nanotubes with a

skeletal density of 0.51g/cm^3. One possible reason for this increase could be a result of the destruction of the nanotube structure and the formation of amorphous carbon.

Figure 3.8 shows the pore size distribution using mercury pycnometry. The disadvantage of Hg pycnometry is the fact that very small pores in the microporous region are not characterised as very high pressure is required for the mercury to penetrate the pores. If the pores are ink bottle shaped, the mercury may not penetrate certain pores at all. With N_2 physisorption, it is possible to analyse much smaller pores. The nanotubes appear to show an increased proportion of pores between 1000nm and 3000nm. This is larger than the diameter of the nanotubes and is probably caused by the gaps between individual nanotubes.

The activated carbon has a smaller average pore diameter than the nanotubes. The porosity is much lower at 60%. The pore size distribution for activated carbon (Figure 3.9) shows a large proportion of the pores in activated carbon are in the microporous/mesoporous region. Only a small portion of the pores are bigger than 10nm. There is a sharp increase in the proportion of pores above 1000nm which is most likely due to gaps between particles of activated carbon.

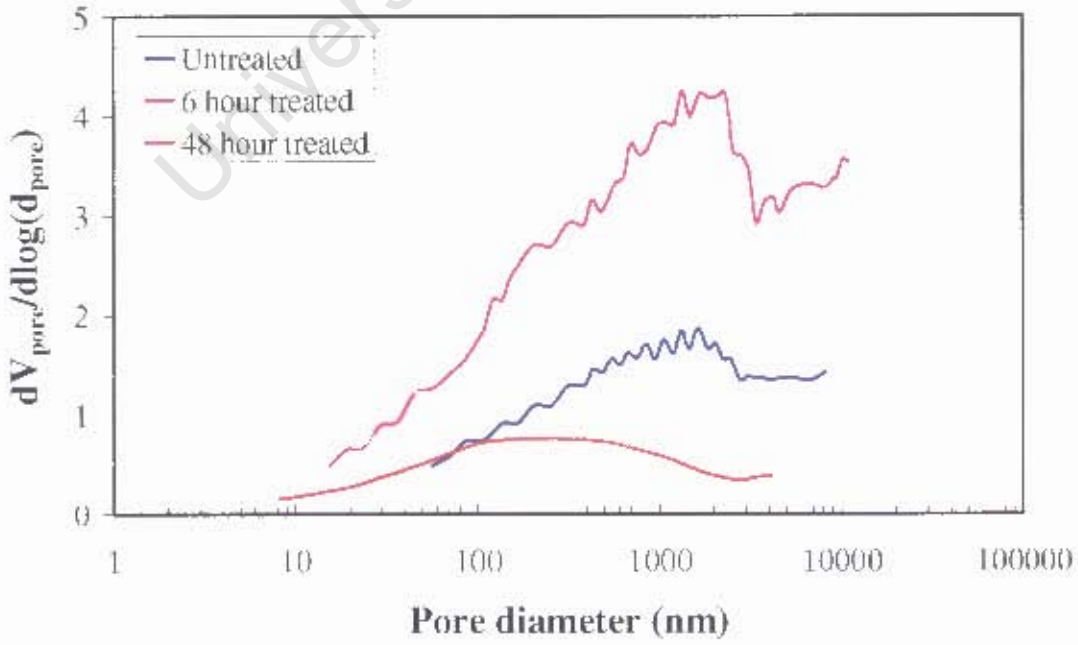

Figure 3.8: Mercury pycnometry pore size distribution for carbon nanotubes

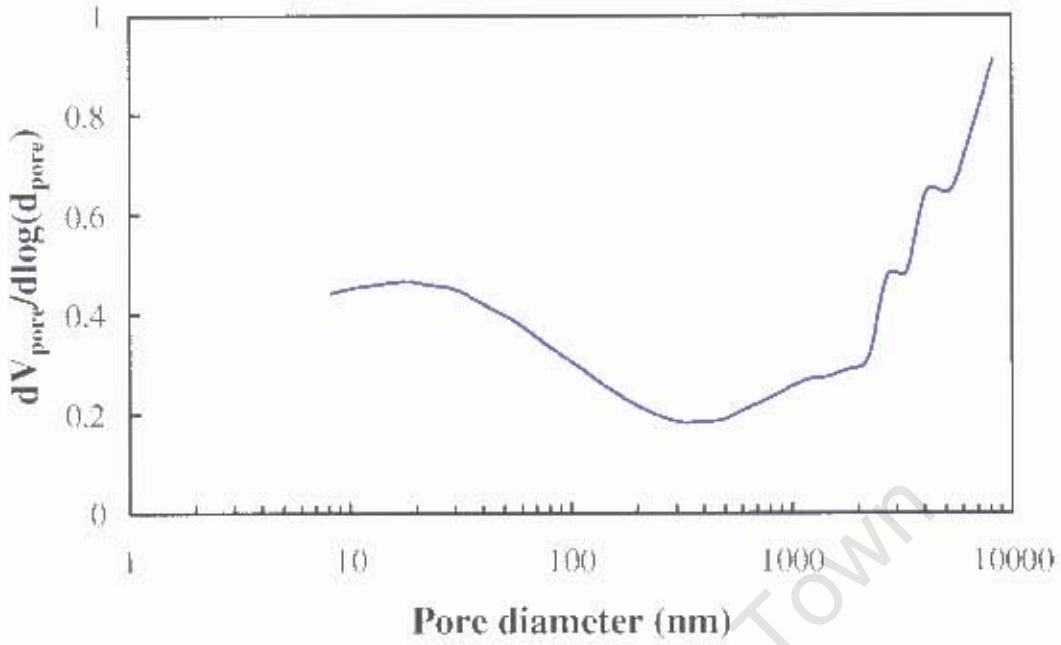

Figure 3.9: Mercury pycnometry pore size distribution for activated carbon

Table 3.4: Mercury Pycnometry Data

	Total Pore Area m^2/g	Total Intrusion Volume ml/g	Average Pore Diameter µm	Bulk Density g/cm^3	Skeletal Density g/cm^3	Porosity %
Untreated CNT	34	3.2	0.37	0.25	1.08	77
6hr boiled CNT	242	8.1	0.13	0.10	0.51	80
48hr boiled CNT	96	1.7	0.07	0.43	1.56	72
Activated Carbon	233	1.6	0.03	0.38	0.95	60

3.2.4 N_2 physisorption

The BET analysis was carried out at 77K using N_2. Untreated, 6 hour and 48 hour acid treated nanotubes were analysed along with activated carbon.

The BET surface area for the untreated carbon nanotubes was $46m^2/g$ (Table 3.5). After boiling the nanotubes in nitric acid, the BET surface area almost doubles to $80m^2/g$ for both the 6 and 48 hour acid treated nanotubes. The doubling of the BET surface area could be a result of the opening of the nanotubes with treatment in nitric acid. A possible reason for the acid treated nanotubes having the same BET surface area could be the fact that a large majority of the nanotubes are in fact open after 6 hours.

The BET surface area for the activated carbon is much higher than the carbon nanotubes (1230m^2/g). This was expected as activated carbon is well known for its microporous structure (Rodríguez-Reinoso, 1998).

Figure 3.10 and figure 3.11 show the BJH pore size distribution for the carbon nanotubes and activated carbon respectively. This shows that the activated carbon has a larger portion of pores between 1 and 10nm compared to the carbon nanotubes. The distributions for the nanotubes are similar. The nanotubes have a higher proportion of pores between 10 and 40nm as the tube diameters are in this range.

The average pore diameter for the untreated nanotubes is 27nm (Table 3.5). This almost doubles to 44nm and 41nm for the 6 and 48 hour acid treated nanotubes. A possible reason for this is the fact that the nanotubes are opened with treatment allowing adsorption on the inside of the tube. As the tubes have a relatively large diameter, this would result in an increase in the average pore diameter. This is further illustrated by the pore volume obtained which triples with treatment. The activated carbon yielded an average pore diameter of 6nm, much smaller than the pore diameters for carbon nanotubes as expected.

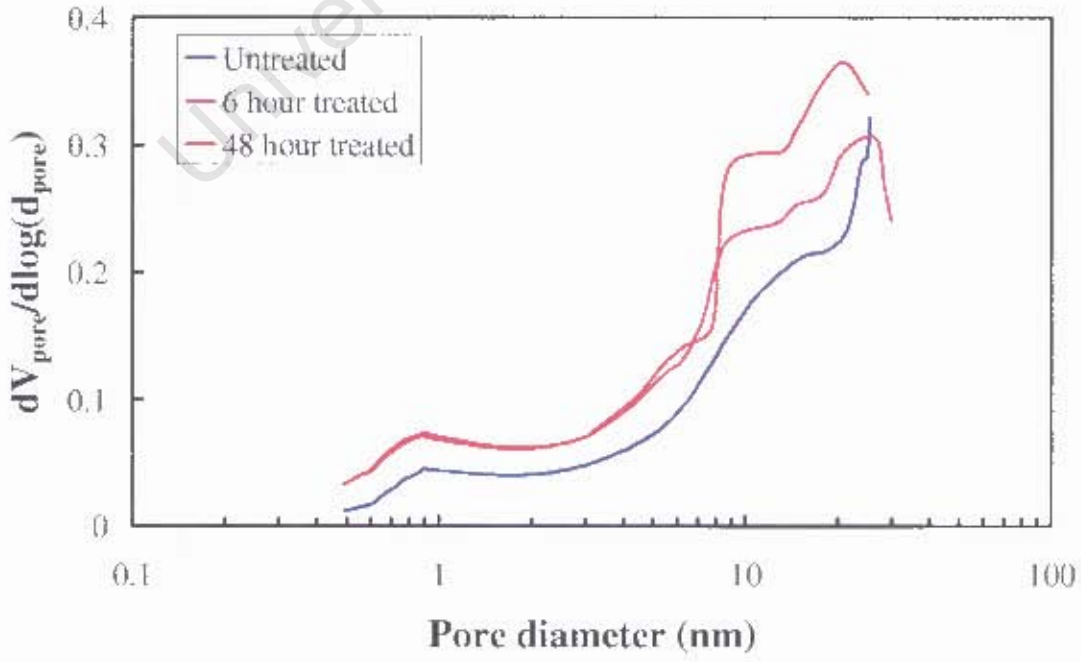

Figure 3.10: The BJH pore size distribution for untreated, 6 hour and 48 hour boiled carbon nanotubes

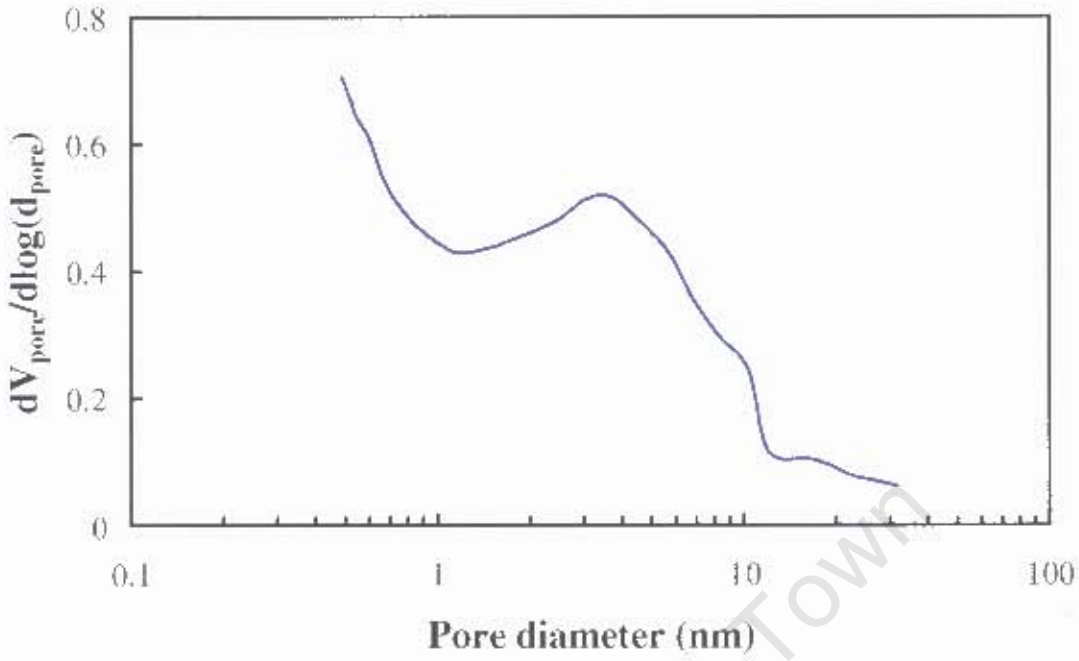

Figure 3.11: The BJH pore size distribution for activated carbon

Table 3.5: BET surface area for the carbon nanotubes

	BET Surface Area m^2/g	Pore Volume cm^3/g	Average Pore Diameter nm
Untreated carbon nanotubes	45	0.3	27
6 hour treated carbon nanotubes	80	1.1	44
48 hour treated carbon nanotubes	80	1.0	41
Activated carbon	1230	0.8	6

3.2.5 Raman spectroscopy

The Raman spectra of the carbon nanotubes (Figure 3.12) show three characteristic peaks at 2570cm^{-1}, 1600cm^{-1} and 1290cm^{-1}. The 48 hour boiled nanotubes also revealed a peak at 170cm^{-1} (Figure 3.13). A peak at about 3400cm^{-1} was seen and was caused by the heating of the carbon nanotube KBr tablet by the laser. The full Raman spectrum of the carbon nanotubes is presented in the appendix (Figure 6.7).

The peaks around 1600cm^{-1} correspond to the G-band of the nanotubes. This refers to the displacement of atoms tangent to the tube. This is one of the characteristic peaks

of carbon nanotubes (Jorio *et al.*, 2003; Rosca *et al.*, 2005; Titus *et al.*, 2007). This G-band (or tangential mode) is observed for graphite at about the same wavelength (Jorio *et al.*, 2003). However, unlike graphite, the peak for carbon nanotubes is actually made up of 6 peaks (Jorio *et al.*, 2003). These 6 peaks are not all visible in Figure 3.12. There are two intense peaks which give the observed signal (Jorio *et al.*, 2003). One of the peaks is caused by atomic displacements along the tube's axis. The other peak which occurs at slightly lower frequencies is caused by atomic displacement in the circumferential direction (Jorio *et al.*, 2003).

The peak at 1300cm^{-1} represents the D-band of the carbon nanotubes. This refers to the disorder induced mode of carbon nanotubes (Jorio *et al.*, 2003; Maultzsch *et al.*, 2001). For most single-walled nanotubes, the D-band signal is much smaller than the G-band signal (Titus *et al.*, 2007; Jorio *et al.*, 2003; Brown *et al.*, 2000). However, large D-band peaks compared with G-band peaks could indicate the presence of amorphous carbon (Ferrari and Robertson, 2000). The peak at 2570cm^{-1} represents a 2nd order D-band (Brown *et al.*, 2000).

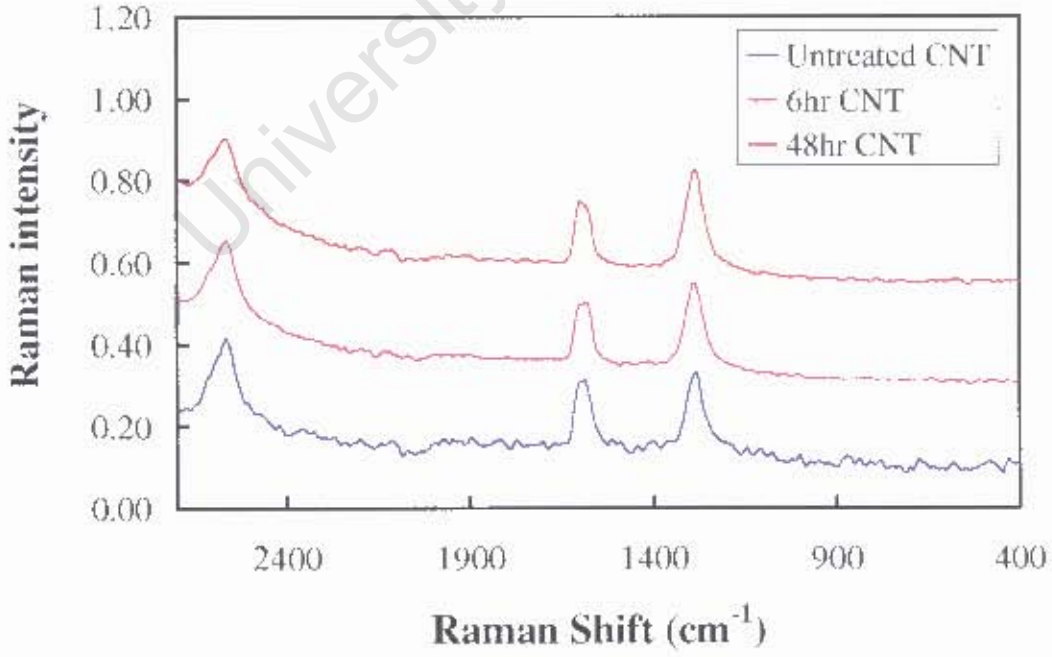

Figure 3.12: Raman spectra for untreated and acid treated carbon nanotubes between 2700cm^{-1} and 400cm^{-1}

The small peak at 170cm^{-1} for the 48 hour acid treated nanotubes in figure 3.13 represents the so-called radial breathing mode in carbon nanotubes. This refers to the atomic vibration of carbon atoms in the radial direction (Jorio *et al.*, 2003).

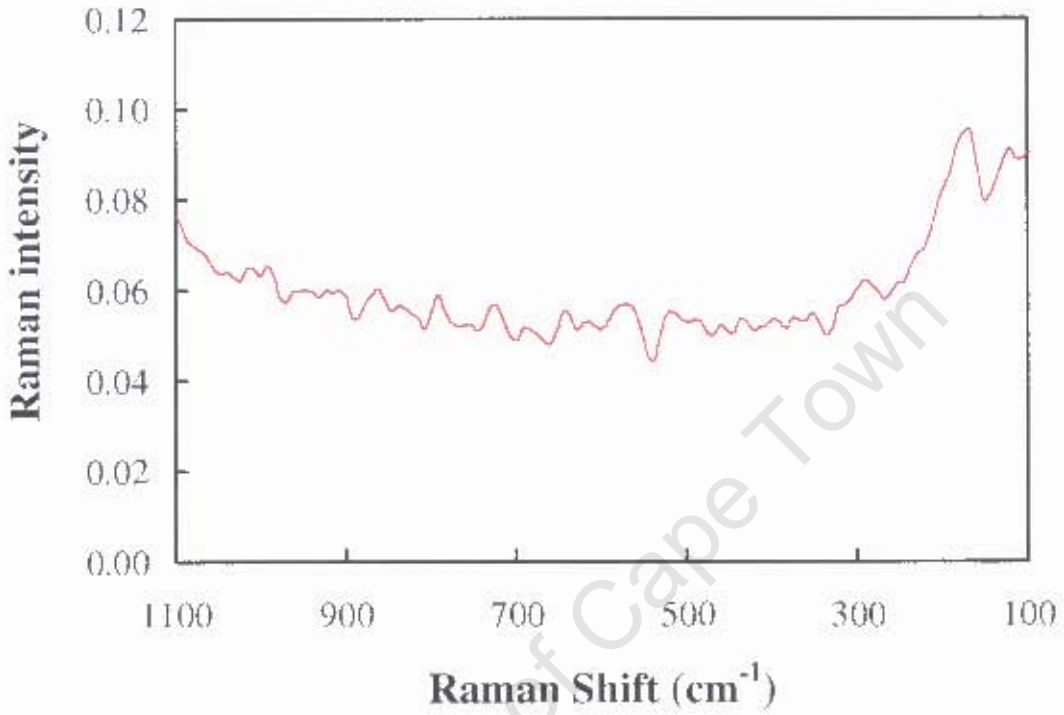

Figure 3.13: Raman spectrum of 48 hour acid treated carbon nanotubes between Raman shifts of 1100 cm^{-1} and 100 cm^{-1}.

Table 3.6 shows the D- and G-band frequencies and the relative intensities of the D-band to the G-band. For most single-walled nanotubes, the intensity of the D-band signal is much smaller than the G-band signal (Titus *et al.*, 2007; Jorio *et al.*, 2003; Brown *et al.*, 2000). Large D-band peaks compared with G-band peaks could indicate the presence of amorphous carbon or sp^3 hybridisation on the surface due to the presence of functional groups (Ferrari and Robertson, 2000). The large D-band peak for the untreated nanotubes indicates the presence of amorphous carbon.

From figure 3.12, the D-band peaks for all the nanotubes are larger than their respective G-band peaks. With increased boiling time, the relative intensities of these peaks (D-band to G-band) increases (Table 3.6). This may indicate the continuous formation of amorphous carbon or the formation of functional groups.

The increased D- to G- band intensity ratio for the 6 and 48 hour treated nanotubes compared to the untreated nanotubes might also be explained by the increased presence of sp^3 hybridisation on the surface due to the presence of functional groups.

Table 3.6: Table of D- and G-band frequencies and relative intensities of carbon nanotubes

	D-band	G-band	Relative Intensities
	cm^{-1}	cm^{-1}	I_D/I_G
Untreated nanotubes	1287	1591	1.06
6hr boiled nanotubes	1290	1586	1.18
48hr boiled nanotubes	1288	1600	1.31

3.2.6 Infrared spectroscopy

The infrared spectra of the activated carbon, untreated, 6 hour and 48 hour nanotubes were collected on a Nicolet 5700 FT-IR with the Smart-OMNI Transmission accessory.

The infrared spectra for the untreated and treated carbon nanotubes showed peaks at $1600cm^{-1}$. This is assigned to the stretching mode of carboxyl groups on the surface. After 48 hours treatment, the concentration of these groups increased. This was expected as untreated carbon nanotubes are relatively inert and were treated in boiling nitric to introduce functional groups onto the surface.

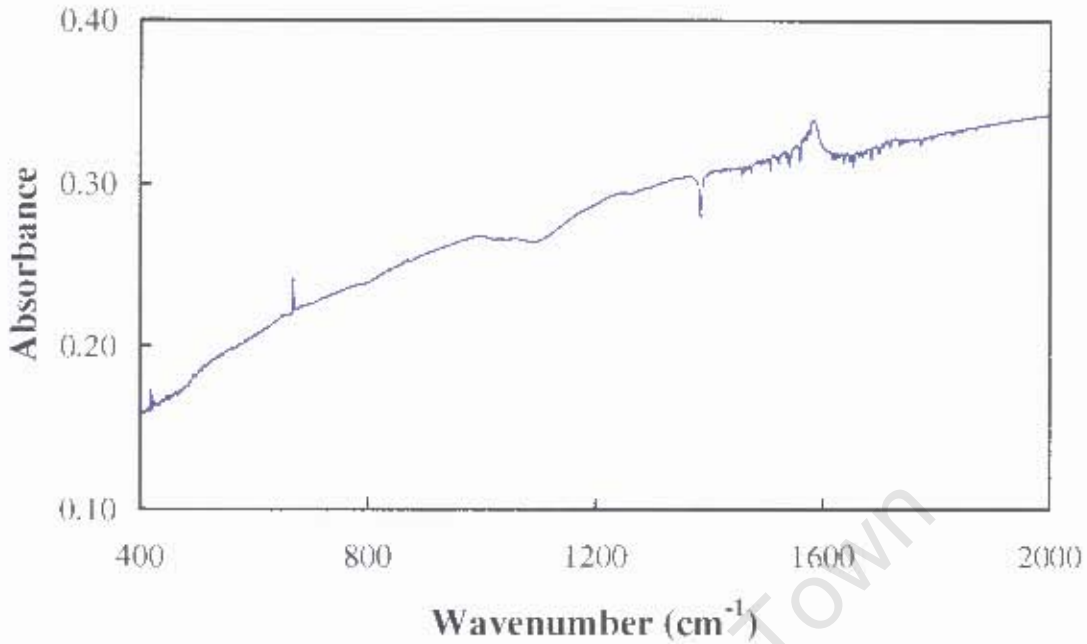

Figure 3.14: Infrared spectrum of 48 hour acid treated carbon nanotubes

3.2.7 Zeta potential

The zeta potential of the 10wt-% suspensions in a 0.1M KCl aqueous solution were measured in a Malvern Zetasizer Nano ZS at 25°C. Dilute solutions of HCl and KOH were used for pH adjustment.

The iso-electric point of the untreated fishbone nanotubes is at pH 2 (Figure 3.15). After treatment by boiling in nitric acid for 6 hours and 48 hours, the iso-electric point shifts to a pH of 1. There does not appear to be a difference in the iso-electric point for the 6 and 48 hour acid treated nanotubes. At pH values above 3, the zeta potential of the 48 hour acid treated nanotubes shows a marked step-wise decrease suggesting the increased concentration of a particular functional group on the surface. The untreated and 6 hour acid treated nanotubes do not appear to show this behaviour possibly suggesting a lower concentration of this functional group.

The iso-electric of activated carbon is at a pH of about 2, the same as the untreated nanotubes. The zeta potential of activated carbon shows different behaviour to that of the carbon nanotubes. Comparing the carbon nanotubes to the activated carbon, only the 48 hour acid treated nanotubes showed a more negative surface charge at pH values above the iso-electric (Figure 3.15 and Figure 3.16).

One of the most distinctive features of the zeta potential of activated carbon (Figure 3.16) is the sharp increase in the zeta potential around the iso-electric. Below the iso-electric the zeta potential is higher than the carbon nanotubes at the equivalent pH. This may suggest an increased concentration of one functional group on the surface of activated carbon. With increasing pH, the zeta of activated carbon does not appear to proceed stepwise.

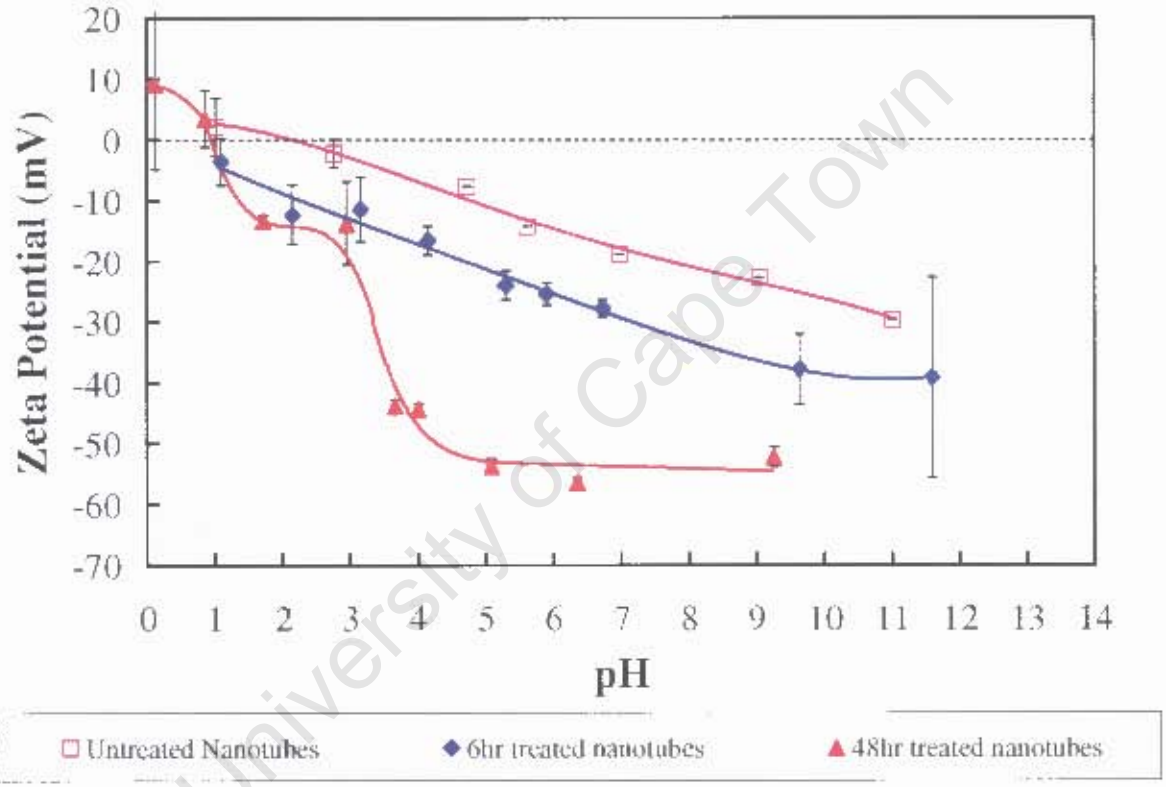

Figure 3.15: Zeta potential of untreated and treated carbon nanotubes

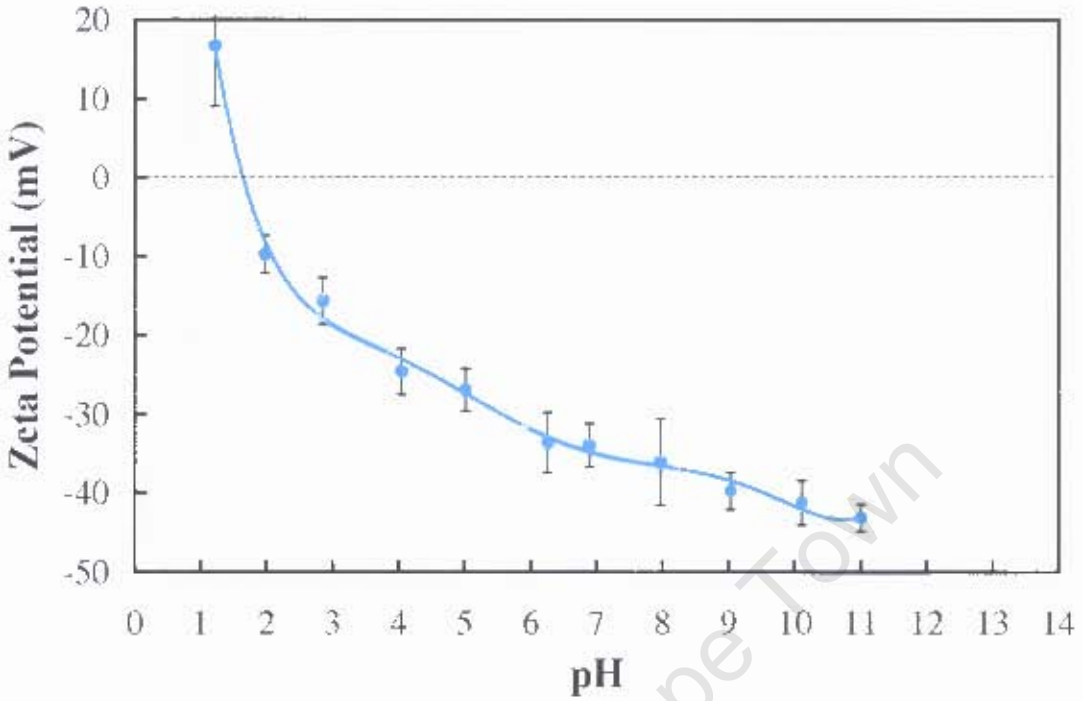

Figure 3.16: Zeta potential of activated carbon

3.3 Catalyst characterisation

3.3.1 Gold loadings

The gold loadings were obtained by dissolving the gold off the surface of the carbon using aqua regia and the resulting filtrate was analysed using AAS.

The catalysts prepared on activated carbon yielded higher loadings than the carbon nanotubes. The catalysts prepared using the tetramminegold (III) nitrate precursor yielded higher loadings when prepared at pH 4 than at pH 2. The 6 hour acid treated nanotubes were the exception, where the loadings were more or less the same probably as a result of the surface charge of the nanotubes being relatively similar at pH 2 (-10mV) and pH 4 (-16mV) for the 6 hour acid treated nanotubes whereas the 48 hour acid treated nanotubes and the activated carbon surface charges change significantly between pH 2 and pH 4 (Figure 3.15). The highest loadings were achieved with the $HAuCl_4$ precursor on all the supports, particularly the 48 hour acid treated carbon nanotubes and the activated carbon.

Table 3.7: Gold loadings

Catalyst	Support	Precursor	Preparation pH	Loading %
1	6hr CNT	$Au(NH_3)_4(NO_3)_3$	4	0.66
2	6hr CNT	$Au(NH_3)_4(NO_3)_3$	2	0.70
3	6hr CNT	$HAuCl_4$	0.8	1.25
4	48hr CNT	$Au(NH_3)_4(NO_3)_3$	4	0.69
5	48hr CNT	$Au(NH_3)_4(NO_3)_3$	2	0.58
6	48hr CNT	$HAuCl_4$	0.8	2.39
7	Activated C	$Au(NH_3)_4(NO_3)_3$	4	2.19
8	Activated C	$Au(NH_3)_4(NO_3)_3$	2	1.71
9	Activated C	$HAuCl_4$	0.8	2.61

3.3.2 TEM

3.3.2.1 Fresh catalyst

The TEM images of the prepared catalysts were analysed using ImageJ©. The gold crystallites were measured along their longest axis. For some of the catalysts analysed, very few crystallites were found. A sample TEM image is shown in figure 3.18.

The catalyst prepared on 6 hour treated nanotubes at pH 4 using tetramminegold (III) nitrate yielded smaller crystallites compared to the catalyst prepared at pH 2 using the same precursor and support. Similar results were obtained on the 48 hour acid treated nanotubes. From figure 3.17, it appears that the catalyst prepared at pH 2 might actually have smaller crystallites. However, the catalyst prepared at pH 2 does contain a number of crystallites above 30nm in size unlike the catalyst prepared at pH 4. The catalysts prepared at pH 2 on both the 6 and 48 hour treated nanotubes gave larger mean crystallite sizes. For the 6 hour treated nanotubes the crystallite size increased from 4.6nm to 9.8nm and for the 48 hour treated nanotubes the crystallite size increased from 8.5nm to 10.3nm.

The catalysts prepared on activated carbon showed very large crystallites with mean crystallite sizes of over 150nm. The catalyst prepared at pH 2 using tetramminegold (III) nitrate showed the largest crystallites with a mean crystallite size of 302nm. Some of the crystallites were as large as 450nm. The catalyst prepared at pH 4 showed much smaller crystallites with a mean crystallite size of 157nm. There is a large error associated with the crystallite sizes measured on the activated carbon (Table 3.8). This may not be an accurate reflection of the size of the crystallites present. Only crystallites that can be seen on the TEM photographs are measured. For the activated carbon, very few crystallites were found. For the catalyst prepared using $HAuCl_4$ as the precursor, only 2 crystallites were found, one of which was over 1000nm in size.

The catalysts prepared using $HAuCl_4$ as the precursor showed much wider crystallite size distributions (Figure 3.17 and Table 3.8). There is no crystallite size distribution for the catalyst prepared using $HAuCl_4$ on activated carbon as only two crystallites were found using TEM. Other crystallites may have been present but were not seen. These catalysts were prepared at pH 0.8 on all the supports. The catalyst prepared on the 48 hour treated nanotubes showed a larger mean crystallite size of 14.4nm compared with 8.1 for the 6 hour acid treated nanotubes, the same trend as observed on the catalysts prepared with tetramminegold (III) nitrate.

The reason for the wide distribution could be explained by the presence of chlorine (Oh *et al.*, 2002; Bollinger and Vannice, 1996). All of the catalysts were first calcined in air for 2 hours. They were subsequently reduced in hydrogen for 6 hours. Normally catalysts prepared using $HAuCl_4$ are calcined and reduced in hydrogen to remove the chlorine as HCl to yield smaller crystallites (Zanella and Louis, 2005). During the 2 hour calcination, it is possible that the chlorine promoted the sintering of the gold. Another possible reason for the wide distribution might lie in the fact that pH 0.8 is very close to the iso-electric point of the carbon nanotubes. This will result in fewer anchoring points available for the anionic gold ($AuCl_4^-$) to attach to compared to if the pH was lower and further away from the iso-electric point. This will result in the same effect as observed with the catalysts prepared with tetramminegold (III) nitrate.

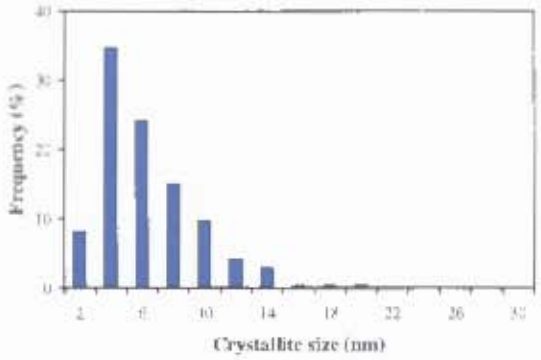

Catalyst No.	1
Support	6hr CNT
Precursor	$Au(NH_3)_4(NO_3)_3$
Preparation pH	4

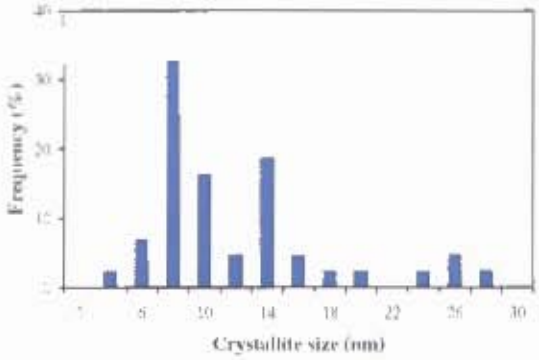

Catalyst No.	2
Support	6hr CNT
Precursor	$Au(NH_3)_4(NO_3)_3$
Preparation pH	2

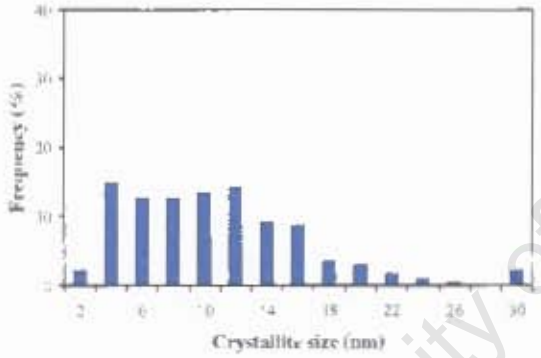

Catalyst No.	3
Support	6hr CNT
Precursor	$HAuCl_4$
Preparation pH	0.8

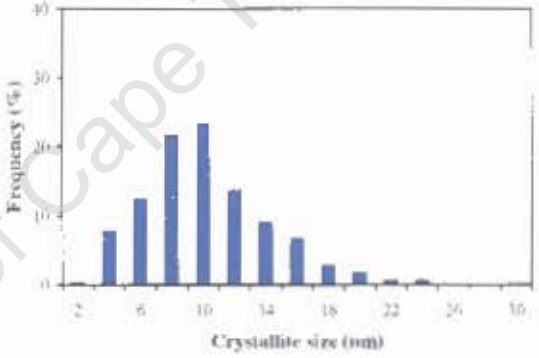

Catalyst No.	4
Support	48hr CNT
Precursor	$Au(NH_3)_4(NO_3)_3$
Preparation pH	4

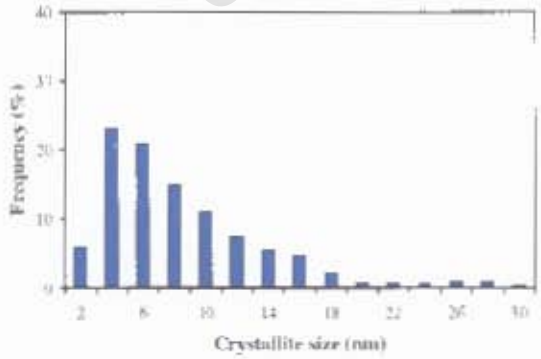

Catalyst No.	5
Support	48hr CNT
Precursor	$Au(NH_3)_4(NO_3)_3$
Preparation pH	2

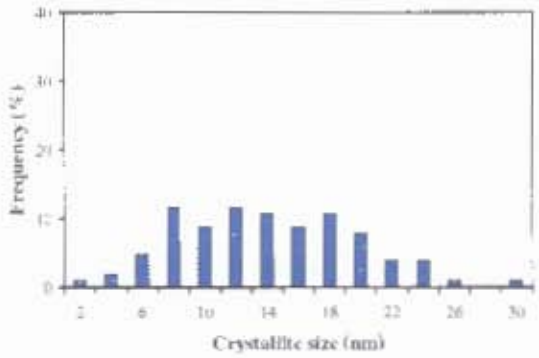

Catalyst No.	6
Support	48hr CNT
Precursor	$HAuCl_4$
Preparation pH	0.8

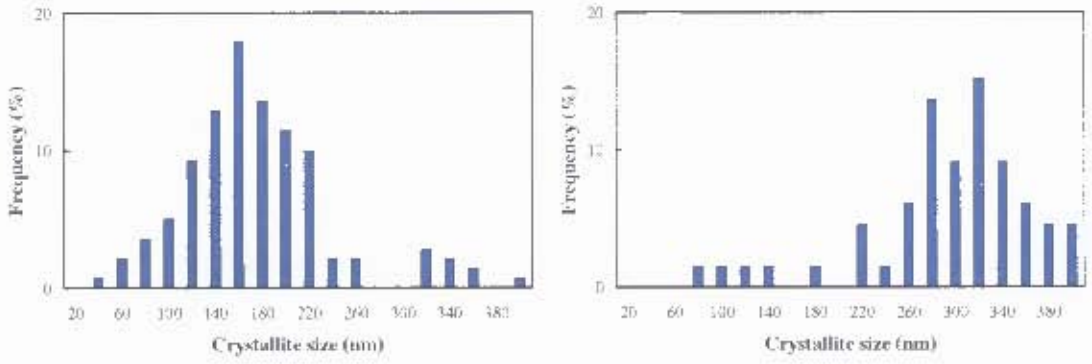

Catalyst No.	7	Catalyst No.	8
Support	Activated C	Support	Activated C
Precursor	$Au(NH_3)_4(NO_3)_3$	Precursor	$Au(NH_3)_4(NO_3)_3$
Preparation pH	4	Preparation pH	2

Figure 3.17: Crystallite size distributions of produced catalysts

Table 3.8: Mean gold crystallite sizes obtained from TEM

Catalyst	Support	Precursor	Preparation pH	Mean Crystallite Size nm	σ	No of crystallites measured
1	6h CNT	$Au(NH_3)_4(NO_3)_3$	4	4.6	3.1	245
2	6h CNT	$Au(NH_3)_4(NO_3)_3$	2	9.8	5.6	43
3	6h CNT	$HAuCl_4$	0.8	8.1	6.0	230
4	48h CNT	$Au(NH_3)_4(NO_3)_3$	4	8.5	3.9	301
5	48h CNT	$Au(NH_3)_4(NO_3)_3$	2	10.3	5.6	725
6	48h CNT	$HAuCl_4$	0.8	14.4	22.9	103
7	Activated C	$Au(NH_3)_4(NO_3)_3$	4	157	82	140
8	Activated C	$Au(NH_3)_4(NO_3)_3$	2	302	107	66
9	Activated C	$HAuCl_4$	0.8	1313 / 42		2

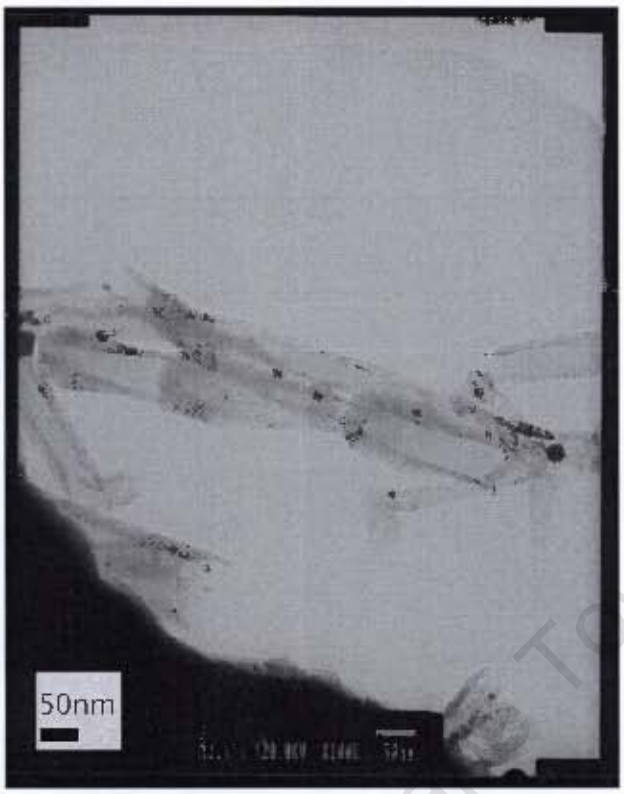

Figure 3.18: TEM image of a gold on carbon nanotube catalyst (Catalyst 2)

3.3.2.2 Catalyst after glucose oxidation

The crystallite sizes were characterised after glucose oxidation using TEM. Significant crystallite growth was observed for the catalysts produced on the 6 hour treated nanotubes (Table 3.9). This growth could have been caused by gluconic acid. Gluconic acid is a chelating agent in alkaline conditions (Ramachandran *et al.*, 2006). Its effect on gold is unclear. It is possible that some of the very small gold crystallites may have been dissolved and redeposited on larger crystallites.

The gold may have been present in the form of the precursor tetramminegold (III) nitrate. This is soluble and may have dissolved and redeposited on larger crystallites. The catalysts were reduced in hydrogen for 6 hours at 200°C and tetramminegold (III) nitrate may slowly start decomposing at temperatures as low as 120°C (Beeming and Bialek, 2006). Therefore the presence of tetramminegold (III) nitrate on the catalysts is unlikely given its unstable nature.

Prado-Burguete *et al.* (1989) investigated the effects of functional groups sintering and agglomeration and found that C−O groups seemed to act as anchors for their

platinum crystallites and carboxylic groups (-COOH) seemed to promote sintering and agglomeration. On the 6 hour treated nanotubes, the concentration of functional groups such as C=O on the surface is most likely lower than on the 48 hour treated nanotubes. The crystallites could therefore be more mobile during the reaction and could agglomerate. The catalysts on the 6 hour treated nanotube support showed significant crystallite growth whereas the catalysts produced on the 48 hour treated carbon nanotube support did not show significant crystallite growth suggesting the gold crystallites on the 48 hour treated nanotubes were more anchored. However, this may be due to the fact that larger crystallites were present on the 48 hour acid treated nanotubes initially.

No crystallites were found on the used activated carbon catalysts using TEM. It is possible that the crystallites were removed from the surface of the support during the reaction leaving colloidal gold as the active species.

Table 3.9: Mean crystallite sizes for fresh catalyst and used catalyst after glucose oxidation

Catalyst	Support	Precursor	Preparation pH	Mean Crystallite Size (fresh) nm	σ	Mean Crystallite Size (used) nm	σ
1	6h CNT	$Au(NH_3)_4(NO_3)_3$	4	4.6	3.1	8.9	6.2
2	6h CNT	$Au(NH_3)_4(NO_3)_3$	2	9.8	5.6	15.6	10.0
3	6h CNT	$HAuCl_4$	0.8	8.1	6.0	9.4	10.2
4	48h CNT	$Au(NH_3)_4(NO_3)_3$	4	8.5	3.9	10.8	4.8
5	48h CNT	$Au(NH_3)_4(NO_3)_3$	2	10.3	5.6	8.9	4.9
6	48h CNT	$HAuCl_4$	0.8	14.4	22.9	12.2	17.7
7	Activated C	$Au(NH_3)_4(NO_3)_3$	4	157	82	*	*
8	Activated C	$Au(NH_3)_4(NO_3)_3$	2	302	107	*	*
9	Activated C	$HAuCl_4$	0.8	1313 / 42		*	*

* no crystallites found using TEM

3.3.3 Oxygen chemisorption

In order to verify the TEM results, oxygen chemisorption was performed on the catalysts at 200°C. O_2 chemisorption was suggested as a means of characterising the gold crystallite size and dispersion on a catalyst by Berndt *et al.* (2003). Negative volumes adsorbed were recorded for some of the catalysts and some of the catalysts

had a very low oxygen uptake and only the catalysts with small crystallites (<8nm) showed good oxygen uptake. Only the carbon nanotube catalysts showed this behaviour. This may be partly down to the fact that the density of the nanotubes is low and only a small mass could be placed in the apparatus (0.07g in some cases). It could also be explained by the fact that larger gold crystallites will begin to behave like bulk gold which does not chemisorb oxygen.

A dual Langmuir isotherm was fitted to the gold on carbon nanotube chemisorption data. The carbon nanotube catalysts and the activated carbon appeared to follow two different adsorption processes (Figure 3.19). The gold on carbon nanotube catalysts appear to show an almost constant amount of adsorbed oxygen at low pressure. This indicates the quick saturation of strongly adsorbed oxygen. Weakly adsorbing oxygen only becomes noticeable at high pressures. For the activated carbon, there is a rapid increase in oxygen at low pressure followed by slower increase at higher pressures.

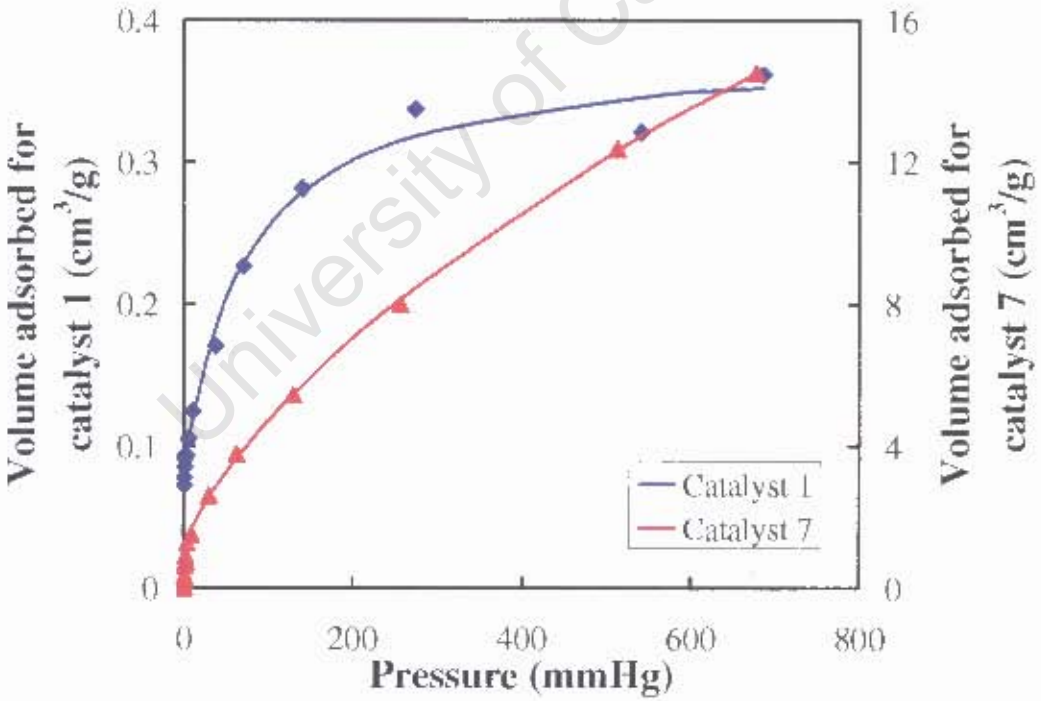

Figure 3.19: Oxygen chemisorption isotherms for a gold on carbon nanotube catalyst (Catalyst 1) and a gold on activated carbon catalyst (Catalyst 7)

Since the strong adsorption of oxygen at low pressure means the adsorption strength cannot be determined accurately, the following isotherm was used:

$$V_{O_2} = V_{m,1} + V_{m,2} \cdot \frac{K_2 . p_{O_2}^m}{1 + K_2 . p_{O_2}^m} \qquad (1)$$

where V_1 and V_2 are the volumes of the monolayers on the gold crystallites and the support surface respectively, K_2 is the adsorption constant for the support, p_{O2} is the oxygen pressure and m is the order of adsorption for the support. A dual isotherm was fitted to the activated carbon data:

$$V_{O_2} = V_{m,1} \cdot \frac{K_1 . p_{O_2}^n}{1 + K_1 . p_{O_2}^n} + V_{m,2} \cdot \frac{K_2 . p_{O_2}^m}{1 + K_2 . p_{O_2}^m} \qquad (2)$$

where K_1 is the adsorption constant for the gold and n is the order of adsorption on the gold.

The parameters were calculated and the results are presented in table 3.10. For the gold on carbon nanotube catalysts, n was more or less equal to one and was set to one. From the volume of the monolayer on the gold crystallites ($V_{m,1}$), a crystallite size and dispersion were calculated based on the calculated parameters (Table 3.11). The gold on carbon nanotube catalyst crystallite size and dispersion were calculated based on a Au:O ratio of 1:1. Based on the statistical analysis of the parameters (95% confidence interval), only the monolayers for catalysts 1 and 4 have a relatively small confidence interval. All the other catalysts have large confidence intervals particularly the gold on activated carbon catalysts. For the gold on activated carbon catalysts the uncertainty is a result of adsorption of oxygen onto the activated carbon (Dastgheib and Karanfil, 2004). The rapid increase in oxygen adsorbed at low pressure for the gold on activated carbon catalysts could be a result of oxygen adsorption on the activated carbon.

The gold on activated carbon catalysts yielded the highest dispersions and smallest crystallites compared to the gold on carbon nanotubes based on the oxygen chemisorption results. These results are based on the monolayer volume obtained. The monolayer volume obtained for the activated carbon catalysts did have a large confidence interval and the dispersions and crystallite sizes are based on the monolayer volume. It is unclear whether or not the adsorption was taking place only on the activated carbon, only the gold or both at low pressure. Based on the results of

adsorbing oxygen at low pressure. This will result in an underestimation of the size of the gold crystallites on the activated carbon. Comparing the results obtained from TEM and O_2 chemisorption for activated carbon (Table 3.12), the gold crystallite size calculated from O_2 chemisorption is significantly smaller than TEM. Diameters calculated from TEM ranged from 157nm to 300nm and 0.6nm to 3.3nm for O_2 chemisorption.

The chemisorption results for catalyst 1 (catalyst prepared on 6 hour treated nanotubes using tetramminegold (III) nitrate at pH 4) and catalyst 4 (catalyst prepared on 48 hour acid treated nanotubes using tetramminegold (III) nitrate at pH 4) showed a crystallite size comparable to that obtained with TEM (Table 3.12). Assuming dissociative chemisorption the diameters calculated for catalysts 1 and 4 are 5.4nm and 8.3nm respectively. These values are very close to the mean crystallite sizes of 4.6nm and 8.5nm obtained using TEM. It might be suggested that the adsorption on the gold crystallites is dissociative. However no conclusions can be drawn from the other catalysts as the crystallite sizes measured from TEM and chemisorption are not comparable.

Owing to the uncertainty with the chemisorption results, all further calculations used the gold crystallite sizes measured using TEM.

Table 3.10: Oxygen chemisorption paramters

Catalyst 1			95% confidence interval
$V_{m,1}$	$cm^3(STP)/g$	0.081	0.0086
$V_{m,2}$	$cm^3(STP)/g$	0.30	0.0238
K_2	$mmHg^{-1}$	0.014	0.0044
Error		4.93	

Catalyst 3			95% confidence interval
$V_{m,1}$	$cm^3(STP)/g$	0.016	0.0043
$V_{m,2}$	$cm^3(STP)/g$	0.14	0.0148
K_2	$mmHg^{-1}$	0.010	0.0036
Error		9.01	

Catalyst 4			95% confidence interval
$V_{m,1}$	$cm^3(STP)/g$	0.055	0.0045
$V_{m,2}$	$cm^3(STP)/g$	0.21	0.0193
K_2	$mmHg^{-1}$	0.007	0.0021
Error		4.60	

Catalyst 5			95% confidence interval
$V_{m,1}$	$cm^3(STP)/g$	0.009	0.0113
$V_{m,2}$	$cm^3(STP)/g$	0.53	0.0959
K_2	$mmHg^{-1}$	0.003	0.0014
Error		14.02	

Catalyst 7			95% confidence interval
$V_{m,1}$	$cm^3(STP)/g$	1.07	0.55
K_1	$mmHg^{-1}$	0.46	0.27
n		2.04	1.49
$V_{m,2}$	$cm^3(STP)/g$	81.7	154
K_2	$mmHg^{-1}$	0.0015	0.0013
m		0.75	0.19
Error		1.79	

Catalyst 8			95% confidence interval
$V_{m,1}$	$cm^3(STP)/g$	0.52	0.51
K_1	$mmHg^{-1}$	0.24	0.33
n		1.76	1.95
$V_{m,2}$	$cm^3(STP)/g$	88	242
K_2	$mmHg^{-1}$	0.0003	0.0003
m		0.98	0.26
Error		2.12	

Catalyst 9			95% confidence interval
$V_{m,1}$	$cm^3(STP)/g$	2.29	1.01
K_1	$mmHg^{-1}$	0.48	0.37
n		1.12	0.63
$V_{m,2}$	$cm^3(STP)/g$	86	44
K_2	$mmHg^{-1}$	0.0006	0.0003
m		1.04	0.17
Error		1.54	

Table 3.11: Dispersion and gold crystallite size from O_2 chemisorption

Catalyst	Loading %	Dispersion %	Crystallite Size nm
1	0.7	11	5.4
2	0.7	-	-
3	1.3	1.1	52
4	0.7	7.0	8
5	0.6	1.4	43
6	2.4	-	-
7	2.2	92	0.6
8	1.7	55	1.1
9	2.6	18	3.3

Table 3.12: Mean gold crystallite sizes from TEM and O_2 chemisorption

Catalyst	Mean Crystallite Size from TEM nm	σ	No of crystallites measured	Mean Crystallite Size from chemisorption nm	95% confidence interval
1	4.6	3.1	245	5.4	0.6
2	9.8	5.6	43	-	-
3	8.1	6.0	230	52.0	14.0
4	8.5	3.9	301	8.3	0.7
5	10.3	5.6	725	42.9	53.8
6	14.4	22.9	103	-	-
7	157	82	140	0.6	0.3
8	302	107	66	1.1	1.0
9	234	899	2	3.3	1.5

3.3.4 Glucose oxidation

3.3.4.1 Preliminary runs

The glucose oxidation runs were initially carried out using a Engelhard 2% platinum on activated carbon catalyst and the World Gold Council 0.8% gold on activated carbon standard catalyst. Initially tests were performed to assess mass transfer limitations in glucose oxidation.

Reactions were carried out at 50°C. The introduction of baffles into the reactor was evaluated (Figure 3.20). The conversion observed after 5 hours increases significantly by the introduction of baffles. This indicates the presence of external mass transfer

limitations. The agitation rate was then varied between 600 and 2200rpm. The conversion increased with increasing agitation (Figure 3.21). There was a smaller increase in conversion from 1800rpm to 2200rpm. It is possible that at 2500rpm the conversion will be the same as the conversion at 2200rpm. Reactions were subsequently performed at 35°C in order to slow down the reaction kinetics. The baffles were then widened from a width of 10mm to 20mm. The conversion after 5 hours increased from about 30% to 40% suggesting mass transfer limitations were still present with the 10mm baffles (Figure 3.22).

The presence of external mass transfer limitations was then tested at 35°C with the 0.8% gold on activated carbon World Gold Council standard catalyst due to limited supply of the platinum catalyst. The existence of oxygen mass transfer limitations was studied. 0.2g of the World Gold Council standard catalyst was tested. This mass was then halved to 0.1g and the conversion measured. The conversion using 0.1g of catalyst was just over half that when 0.2g was used.

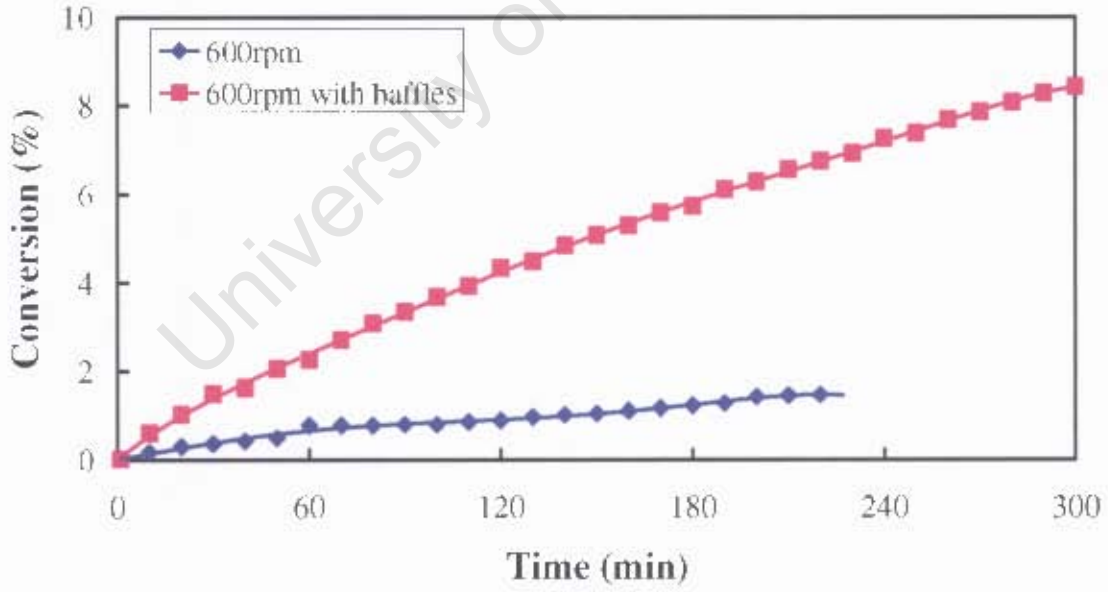

Figure 3.20: Glucose oxidation with 0.25g 2% Pt/C catalyst at 50°C with and without baffles

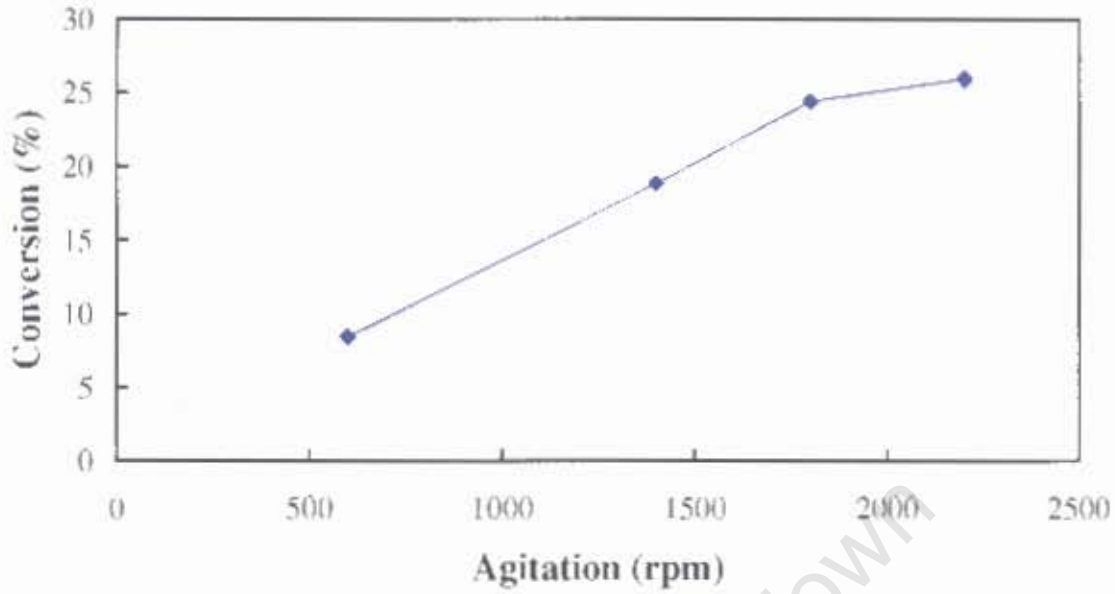

Figure 3.21: Plot of conversion after 5 hours vs. agitation (0.25g 2% Pt/C catalyst at 50°C with 3 10mm baffles

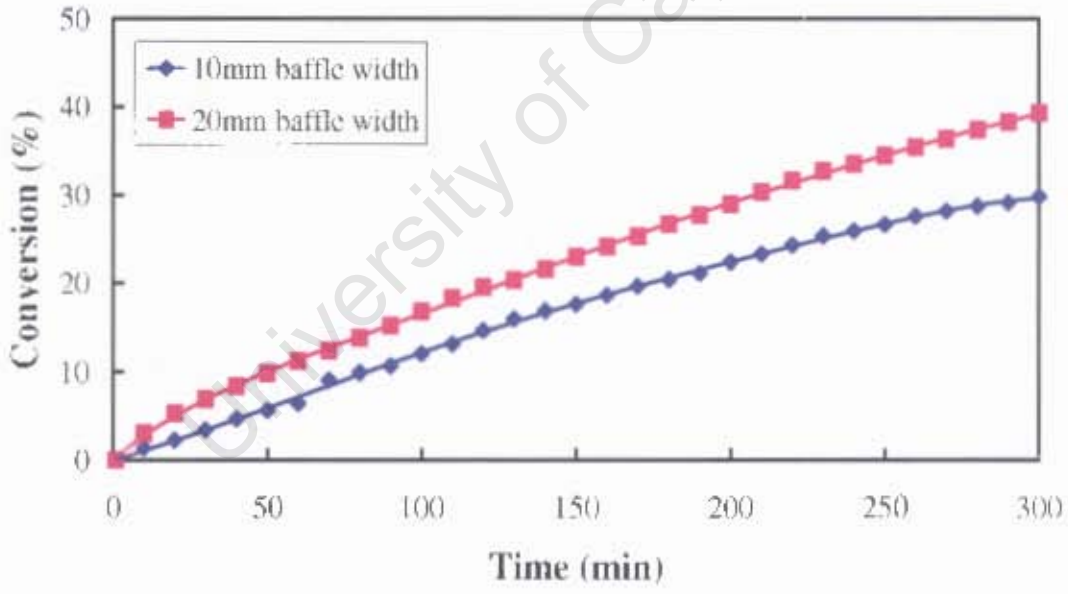

Figure 3.22: Effect of baffle width on conversion (2200rpm, 35°C, 0.25g 2% Pt/C catalyst)

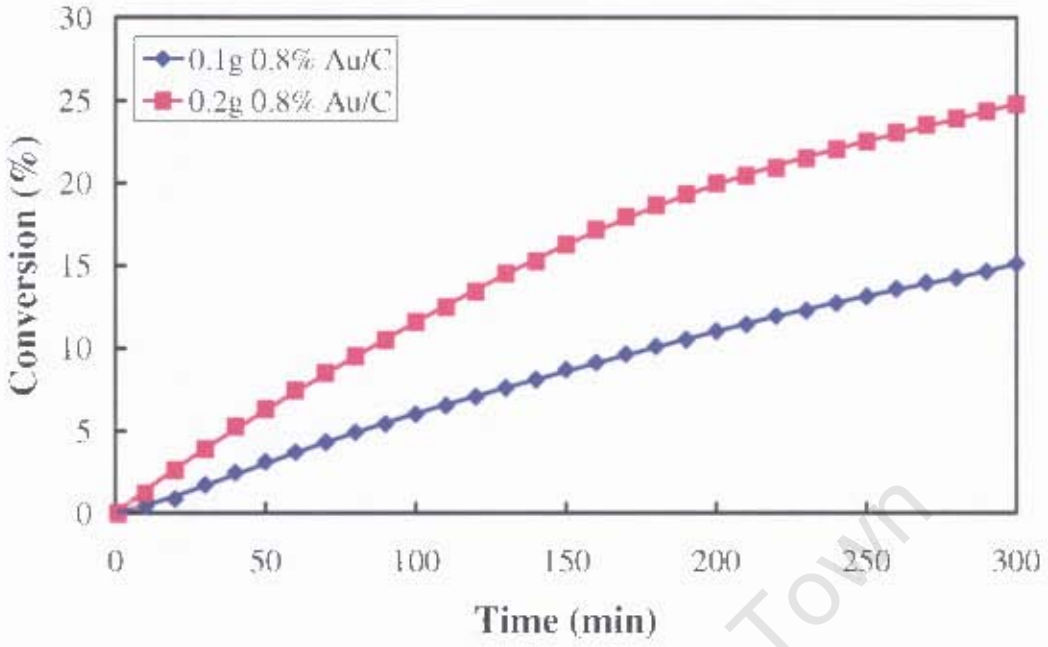

Figure 3.23: Glucose oxidation with World Gold Council standard catalyst evaluating the presence of oxygen mass transfer limitations (2200rpm, 35°C, 0.1g 0.8% Au/C, 3 20mm baffles)

3.3.4.2 Testing of produced catalysts

All the catalysts produced were tested at 35°C at an agitation rate of 2200rpm with three 20mm width glass baffles. 0.1g of each catalyst was used for the reaction.

The catalysts produced using the $HAuCl_4$ precursor were more active than the catalysts produced using the tetramminegold (III) nitrate precursor (Figures Figure 3.24, Figure 3.25, Figure 3.26 and Table 3.13). This was followed by the tetramminegold (III) nitrate precursor prepared at pH 2 and the catalysts prepared at pH 4. This was unexpected as smaller crystallites were expected to be more active for glucose oxidation. Despite the large crystallites seen in TEM, the catalysts prepared on activated carbon were active for glucose oxidation.

The catalysts prepared on the 48 hour acid treated nanotubes showed a higher conversion after 5 hours oxidation compared to the 6 hour acid treated nanotubes (Figure 3.27, Figure 3.28, Figure 3.29 and Table 3.13). This may be due to the hydrophobic nature of carbon nanotubes. The 48 hour acid treated nanotubes dispersed more easily in the reaction mixture compared to the 6 hour acid treated

nanotubes. The most active carbon nanotube catalyst tested was the catalyst prepared using the $HAuCl_4$ precursor on the 48 hour acid treated nanotubes.

The catalysts produced using the $HAuCl_4$ precursor showed the highest activity compared to the catalysts prepared using tetramminegold (III) nitrate (Figure 3.27, figure 3.28 and figure 3.29). The catalysts prepared on the 48 hour treated nanotube support were the most active catalysts for all the preparation conditions used. The activated carbon catalysts showed activity comparable to the 6 hour treated nanotubes. This was unexpected as the activated carbon catalyst contained much larger crystallites than the nanotube catalysts.

The most active catalysts were prepared on the 48 hour acid treated nanotubes (Figure 3.27, Figure 3.28 and Figure 3.29). The catalyst prepared using $HAuCl_4$ was the most active. For the catalysts prepared on the 6 hour treated carbon nanotube support, the catalyst prepared at pH 2 using tetramminegold nitrate was more active than its $HAuCl_4$ equivalent (Figure 3.27 and Figure 3.28).

The catalysts prepared at pH 2 using tetramminegold (III) nitrate were more active on all the supports. This was unexpected as the pH 4 catalysts contained smaller crystallites. There may be a crystallite size effect where larger crystallites are more active.

It was also noted that the increase in conversion with time appeared to slow down for all the catalysts. This may have been caused by the poisoning of active sites by the gluconate ion or the growth of the gold crystallites.

Table 3.13: Table of conversion achieved after 5 hours

Catalyst	Support	Precursor	Preparation pH	Conversion after 5 hours %
1	6h CNT	$Au(NH_3)_2(NO_3)_3$	4	5.15
2	6h CNT	$Au(NH_3)_2(NO_3)_3$	2	9.45
3	6h CNT	$HAuCl_4$	0.8	6.28
4	48h CNT	$Au(NH_3)_2(NO_3)_3$	4	6.72
5	48h CNT	$Au(NH_3)_2(NO_3)_3$	2	11.65
6	48h CNT	$HAuCl_4$	0.8	13.1
7	Activated C	$Au(NH_3)_2(NO_3)_3$	4	5.17
8	Activated C	$Au(NH_3)_4(NO_3)_3$	2	6.92
9	Activated C	$HAuCl_4$	0.8	10.96

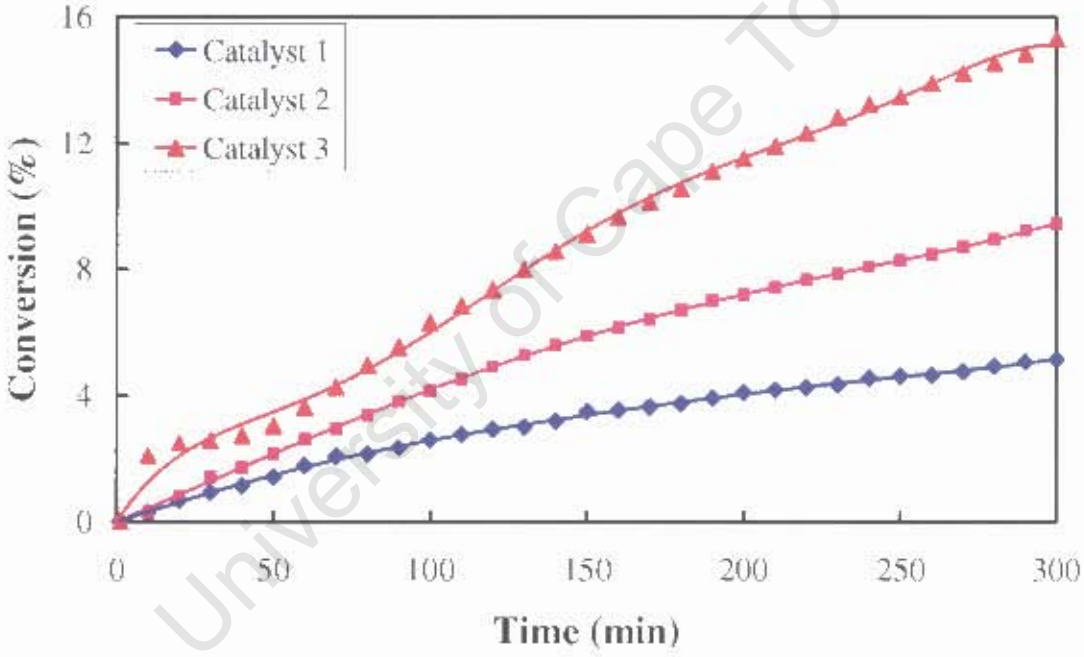

Figure 3.24: Glucose oxidation using catalysts prepared on 6 hour acid treated carbon nanotubes (2200rpm, 35°C, 0.1g Au/C catalyst, 3 20mm baffles)

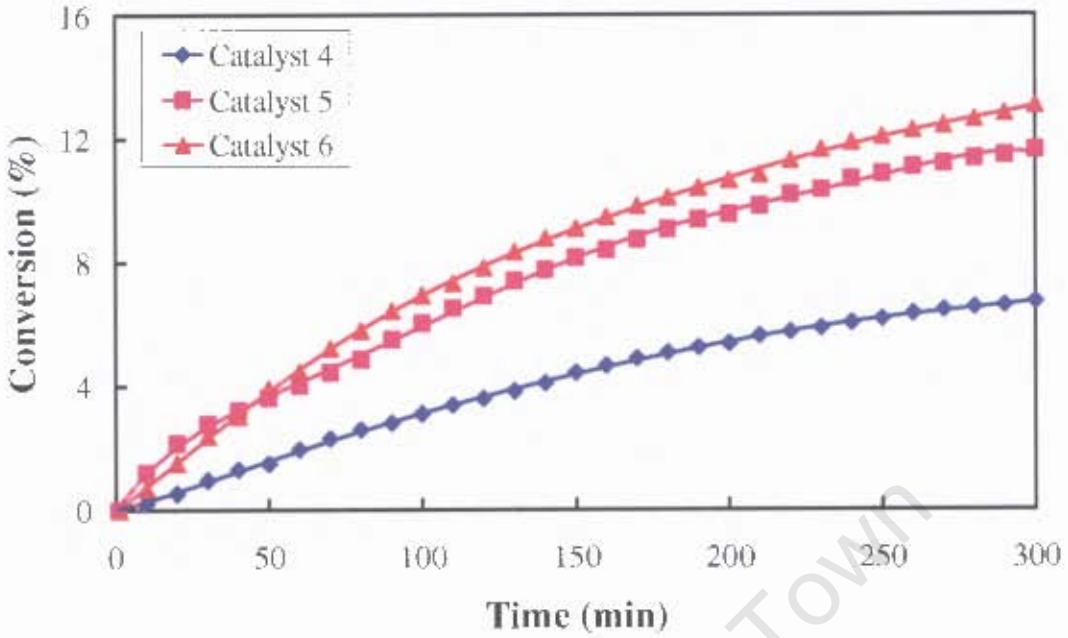

Figure 3.25: Glucose oxidation using catalysts prepared on 48 hour acid treated carbon nanotubes (2200rpm, 35°C, 0.1g Au/C catalyst, 3 20mm baffles)

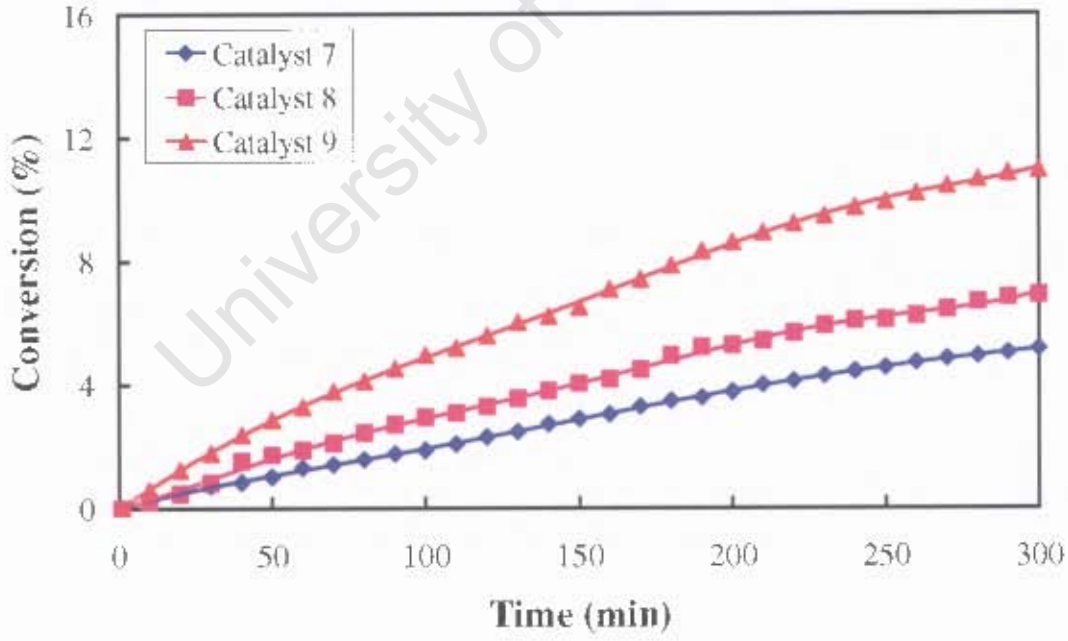

Figure 3.26: Glucose oxidation using catalysts prepared on activated carbon (2200rpm, 35°C, 0.1g Au/C catalyst, 3 20mm baffles)

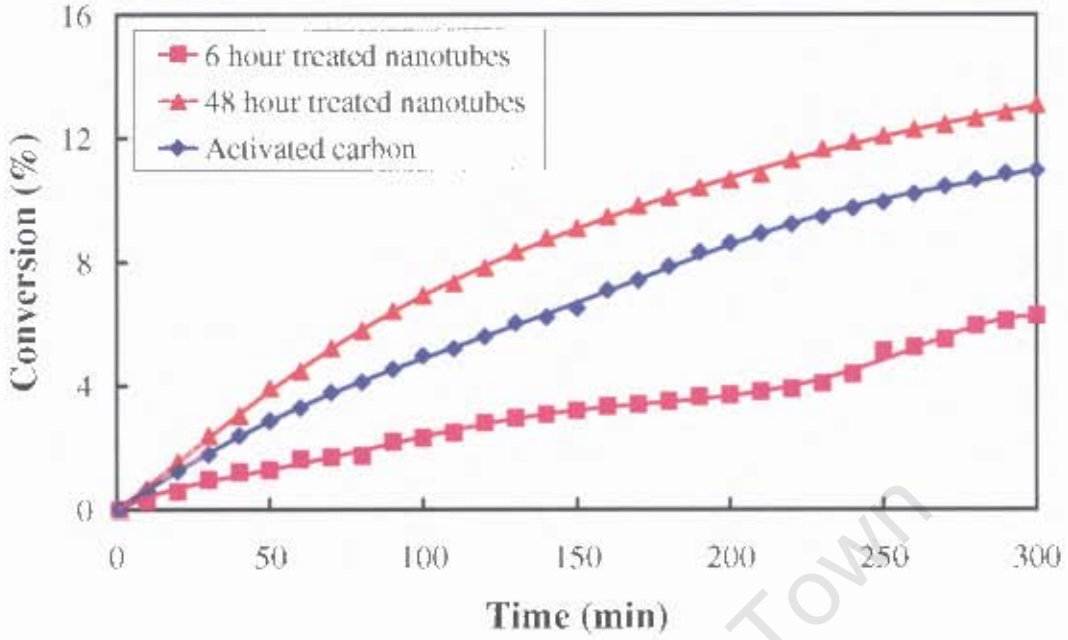

Figure 3.27: Glucose oxidation using catalysts prepared with the $HAuCl_4$ precursor (2200rpm, 35°C, 0.1g Au/C catalyst, 3 20mm baffles)

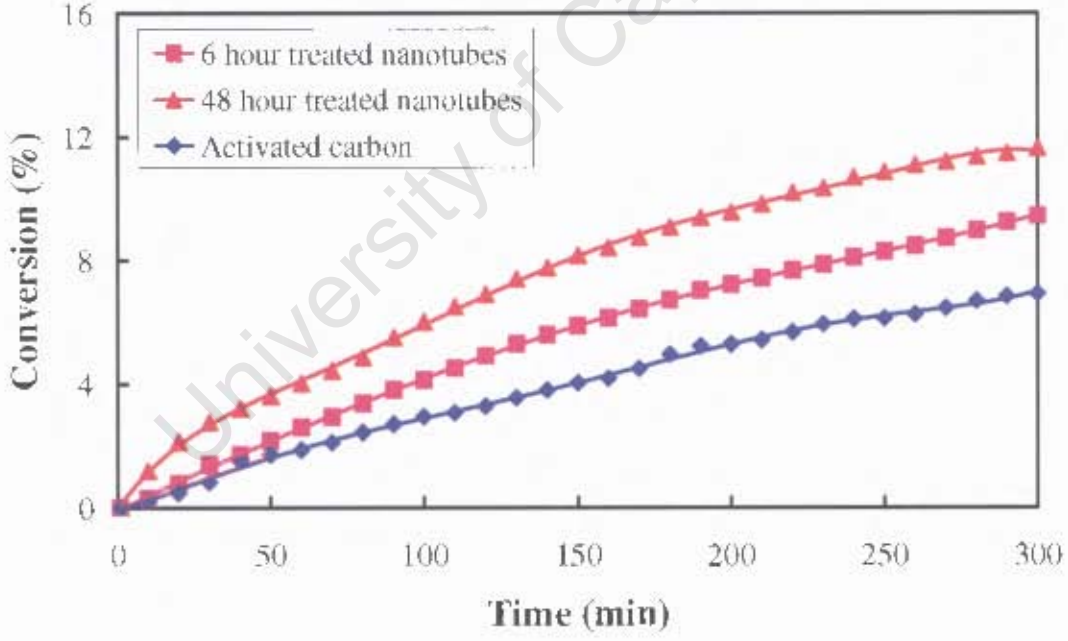

Figure 3.28: Glucose oxidation using catalysts prepared with the tetramminegold (III) nitrate precursor at pH 2 (2200rpm, 35°C, 0.1g Au/C catalyst, 3 20mm baffles)

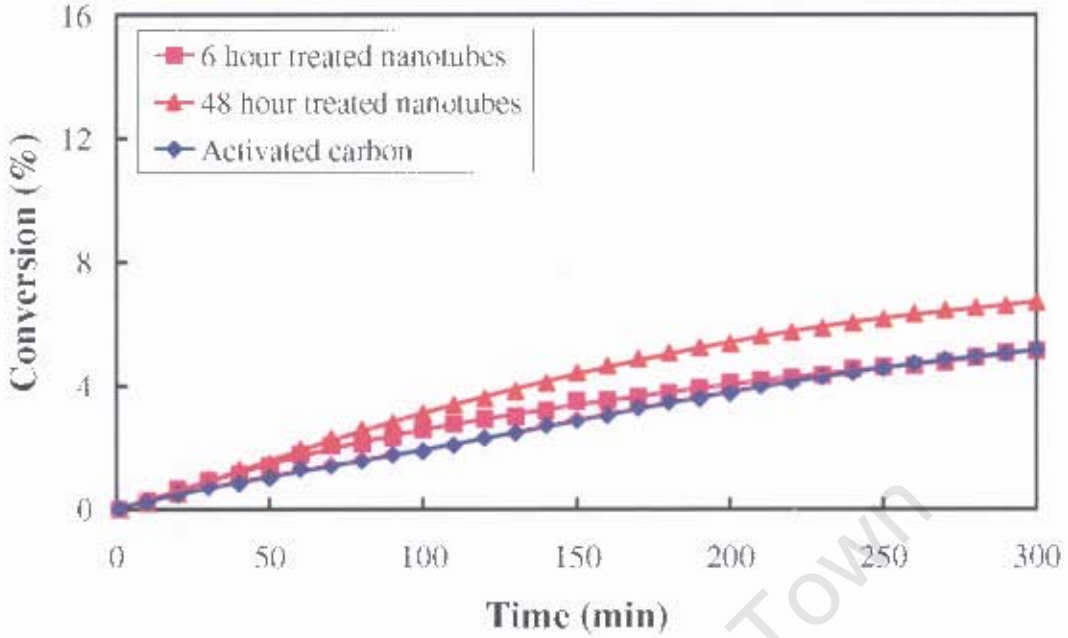

Figure 3.29: Glucose oxidation using catalysts prepared with the tetramminegold (III) nitrate precursor at pH 4 (2200rpm, 35°C, 0.1g Au/C catalyst, 3 20mm baffles)

3.3.4.3 Analysis of reaction products

The analysis of the reaction products was performed using HPLC. Sample chromatograms are given in figure 3.30, Figure 3.31, Figure 3.32. A chromatogram of an RI signal is gien in the appendix.

The gluconic acid peak in the UV chromatogram is used to calculate the conversion of the glucose to gluconic acid. The glucose peak in a RI chromatogram includes the gluconic acid. This may introduce some inaccuracy when the glucose concentration is calculated. The contribution of the gluconic acid signal in RI is calculated and is subtracted to obtain the glucose concentration. The accuracy of this calculation is unclear. The relative contributions in RI may vary with concentration. A standard was produced containing a mixture of glucose and gluconic acid. However, the gluconic acid split into its various forms and numerous peaks were observed. It is known gluconic acid may exist as 2-keto- and 5-keto-gluconic acid (Berndt *et al.*, 2004).

The selectivity for the catalysts was very good except for catalyst 2 (catalyst prepared on 6 hour treated nanotubes using the tetramminegold (III) nitrate precursor at pH 2). No gluconic acid was formed. However another unidentified acid was formed. For 2

of the most active catalysts 6 and 7, another unidentified acid was formed. Catalyst 6 was about 58% selective and catalyst 7 was about 95% selective towards gluconic acid.

Table 3.14: Table of the selectivity of the catalysts to gluconic acid

Catalyst	Precursor	Support	Preparation pH	Conversion %	Selectivity %
1	$Au(NH_3)_4(NO_3)_3$	6 hour CNT	4	5.15	100
2	$Au(NH_3)_4(NO_3)_3$	6 hour CNT	2	9.45	0
3	$HAuCl_4$	6 hour CNT	0.8	6.28	100
4	$Au(NH_3)_4(NO_3)_3$	48 hour CNT	4	6.72	100
5	$Au(NH_3)_4(NO_3)_3$	48 hour CNT	2	11.65	100
6	$HAuCl_4$	48 hour CNT	0.8	13.10	58
7	$Au(NH_3)_4(NO_3)_3$	Activated C	4	5.17	100
8	$Au(NH_3)_4(NO_3)_3$	Activated C	2	6.92	100
9	$HAuCl_4$	Activated C	0.8	10.96	95

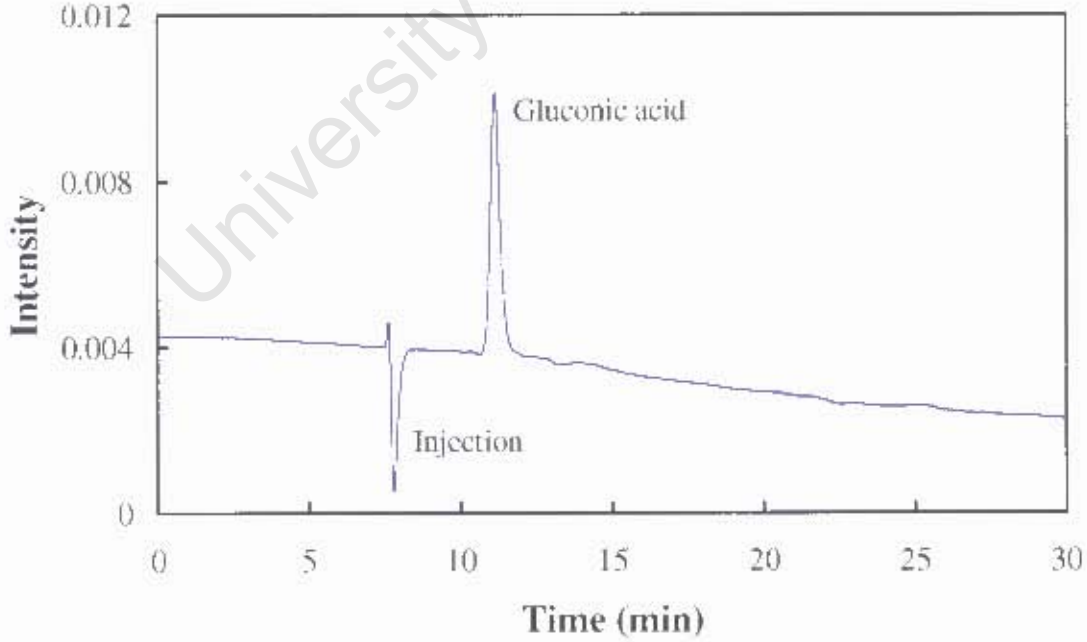

Figure 3.30: UV signal for the analysis of the glucose oxidation products for catalyst 7 (Tetramminegold (III) nitrate precursor on activated carbon at pH 4)

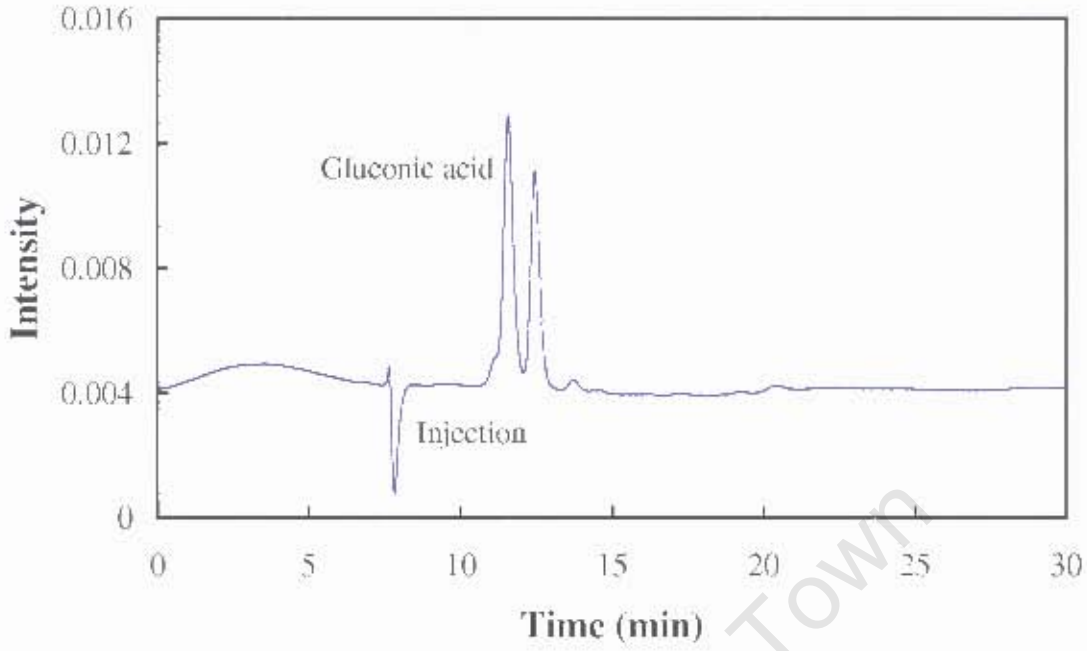

Figure 3.31: UV signal for catalyst 6 (Catalyst prepared on 48 hour treated nanotubes using $HAuCl_4$)

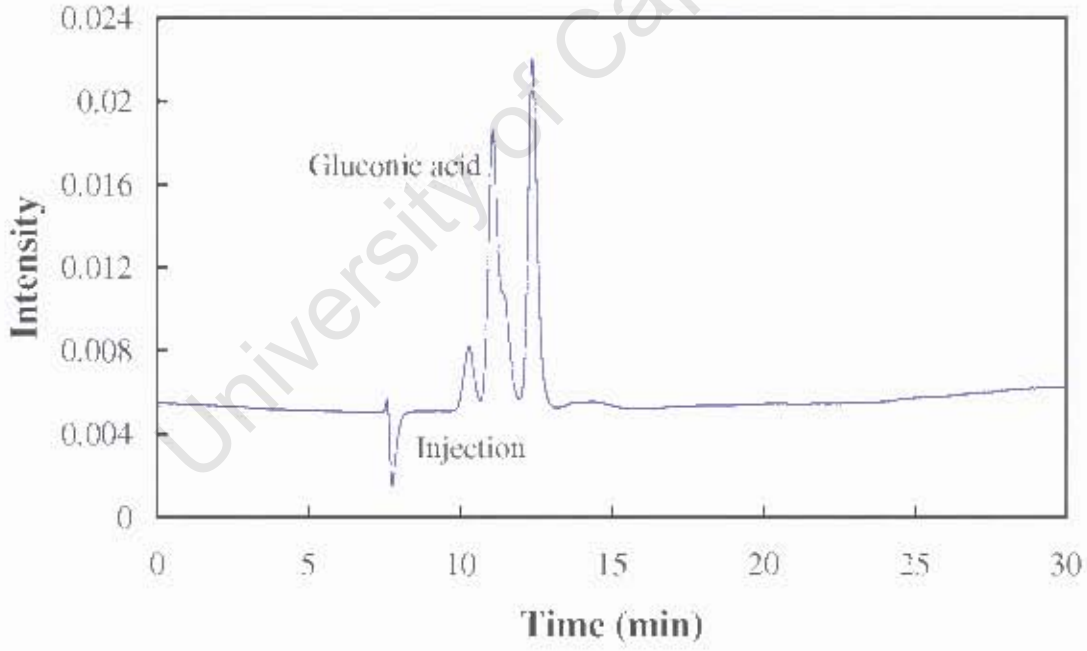

Figure 3.32: UV signal for catalyst 9 (Catalyst prepared on activated carbon using $HAuCl_4$)

4 Discussion

4.1 Carbon support

4.1.1 Acid treatment

As carbon nanotubes are relatively inert, they were treated in concentrated nitric acid in order to introduce functional groups onto the surface. The introduction of functional groups such as carboxylic groups made the carbon nanotubes less hydrophobic which is vital as they were tested using a liquid phase reaction. The nitric acid treatment not only introduced functional groups onto the surface, but it also modified the nanotube structure to a degree.

The bulk density of the 48 hour nanotubes obtained from Hg pycnometry is 0.43g/cm^3, higher than the 6 hour nanotubes with a bulk density of 0.13g/cm^3 indicating the presence of less porous material. Evidence of amorphous carbon was seen in the TEM images of the 48 hour treated nanotubes which would explain the decrease in the total pore area and porosity (Figure 3.6). The density of graphitic carbon is 2.09g/cm^3. The bulk density of the 48 hour boiled nanotubes of 0.43g/cm^3 would suggest that amorphous carbon is being formed. The 48 hour boiled nanotubes also gave the lowest volume of mercury intrusion of all the nanotubes signifying the presence of less porous material (Table 3.4).

Part of the loss of mass during the acid treatment is a result of the removal of the amorphous carbon layer seen in the TEM images. The actual loss of carbon nanotubes would therefore be less than the results suggest. It is suggested that this layer has in effect protected the carbon nanotube structure from breaking apart and forming amorphous carbon itself. The wall thicknesses of the carbon nanotubes were measured using the TEM images. There was no significant difference between the untreated and 48 hour boiled nanotubes. However the 6 hour treated nanotubes had thinner walls. It is proposed that the fishbone nanotubes break apart once the walls reach a certain thickness from the action of the nitric acid, thus weakening the tube structure. After 6 hours treatment many of the nanotube walls were thinner, but did not appear to be breaking apart. From the TEM images, very little evidence was seen for the destruction of the nanotube structure, whereas for the 48 hour nanotubes, this was

seen in abundance. It is suggested that the 48 hour treated nanotubes have a similar wall thickness to the untreated nanotubes because only nanotubes with thicker walls would be left behind. The tubes with thinner walls are preferentially destroyed.

A BET analysis was also performed on the nanotubes. With treatment, the BET surface area almost doubles from $45m^2/g$ for the untreated nanotubes to $80m^2/g$. This can be explained by the opening of the nanotubes during treatment. From the TEM images, a large portion of the untreated nanotubes appeared to be closed. For the 6 hour treated nanotubes, a very small portion of the nanotubes appeared to be closed. No closed nanotubes were seen in the TEM images of the 48 hour treated nanotubes.

The BET surface area for untreated carbon nanotubes of $45m^2/g$ is low compared to the values obtained in literature. Values of close to $1000m^2/g$ have been quoted in literature (Ning et al., 2005). This more than likely down to the fact that the higher values quoted in literature are for nanotubes with much smaller diameters. With tube diameters of about 60nm, the surface area will be considerably lower than some of the nanotubes with diameters of a few nanometers. Figure 4.1 shows some of the values obtained in literature. The solid line represents the surface area obtained assuming cylindrical geometry and open tubes using the skeletal density of the untreated carbon nanotubes from Hg pycnometry. The BET surface areas obtained in literature are closely linked to the tube diameter.

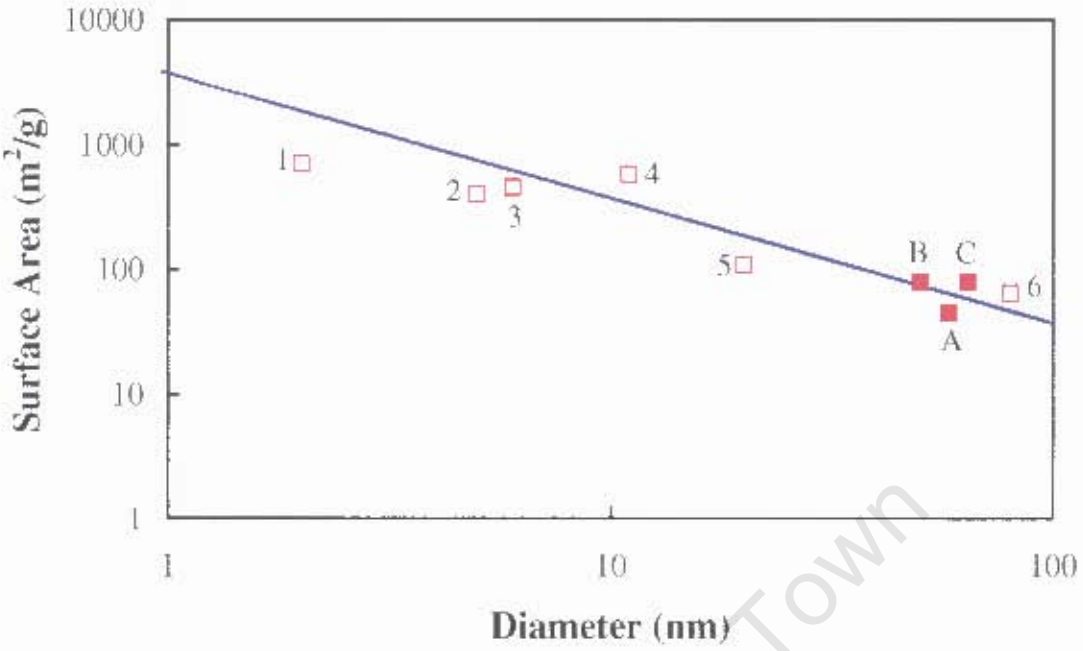

Figure 4.1: Comparison of BET surface areas of the nanotubes used (A – untreated, B – 6 hour acid treated, C – 48 hour acid treated) and those obtained in literature (1 – Ning *et al.*, 2005; 2 – Lee *et al.*, 2005; 3 – Ning *et al.*, 2005; 4 – Niu and Wang, 2008; 5 – Jiang and Zhao, 2004; 6 – Niu and Wang, 2008). The solid line represents the surface are calculated using the diameter of the tubes assuming cylindrical geometry, closed tubes and a skeletal density of 1.08g/cm^3

Pore size distributions were obtained from both N_2 physisorption and Hg pycnometry. Comparing the average pore diameters, the diameters obtained from Hg pycnometry were much larger than that obtained from N_2 physisorption. This is because mercury cannot penetrate very small pores, unless under very high pressure. N_2 physisorption has the ability to penetrate much smaller pores and therefore give a more accurate description of pores in the micro- and mesoporous region (Leofanti *et al.*, 1998).

The results obtained from these two analysis techniques did not follow the same trends. For example, according to Hg pycnometry, the average pore diameter of the carbon nanotubes decreased after treatment, whereas N_2 physisorption results suggest that the average pore size increased. The increase in pore size in the N_2 physisorption results was caused by the nitric acid treatment opening the closed nanotubes, thus exposing a large hollow in many of the tubes that were previously closed. As some of the nanotubes are quite large with inner diameters as big as 50nm, this explains the

increase in average pore size. For the Hg pycnometry, the mercury will initially penetrate the spaces and gaps in between individual nanotubes could be quite large hence the big deviation from the N_2 physisorption results for the untreated nanotubes. For the treated nanotubes, the opening of the nanotubes allowed the mercury to penetrate the nanotubes, resulting in the decrease in average pore diameter. This is further illustrated by the fact that the mercury intrusion volume for the treated nanotubes is considerably higher than the intrusion volume for the untreated nanotubes (Table 3.4).

The pore size distributions obtained using N_2 physisorption and Hg pycnometry were combined. Hg pycnometry is used to characterise large pores up to about 15000nm and was therefore used to characterise larger pores. N_2 physisorption was used for smaller pores. Hg pycnometry is used for meso- and macropore charaterisation and N_2 physisorption is not a suitable technique in the macroporous region (Leofanti *et al.*, 1998).

The combined pore size distributions for the carbon nanotubes followed similar trends. There was an increase in the proportion of pores above 20nm. This is in the region of the inner diameters of the carbon nanotubes. This increase was larger for the treated nanotubes due to the opening of the tubes with treatment. The combined pore size distribution for the activated carbon showed a greater proportion of pores in the microporous region as expected due to activated carbon's microporous nature.

A single combined pore size was calculated by combining the mercury intrusion volumes and the BJH pore volumes along with their respective pore areas over the appropriate pore size ranges (Table 4.1).

The results obtained for the nanotubes showed a much larger pore size compared to the pore sizes obtained with the individual methods. From table 4.1, the volume contribution from Hg pycnometry was quite large compared to the BJH pore volume. Due to the structure of the carbon nanotubes, the mercury will intrude into the spaces in between individual nanotubes thereby inflating the intrusion volume for larger pores. The combined mean pore sizes for the nanotubes are actually much larger than

the diameters of the actual tubes. The mean pore size obtained for activated carbon was comparable to the pore size obtained by the individual methods.

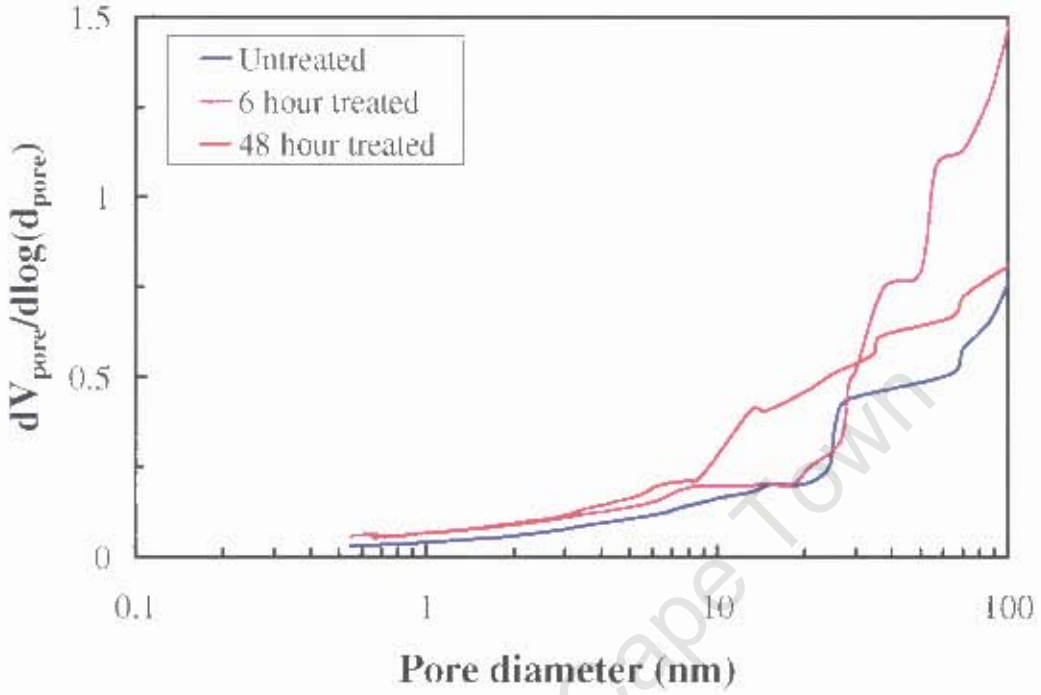

Figure 4.2: Combined BJH and Hg pycnometry pore size distribution for carbon nanotubes

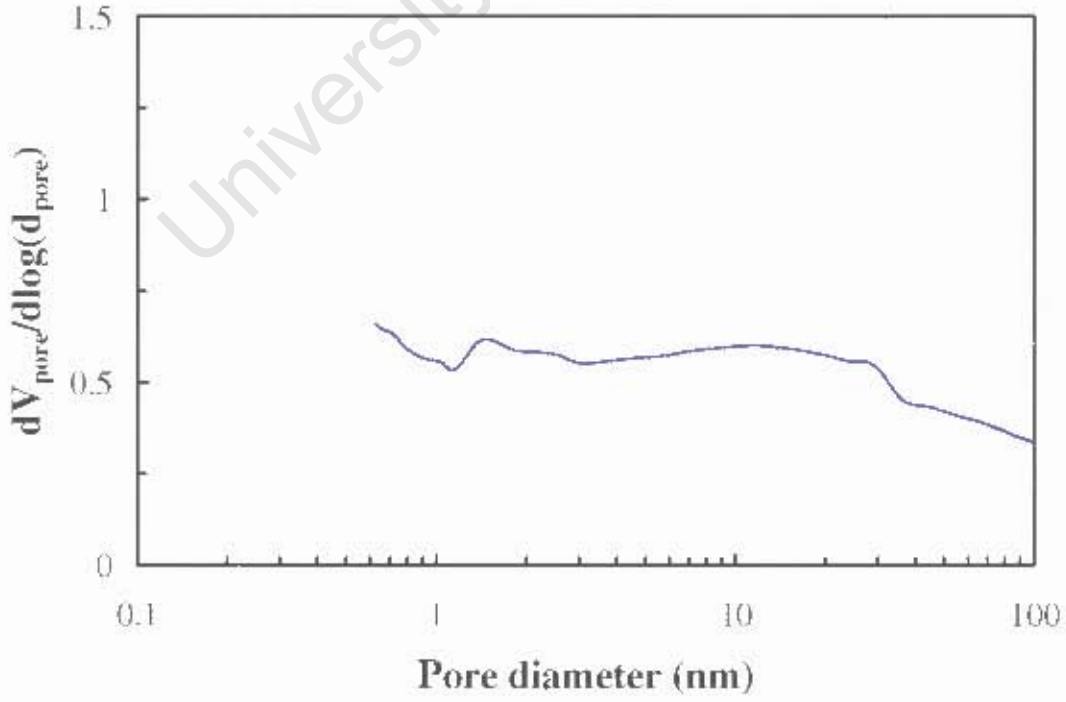

Figure 4.3: Combined pore size distribution for activated carbon

Table 4.1: Combined mean pore size

	BJH Pore Surface Area m^2/g	Hg Pore surface area m^2/g	BJH Pore volume cm^3/g	Hg pore volume cm^3/g	Mean Pore Diameter nm
Untreated carbon nanotubes	46	5.1	0.2	2.9	692
6 hour treated carbon nanotubes	76	16.7	0.3	7.0	1244
48 hour treated carbon nanotubes	74	13.1	0.2	1.2	774
Activated carbon	826	1.4	0.8	0.8	11

4.1.2 Changes to the surface chemistry of the nanotubes

The infrared spectra of the carbon nanotubes were taken to characterise the effect of the nitric acid treatment on the surface of the nanotubes. The infrared spectra of the nanotubes revealed one characteristic peak at $1650cm^{-1}$. This is assigned to the stretching mode of carboxylic groups on the surface. The intensity of this peak was greatest for the 6 hour treated nanotubes and slightly lower for the 48 hour treated nanotubes. The intensity of this peak for the treated nanotubes was significantly greater than the untreated nanotubes suggesting the treatment in nitric acid did introduce functional groups onto the surface.

The zeta potential of the untreated and treated nanotubes was also measured. The iso-electric point of the untreated fishbone nanotubes is at pH 2 (Figure 3.15). This low iso-electric point suggests that the functional groups responsible for charging the nanotubes are acidic in nature (Kongolo *et al.*, 1997). After treatment by boiling in nitric acid for 6 hours and 48 hours, the iso-electric point drops to a pH of 1 indicating the addition of more acidic groups. There does not appear to be a significant difference in the iso-electric point for the 6 and 48 hour boiled nanotubes. At pH values above 3, the zeta potential of the 48 hour nanotubes is much lower than 6 hour acid treated carbon nanotubes. This indicates the presence of additional acidic functional groups on the surface of the 48 hour nanotubes.

With increasing pH, the zeta potential of the 6 and 48 hour nanotubes appears to proceed stepwise (Figure 3.15). This indicates the presence of more than one functional group on the surface as these functional groups should dissociate at particular pH values. It has been suggested in literature that the acidic functional

groups present on carbon nanotubes are hydroxyl (-OH) and carboxyl (-COOH) groups (Liu and Gao, 2005). These steps are more pronounced for the 48 hour nanotubes further suggesting the increased concentration of one of these functional groups on the nanotubes, most likely the carboxylic groups based on the infrared spectra.

It was also noted during the experimental work that the carbon nanotubes used were hydrophobic. This behaviour has been observed in literature (Rosca *et al.*, 2005). The introduction of functional groups onto the surface makes them less hydrophobic allowing easier dispersion in solution. A consequence of this is that a catalyst precursor in solution will have easier access to the solid support surface from the solution.

4.2 Catalysts produced

4.2.1 Chemistry of Preparation

The catalysts were produced using ion-exchange with the aim of producing small and well dispersed gold crystallites with a narrow crystallite size distribution. The crystallite size distribution was obtained using TEM. A mean crystallite size was acquired using O_2 chemisorption and compared with the TEM results.

Small gold crystallites were obtained on the catalyst prepared on 6 hour acid treated carbon nanotubes at pH 4 using tetramminegold (III) nitrate. The mean crystallite size is 4.6nm (Table 3.8). Almost all the crystallites measured were below 10nm in size (Figure 3.17). Using the same precursor and support at pH 2, the mean crystallite size is 9.8nm. The crystallite size distribution is also not as narrow as the catalyst prepared at pH 4. At pH 2, the zeta potential for 6 hour treated nanotubes is about -10mV and at pH 4 it is about -16mV. At pH 4, there will be more anchoring points for the positively charged gold ammine complex ($Au(NH_3)_4^{3+}$) to attach to on the surface of the nanotube. This should allow for greater dispersion of gold on the nanotube surface. At pH 2, there are fewer anchoring points and therefore more cationic gold will attach to a single anchoring point. This will explain the larger crystallites obtained using ion-exchange at pH 2 and the wider crystallite size distribution.

Comparing catalysts using the 6 and 48 hour treated nanotube supports prepared at pH 4 with tetramminegold (III) nitrate, the 6 hour treated nanotubes have a much smaller mean crystallite size of 4.6nm compared to 8.5nm for the 48 hour treated nanotubes. The 48 hour treated nanotubes have a much lower zeta potential at pH 4 of about -50mV, compared with -16mV for the 6 hour treated nanotubes. This gives the 48 hour acid treated nanotubes far more anchoring points for the cationic gold to attach. During calcination and reduction, the gold on the 48 hour acid treated nanotubes has most likely sintered. The increased concentration of anchoring points means these anchoring points are closer together. The result of this is the gold will sinter during calcination and reduction, forming larger crystallites. However, the functional groups present on the surface of the nanotubes plays a role in the sintering process and are discussed later.

The catalysts produced on the 48 hour acid treated nanotubes showed larger crystallites in TEM compared to the 6 hour acid treated nanotubes. This is most likely due to sintering during calcination and reduction. The 48 hour treated nanotubes have a lower zeta potential at pH 2 and pH 4 compared to the 6 hour acid treated nanotubes. This means the concentration of anchoring points is higher at a given pH and they are therefore closer together. This will result in the sintering of the gold crystallites at elevated temperature. However the loadings of the 6 and 48 hour acid treated nanotube catalysts prepared using the tetramminegold (III) nitrate precursor are very similar. This may suggest there is another effect which is causing the gold crystallites to sinter on the 48 hour treated nanotubes.

Prado-Burguete et al. (1989) looked at the effect of oxygen containing surface groups on their activated carbon support on platinum crystallite dispersion after impregnation and sintering during reduction. They found that the increased concentration of carboxylic groups on the carbon surface gave a more homogeneous dispersion due to the decrease in hydrophobicity. However the carboxylic groups also promoted sintering during reduction. They also found the less acidic groups such as oxygen (C=O) are responsible for the anchorage of the platinum crystallites.

The increased concentration of carboxylic groups on the surface of the 48 hour treated nanotubes will also explain the larger mean crystallite sizes obtained after reduction

compared to the 6 hour treated nanotubes. The relative concentrations of the carboxylic groups compared to the oxygen groups are unknown, however from the zeta potential results, it might be concluded that the carboxylic groups are in much greater concentration on the 48 hour acid treated nanotubes due to the significant step wise decrease in zeta potential with increasing pH compared to the 6 hour acid treated nanotubes (Figure 3.15).

The activated carbon support showed very large crystallites with mean crystallite sizes of over 150nm (Table 3.8). When the loading is considered, the large crystallites could simply be the result of sintering during calcination and reduction. The loadings on the activated were higher than the carbon nanotube catalysts (Table 3.7).

4.3 Glucose oxidation

The catalysts produced were tested with glucose oxidation in a batch reactor. However, before testing commenced, an Engelhardt 2% Pt/C catalyst and the World Gold Council standard catalyst 0.8% Au/C were tested to evaluate the presence of any mass transfer limitations. The produced catalysts were then tested at 35°C with an agitation rate of 2200rpm and an air flow rate of 800ml/min, with the assumption that the activity would be sufficiently low to avoid the influence of external mass transfer limitations.

4.3.1 Effect of crystallite size

For the catalysts prepared using the tetramminegold (III) nitrate precursor, the catalysts prepared at pH 2 with the larger crystallites showed greater activity than the catalysts prepared at pH 4 with the smaller crystallites. The most active catalyst produced with the tetramminegold (III) nitrate precursor was prepared at pH 2 on the 48 hour treated nanotubes. Considering only the crystallite size, it appears that the catalysts with larger crystallites in the region of 10nm to 15nm are more active than smaller crystallites.

For the glucose oxidations runs, the same mass of catalyst (0.1g) was used throughout. Therefore, the mass of gold present in each reaction was different. From table 4.2 considering each support, the supports with the higher gold loadings were more active with the exception of the 6 hour treated nanotubes. More gold present in the reactor means more active sites and higher activity. However, larger crystallites means less gold surface area and lower activity. In order to quantify the catalytic activity, the rate constants were calculated using first order kinetics and subsequently the rate constant per unit surface area of gold was evaluated.

The surface area of gold available for adsorption during reaction will have an effect on the activity of the catalysts. Greater gold surface area will yield more active sites for the reactants to adsorb therefore increasing activity. Table 4.2 shows the rate constants expressed per unit surface area of gold actually present in the reactor. The specific surface area of gold on each catalyst was calculated from the crystallite sizes obtained from TEM and the gold loading on each catalyst.

For the nanotube catalysts, the conversion achieved after 5 hours oxidation appears to pass through a minimum with increasing gold surface area (Table 4.2 and Figure 4.4). The conversion then increases with increasing surface area. The activated carbon also showed similar behaviour and also passed through a minimum. The activity of the activated carbon catalysts was comparable to the carbon nanotubes catalysts. It is possible that the activated carbon catalysts contained similar crystallite sizes to the carbon nanotubes catalysts. The gold crystallites on activated carbon were found with great difficulty in TEM and its possible that the smaller crystallites were simply not seen.

Considering the data for the nanotube catalysts, the activity was expected to increase with increasing surface area of gold. The activity did increase with gold surface area except the activity of each support appeared to pass through a minimum. This may suggest there is a crystallite size effect and there may be an optimum crystallite size.

Table 4.2: Table of glucose conversion achieved after 5 hours and the specific surface area of gold per unit mass catalyst

Catalyst	Support	Precursor	Preparation pH	Mean Crystallite Size nm	Loading %	Specific Surface Area of Gold m^2/g_{cat}	Conversion after 5 hours %
1	6h CNT	$Au(NH_3)_4(NO_3)_3$	4	4.6	0.66	0.44	5.15
2	6h CNT	$Au(NH_3)_4(NO_3)_3$	2	9.8	0.70	0.22	9.45
3	6h CNT	$HAuCl_4$	0.8	8.1	1.25	0.47	6.28
4	48h CNT	$Au(NH_3)_4(NO_3)_3$	4	8.5	0.69	0.25	6.72
5	48h CNT	$Au(NH_3)_4(NO_3)_3$	2	10.3	0.58	0.17	11.65
6	48h CNT	$HAuCl_4$	0.8	14.4	2.39	0.51	13.1
7	Activated C	$Au(NH_3)_4(NO_3)_3$	4	234.4	2.19	0.03	5.17
8	Activated C	$Au(NH_3)_4(NO_3)_3$	2	157.5	1.71	0.03	6.92
9	Activated C	$HAuCl_4$	0.8	302.4	2.61	0.03	10.96

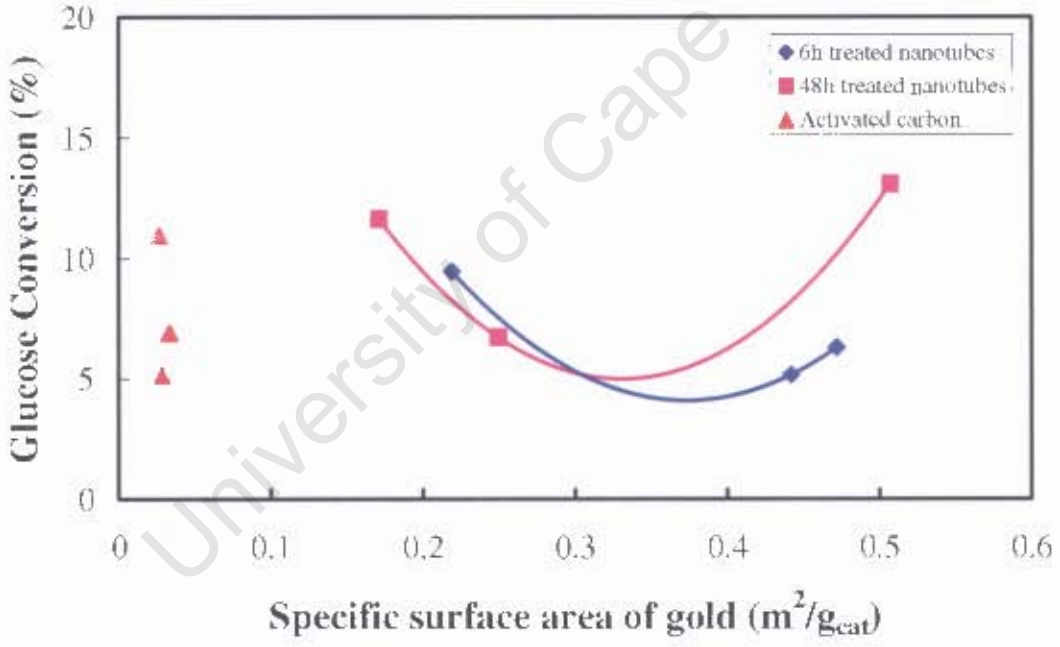

Figure 4.4: Glucose conversion after 5 hours vs. specific surface area of gold per gram of catalyst used in the reaction

4.3.2 Kinetic modelling

In order to evaluate the catalytic activity, the reaction was initially modelled according to the Eley-Rideal mechanism as suggested by Beltrame *et al.* (2006):

$$r = \frac{k_{cat} K_G C_{Au} C_G C_{O2}}{1 + K_G C_G}$$

where C_{Au}, C_G and C_{O2} are the concentrations of gold, glucose and oxygen respectively in the reaction mixture. The parameters k_{cat} and K_G are the kinetic coefficient of the rate determining step and the adsorption constant. When the parameters were fitted to the data, the adsorption constant K_G became very small and the inhibition term in the denominator tends to one. Therefore the reaction was modelled using first order kinetics:

$$r = k \cdot C_G$$

where k is the first order rate constant. The rate constants were evaluated using non-linear regression. The rate constants are expressed per unit surface area gold present on the catalyst in table 4.3.

The most active catalyst per gram gold present on the surface of the support was the catalyst prepared using the $HAuCl_4$ precursor on the 6 hour treated nanotubes (Catalyst 3). The next most active catalyst was also prepared using the $HAuCl_4$ precursor, this time on the 48 hour acid treated nanotubes. Considering individual supports, the most active catalysts prepared were prepared using the $HAuCl_4$ precursor. This was unexpected as the crystallites were generally larger than the catalysts prepared using the tetramminegold (III) nitrate precursor at pH 4. The least active catalysts on each support were the catalysts prepared using the tetramminegold (III) nitrate precursor at pH 4 even though these catalysts contained the smallest crystallites.

Table 4.3: First order rate constants

Catalyst	Support	Precursor	Preparation pH	Loading %	Mean Crystallite Size nm	Conversion after 5 hours %	k $h^{-1}.g_{cat}^{-1}$	Error $h^{-1}.g_{cat}^{-1}$
1	6h CNT	$Au(NH_3)_4(NO_3)_3$	4	0.7	4.6	5.15	0.12	0.002
2	6h CNT	$Au(NH_3)_4(NO_3)_3$	2	0.7	9.8	9.45	0.22	0.002
3	6h CNT	$HAuCl_4$	0.8	1.3	8.1	6.28	0.36	0.003
4	48h CNT	$Au(NH_3)_4(NO_3)_3$	4	0.7	8.5	6.72	0.16	0.001
5	48h CNT	$Au(NH_3)_4(NO_3)_3$	2	0.6	10.3	11.65	0.29	0.002
6	48h CNT	$HAuCl_4$	0.8	2.4	14.4	13.1	0.33	0.005
7	Activated C	$Au(NH_3)_4(NO_3)_3$	4	2.2	234.4	5.17	0.11	0.005
8	Activated C	$Au(NH_3)_4(NO_3)_3$	2	1.7	157.5	6.92	0.16	0.001
9	Activated C	$HAuCl_4$	0.8	2.6	302.4	10.96	0.26	0.002

The most active catalyst was expected to be the catalyst with the smallest crystallites. The catalyst with the smallest crystallites was not the most active (Table 4.2 and Figure 4.4). From the data, considering only the gold crystallite size, there seems to be an optimum point at a crystallite size of between 10nm and 15nm. It is possible that smaller crystallites could adsorb the glucose molecule quite strongly and therefore the molecule will not desorb as easily. If the crystallites are too large, they may not adsorb the reactant strongly enough thus slowing the rate of reaction. For the catalysts produced on the 6 hour treated nanotubes, a mean crystallite size lower than 8nm showed lower activity and the mean crystallite size above this point also showed higher activity. The same can be said for the catalysts produced on the 48 hour treated nanotubes. The lowest crystallite size obtained was 8.5nm which showed the lowest activity per unit area gold. The other two catalysts contained larger crystallites which showed higher activity.

The catalysts produced on activated carbon contained much larger crystallites according to the TEM. These catalysts were active for glucose oxidation and therefore may contain a significant number of crystallites of a similar size to the carbon nanotube catalysts as discussed earlier. It is difficult to draw any conclusions from the data obtained for the activated carbon catalysts due to the uncertainty of the crystallite size obtained from TEM (Figure 4.6). If the crystallite sizes obtained from TEM are accurate, the rate per unit area gold is much higher than the carbon nanotube catalysts. It is possible that the activated carbon is adsorbing oxygen based on the oxygen chemisorption results. The glucose may be reacting with this adsorbed oxygen on the activated carbon surface therefore inflating the rate constant.

The World Gold Council standard catalyst (0.8% Au/C) has a mean crystallite size of 9.6nm and showed slightly higher activity than the catalysts produced. An optimum crystallite size of about 8nm has been observed in literature for a gold on activated carbon catalyst for the liquid phase oxidation of ethylene glycol (Bianchi *et al.*, 2000). This is relatively large for a gold catalyst as for other such as CO oxidation, smaller crystallites are desired (Choudhary and Goodman, 2002). For the carbon nanotube catalysts using glucose oxidation as the reaction, the optimum appears to be between 10nm to 13nm.

Table 4.4: Rate constants per unit mass gold for produced catalysts for glucose oxidation

Catalyst	Precursor	Preparation pH	Support	Loading %	Mean Crystallite Size nm	Conversion after 5 hours %	k $h^{-1}.m^{-2}_{gold}$
1	$Au(NH_3)_4(NO_3)_3$	4	6h CNT	0.7	4.6	5.15	0.27
2	$Au(NH_3)_4(NO_3)_3$	2	6h CNT	0.7	9.8	9.45	0.98
3	$HAuCl_4$	0.8	6h CNT	1.3	8.1	6.28	0.75
4	$Au(NH_3)_4(NO_3)_3$	4	48h CNT	0.7	8.5	6.72	0.63
5	$Au(NH_3)_4(NO_3)_3$	2	48h CNT	0.6	10.3	11.65	1.69
6	$HAuCl_4$	0.8	48h CNT	2.4	14.4	13.1	0.64
7	$Au(NH_3)_4(NO_3)_3$	4	Activated C	2.2	234.4	5.17	5.42
8	$Au(NH_3)_4(NO_3)_3$	2	Activated C	1.7	157.5	6.92	7.7
9	$HAuCl_4$	0.8	Activated C	2.6	302.4	10.96	4.22

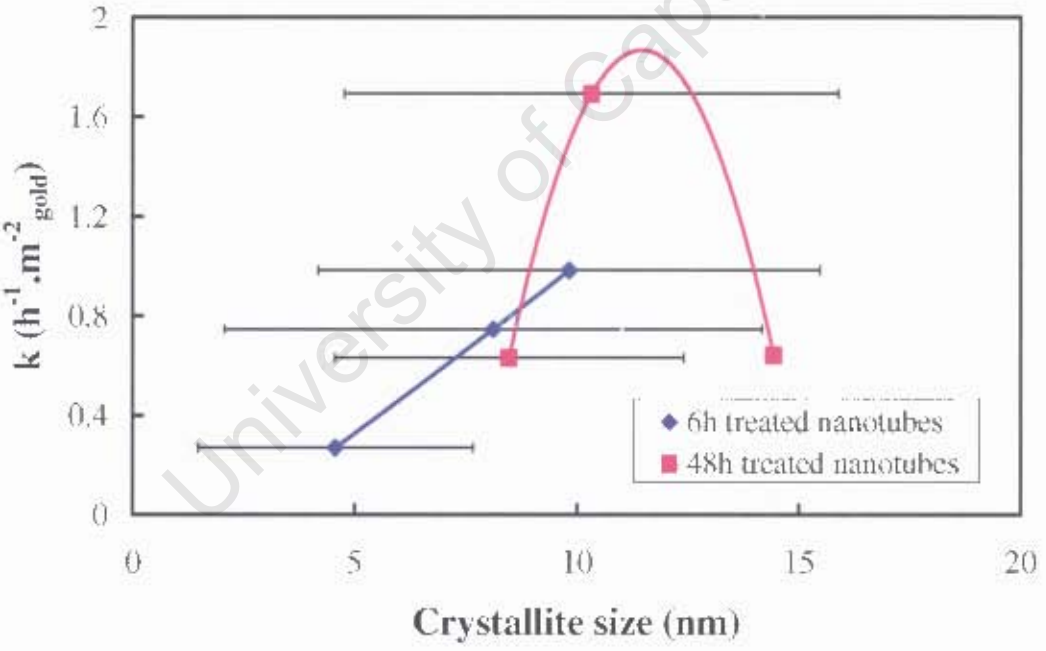

Figure 4.5: Rate constant per unit surface area of gold vs. gold crystallite size for the carbon nanotube catalysts

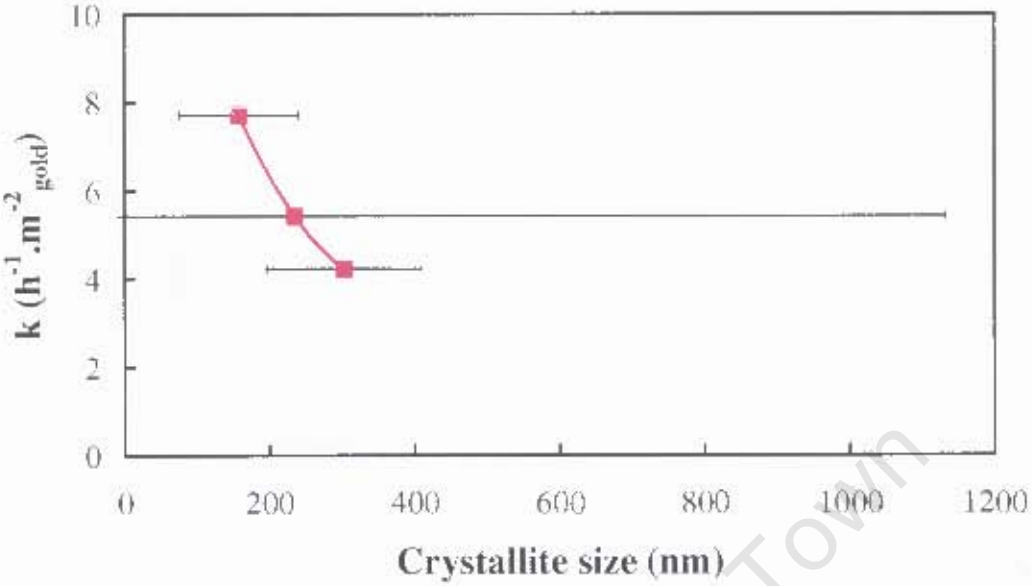

Figure 4.6: Rate constant per unit surface area of gold vs. gold crystallite size for the activated carbon catalysts

5 Conclusions

The gold crystallite size was affected by the pH and the support used during preparation. Smaller crystallites were obtained using a preparation pH of 4 compared to pH 2. The catalysts prepared using the $HAuCl_4$ precursor contained the largest crystallites. This is most likely caused by sintering during calcination and reduction due to the presence of the chlorine.

The catalysts produced using ion-exchange were active for glucose oxidation. Ion-exchange did produce very small and highly dispersed gold crystallites especially on the 6 hour acid treated nanotubes at a preparation pH of 4. The surface groups present on the support appear to affect the size of the crystallites obtained after calcination and reduction. More acidic functional groups such as –COOH seem to promote sintering during calcination.

The smaller gold crystallites were not as active as the larger crystallites for glucose oxidation. Crystallites below 5nm in size were not as active as crystallites between 5nm and 15nm in size. There appears to be optimum point of between 10nm and 15nm for the catalysts prepared on carbon nanotubes.

Oxygen chemisorption was attempted on the catalysts. However the crystallite sizes could not be determined with any degree of accuracy. Activated carbon appeared to adsorb oxygen. Oxygen chemisorption on the supports should be carried out in order to determine the oxygen uptake on the supports.

References

Andreeva D, 2002, 'Low Temperature Water Gas Shift over Gold Catalysts', *Gold Bulletin*, **35**, 3, 82-88

Azar M, Caps V, Morfin F, Rousset J, Piednoir A, Bertolini J, Piccolo L, 2006, 'Insights into activation, deactivation and hydrogen-induced promotion of a Au/TiO_2 reference catalyst in CO oxidation', *Journal of Catalysis*, **239**, 307-312

Baatz C, Prüße U, 2007, 'Preparation of gold catalysts for glucose oxidation', *Catalysis Today*, **249**, 34-40

Baatz C, Thielecke N, Prüße U, 2007, 'Influence of the preparation conditions on the properties of gold catalysts for the oxidation of glucose', *Applied Catalysis B: Environmental*, **70**, 653-660

Bailar JC, Emelius HJ, Nyholm R, Trotman-Dickenson AF, 1973, 'Comprehensive Inorganic Chemistry', Vol. 3, Pergamon Press, Oxford, 129-186

Barkhuizen D, Mabaso I, Viljoen E, Welker C, Claeys M, van Steen E, Fletcher JCQ, 2006, 'Experimental approaches to the preparation of supported metal nanoparticles', *Pure and Applied Chemistry*, **78**, 1759-1769

Bartholomew CH, 2001, 'Mechanisms of catalyst deactivation', *Applied Catalysis A: General*, **212**, 17-60

Bartlett N, 1998, 'Relativistic effects and the chemistry of gold', *Gold Bulletin*, **31**, 22-25

Bayler A, Schier A, Bowmaker GA, Schmidbaur H, 1996, 'Gold is smaller than silver. Crystal structures of [Bis(trimesitylphosphine)gold(I)] and [Bis(trimesitylphosphine)silver(I)] Tetrafluoroborate', *Journal of the American Chemical Society*, **118**, 7006-7007

Beeming BA, Bialek KH, 2006, 'Synthesis and Testing of Gold Catalysts Prepared by Ion-exchange', Undergraduate project, University of Cape Town

Beltrame P, Comotti M, Della Pina C, Rossi M, 2006, 'Aerobic oxidation of glucose II. Catalysis by colloidal gold', *Applied Catalysis A: General*, **297**, 1-7

Berndt H, Pitsch I, Evert S, Stuve K, Pohl M, Radnik J, Martin A, 2003, 'Oxygen adsorption on Au/Al_2O_3 catalysts and relation to the catalytic oxidation of ethylene glycol to glycolic acid', *Applied Catalysis A: General*, **244**, 169-179

Biella S, Prati L, Rossi M, 2002, 'Selective Oxidation of D-Glucose on Gold Catalyst', *Journal of Catalysis*, **206**, 242-247

Bollinger MA, Vannice MA, 1996, 'A kinetic and DRIFTS study of low-temperature carbon monoxide oxidation over $Au-TiO_2$ catalysts', *Applied Catalysis B: Environmental*, **8**, 417-443

Bond GC, Thompson DT, 1999, 'Catalysis by Gold', *Catalysis Review*, **41**, 3-4, 319-388

Bonivardi AL, Baltanás MA, 1990, 'Preparation of Pd/SiO_2 Catalysts for Methanol Synthesis I. Ion exchange of $[Pd(NH_3)_4](AcO)_2$', *Journal of Catalysis*, **125**, 243-259

Boyd D, Golunski S, Hearne GR, Magadzu T, Mallick K, Raphulu MC, Venugopal A, Scurrell MS, 2005, 'Reductive routes to stabilized nanogold and relation to catalysis by supported gold', *Applied Catalysis A: General*, **292**, 76-81

Broqvist P, Molina LM, Grönbeck H, Hammer B, 2004, 'Promoting and poisoning effects of Na and Cl coadsorption on CO oxidation over MgO-supported Au nanoparticles', *Journal of Catalysis*, **227**, 217-226

Brown SDM, Corio P, Marucci A, Pimenta MA, Dresselhaus MS, Dresselhaus G, 2000, 'Second-order Raman spectra of single-walled carbon nanotubes', *Physical Review B*, **61**, 7734-7742

Burda C, Chen X, Narayanan R, El-Sayed MA, 2005, 'Chemistry and properties of nanocrystals of different shapes', *Chemical Reviews*, **105**, 1025-1102

Chingombe P, Saha B, Wakeman RJ, 2005, 'Surface modification and characterisation of a coal-based activated carbon', *Carbon*, **43**, 3132-3143

Choudhary TV, Goodman DW, 2002, 'Oxidation catalysis by supported gold nano-clusters', *Topics in Catalysis*, **21**, 1-3, 25-34

Comotti M, Della Pina C, Falletta E, Rossi M, 2006, 'Is the biochemical route always advantageous? The case of glucose oxidation', *Journal of Catalysis*, **244**, 122-125

Comotti M, Della Pina C, Rossi M, 2006, 'Mono- and bimetallic catalysts for glucose oxidation', *Journal of Molecular Catalysis A: Chemical*, **251**, 89-92

Dastgheib SA, Karanfil T, 2004, 'Adsorption of oxygen by heat-treated granular and fibrous activated carbons', *Journal of Colloid and Interface Science*, **274**, 1-8

Debeila MA, Coville NJ, Scurrell MS, Hearne GR, 2005, 'The effect of calcination temperature on the adsorption of nitric oxide on Au-TiO_2: Drifts studies', *Applied Catalysis A: General*, **291**, 98-115

de Wilt HGJ, 1972, 'Part I. Oxidation of glucose to gluconic acid', *Industrial & Engineering Chemistry Product Research and Development*, **11**, 370-373

Dirkx JMH, van der Baan HS, 1981, 'The oxidation of glucose with platinum on carbon as catalyst', *Journal of Catalysis*, **67**, 1-13

Fierro-Gonzalez JC, Gates BC, 2007, 'Evidence of active species in CO oxidation catalyzed by highly dispersed supported gold', *Catalysis Today*, **122**, 201-210

Franceschetti A, Pennycook SJ, Pantelides ST, 2003, 'Oxygen chemisorption on Au nanoparticles', *Chemical Physics Letters*, **374**, 471-475

Fu Q, Saltsburg H, Flytzani-Stephanopoulos M, 2003, 'Active Nonmetallic Au and Pt Species on Ceria-Based Water-Gas Shift Catalysts', *Science*, **301**, 935-938

Fu Q, Deng W, Saltsburg H, Flytzani-Stephanopoulos M, 2005, 'Activity and stability of low-content gold-cerium oxide catalysts for the water-gas shift reaction', *Applied Catalysis B: Environmental*, **56**, 57-68

Fukushima T, Galvagno S, Parravano G, 1979, 'Oxygen chemisorption on supported gold', *Journal of Catalysis*, **57**, 177-182

Gluhoi AC, 2005, 'Fundamental studies focused on understanding of gold catalysis', PhD Thesis, Leiden University

Goguet A, Aouine M, Cadete Santos Aires FJ, Schweich D, Candy J-P, 2000, 'Silica grain labelling and EDX spectroscopy; evidence for inter-grain diffusion of $Pt(NH_3)_4^{2+}$ species during Pt/SiO_2 catalyst preparation by ionic exchange', *Chemical Communications*, 1417-1418

Gorin, DJ, Toste FD, 2007, 'Relativistic effects in homogeneous gold catalysis', *Nature*, **466**, 395-403

Haruta M, 2004, 'Gold as a Novel Catalyst in the 21st Century: Preparation, Working Mechanism and Applications', *Gold Bulletin*, **37**, 1-2, 27-36

Haruta M, 1997, 'Size- and support-dependency in the catalysis of gold', *Catalysis Today*, **36**, 153-166

Haruta M, Daté M, 2001, 'Advances in the catalysis of Au nanoparticles', *Applied Catalysis A: General*, **222**, 427-437

Haruta M, Yamada N, Kobayashi T, Iijima S, 1989, 'Gold Catalysts Prepared by Coprecipitation for Low-Temperature Oxidation of Hydrogen and of Carbon Monoxide', *Journal of Catalysis*, **115**, 301-309

Higby GJ, 1982, 'Gold in medicine: a review of its use in the west before 1900', *Gold Bulletin*, **15**, 130-140

Hoogenraad M, 1995, 'Growth and utilization of carbon fibrils', PhD Thesis, University Utrecht Netherlands

Hutchings GJ, 2007, 'A golden future for green chemistry', *Catalysis Today*, **122**, 196-200

Hutchings GJ, 1996, 'Catalysis: A Golden Future', *Gold Bulletin*, **29**, 4, 123-130

Hutchings GJ, 2005, 'Catalysis by Gold', *Catalysis Today*, **100**, 55-61

Hutchings GJ, 2002, 'Gold catalysis in chemical processing', *Catalysis Today*, **72**, 11-17

Hutchings GJ, Grady DT, 1985, 'Effect of drying conditions on carbon supported mercuric chloride catalysts', *Applied Catalysis*, **16**, 411-415

Hutchings GJ, Grady DT, 1985, 'Hydrochlorination of acetylene: The effect of mercuric chloride concentration on catalyst life', *Applied Catalysis*, **17**, 155-160

Jiang Q, Zhao Y, 2004, 'Effects of activation conditions on BET specific surface area of activated carbon nanotubes', *Microporous and Mesoporous Materials*, **76**, 215-219

Jorio A, Pimenta MA, Souza Filho AG, Saito R, Dresselhaus G, Dresselhaus MS, 2003, 'Characterizing carbon nanotube samples with resonance Raman scattering', *New Journal of Physics*, **5**, 139.1-139.17

Kim CH, Thompson LT, 2006, 'On the importance of nanocrystalline gold for Au/CeO_2 water-gas shift catalysts', *Journal of Catalysis*, **244**, 248-250

Kirk-Othmer, 1995, "Encyclopedia of Chemical Technology", 4th ed., Vol.13, Wiley, New York

Kleinsmidt JN, 2005, 'The Effect of Temperature and Crystallite Size on the Growth and Morphology of Carbon Nanotubes', Masters thesis, University of Cape Town

Kohler MA, Curry-Hyde HE, Hughes AE, Sexton BA, Cant NW, 1987, 'The structure of Cu/SiO_2 catalysts prepared by the ion-exchange technique', *Journal of Catalysis*, **108**, 323-333

Kohler MA, Lee JC, Trimm DL, Cant NW, Wainwright MS, 1987, 'Preparation of Cu/SiO_2 catalysts by the ion-exchange technique', *Applied Catalysis*, **31**, 309-321

Kongolo K, Kinabo C, Bahr A, 1997, 'Electrophoretic studies of the adsorption of gold and silver from aqueous cyanide solutions onto activated carbon', *Hydrometallurgy*, **44**, 191-202

Lagowski JJ, 1983, 'Anionic gold', *Gold Bulletin*, **16**, 8-11

Lee S, Gavriilidis A, 2002, 'Supported Au Catalysts for Low-Temperature CO Oxidation Prepared by Impregnation', *Journal of Catalysis*, **206**, 305-313

Lee SM, Lee SC, Jung JH, Kim HJ, 2005, 'Pore characterization of multi-walled carbon nanotubes modified by KOH', *Chemical Physics Letters*, **416**, 251-255

Lee W, Wan B, Kuo C, Lee W, Cheng S, 2007, 'Maintaining catalytic activity of Au/TiO_2 during the storage at room temperature', *Catalysis Communications*, **8**, 1604-1608

Leofanti G, Padovan M, Tozzola G, Venturelli B, 1998, 'Surface area and pore texture of catalysts', *Catalysis Today*, **41**, 207-219

Li W, Comotti M, Schüth F, 2006, 'Highly reproducible syntheses of active Au/TiO_2 catalysts for CO oxidation by deposition-precipitation or impregnation', *Journal of Catalysis*, **237**, 190-196

Lichtenthaler FW, 2002, 'Unsaturated O- and N-Heterocycles from carbohydrate feedstocks', *Accounts of Chemical Research*, **35**, 728-737

Link S, El-Sayed MA, 2000, 'Shape and size dependence of radiative, non-radiative and photothermal properties of gold nanocrytals', *International Reviews in Physical Chemistry*, **19**, 409-453

Link S, El-Sayed MA, 1999, 'Size and temperature dependence of the Plasmon absorption of colloidal gold nanoparticles', *Journal of Physical Chemistry B*, **103**, 4212-4217

Liu Y, Gao L, 2005, 'A study of the electrical properties of carbon nanotube-$NiFe_2O_4$ composites: Effect of the surface treatment of the carbon nanotubes', *Carbon*, **43**, 47-52

Ma X, Li X, Lun N, Wen S, 2006, 'Synthesis of gold nano-catalysts supported on carbon nanotubes by using electroless plating technique', *Materials Chemistry and Physics*, **97**, 351-356

Maultzsch J, Reich S, Thomsen C, 2001, 'Chirality-selective Raman scattering of the D mode in carbon nanotubes', *Physical Review B*, **64**, 121407-1 – 121407-4

Menegazzo F, Manzoli M, Chiorino A, Boccuzzi F, Tabakova T, Signoretto M, Pinna F, Pernicone N, 2006, 'Quantitative determination of gold active sites by chemisorption and by infrared measurements of adsorbed CO', *Journal of Catalysis*, **237**, 431-434

Meyer R, Lemire C, Shaikhutdinov ShK, Freund H-J, 2004, 'Surface chemistry of catalysis by gold', *Gold Bulletin*, **37**, 73-124

Min BK, Wallace WT, Goodman DW, 2006, 'Support effects on the nucleation, growth, and morphology of gold nano-clusters', *Surface Science*, **600**, L7-L11

Mirescu A, Prüße U, 2007, 'A new environmentally friendly method for the preparation of suger acids via catalytic oxidation on gold catalysts', *Applied Catalysis B: Environmental*, **70**, 644-652

Moreau F, Bond GC, 2007, 'Influence of the surface area of the support on the activity of gold catalysts for CO oxidation', *Catalysis Today*, **122**, 215-221

Moreau F, Bond GC, 2007, 'Preparation and reactivation of Au/TiO_2 catalysts', *Catalysis Today*, **122**, 260-265

Ning G, Wei F, Luo G, Jin Y, 2005, 'Online BET analysis of single-wall carbon nanotube growth and its effect on catalyst reactivation', *Carbon*, **43**, 1439-1444

Nirmala Grace A, Pandian K, 2007, 'Organically dispersible gold and platinum nanoparticles using aromatic amines as phase transfer and reducing agent and their applications in electro-oxidation of glucose', *Colloids and Surfaces A*, **302**, 113-120

Niu JJ, Wang JN, 2008, 'Effect of temperature on chemical activation of carbon nanotubes', *Solid State Sciences*, article in press

Odom TW, Huang J, Kim P, Lieber CM, 2000, 'Structure and Electronic Properties of Carbon Nanotubes', *Journal of Physical Chemistry B*, **104**, 2794-2809

Oh H, Yang JH, Costello CK, Wang YM, Bare SR, Kung HH, Kung MC, 2002, 'Selective Catalytic Oxidation of CO: Effect of Chloride on Supported Au Catalysts', *Journal of Catalysis*, **210**, 375-386

Okumura M, Tanaka K, Ueda A, Haruta M, 1997, 'The reactivities of dimethylgold(III)β-diketone on the surface of TiO_2', *Solid State Ionics*, **95**, 143-149

Okumura M, Tsubota S, Haruta M, 2003, 'Preparation of supported gold catalysts by gas-phase grafting of gold acethylacetonate for low-temperature oxidation of CO and of H_2', *Journal of Molecular Catalysis A: Chemical*, **199**, 73-84

Önal Y, Schimpf S, Claus P, 2004, 'Structure sensitivity and kinetics of D-glucose oxidation to D-gluconic acid over carbon-supported gold catalysts', *Journal of Catalysis*, **223**, 122-133

Parish RV, 1997, 'Organogold Chemistry: I Structure and Synthesis', *Gold Bulletin*, **30**, 1, 3-12

Parish RV, 1998, 'Organogold Chemistry: III Applications', *Gold Bulletin*, **31**, 1, 14-21

Parkes G D, 1960, 'Mellor's Modern Inorganic Chemistry', Revised Edition, Longmans Green and Co., London, 633-642

Phala NS, Klatt G, van Steen E, French SA, Sokol AA, Catlow CRA, 2005, 'The nature of the oxidation states of gold on ZnO', *Physical Chemistry and Chemical Physics*, **7**, 2440-2445

Phala NS, van Steen E, 2007, 'Intrinsic reactivity of gold nanoparticles: classical, semi-empirical and DFT studies', *Gold Bulletin*, **40**, 150-153

Popp A, 2004, 'Preparation and characterisation of a series of gold-based catalysts for methanol synthesis', Project, University of Cape Town

Prado-Burguete C, Linares-Solano A, Rodríguez-Reinoso F, Salinas-Martínez de Lecea C, 1989, 'The effect of Oxygen Surface Groups of the Support on Platinum Dispersion in Pt/Carbon Catalysts', *Journal of Catalysis*, **115**, 98-106

Prati L, Martra G, 1999, 'New Gold Catalysts for Liquid Phase Oxidation', *Gold Bulletin*, **32**, 3, 96-101

Prinsloo FF, 2000, 'Fischer-Tropsch synthesis over carbon nanotube supported iron catalysts', Masters thesis, University of Cape Town

Puddephatt RJ, 1978, 'The chemistry of gold', Elsevier Scientific Publishing Company, Amsterdam, 7-9

Qiu Y, Cheng H, Xu C, Sheng GD, 2008, 'Surface characteristics of crop-residue-derived black carbon and lead(II) adsorption', *Water Research*, **42**, 567-574

Ramachandran S, Fontanille P, Pandey A, Larroche C, 2006, 'Gluconic acid: Properties, applications and microbial production', *Food Technology and Biotechnology*, **44**, 185-195

Rodríguez-Reinoso F, 1998, 'The role of carbon materials in heterogeneous catalysis', *Carbon*, **36**, 3, 159-175

Rosca ID, Watari F, Uo M, Akasaka T, 2005, 'Oxidation of multiwalled nanotubes by nitric acid', *Carbon*, **43**, 3124-3131

Schmidbaur H, Cronje S, Djordjevic B, Schuster O, 2005, 'Understanding gold chemistry through relativity', *Chemical Physics*, **311**, 151-161

Schubert MM, Hackenberg S, van Veen A, Muhler M, Plzak V, Behm J, 2001, 'CO Oxidation over Supported Gold Catalysts – "Inert" and "Active" Support Materials and Their Role for the Oxygen Supply during Reaction', *Journal of Catalysis*, **197**, 113-122

Shastri AG, Datye AK, Schwank J, 1984, 'Gold-titania interactions: Temperature dependence of surface area and crystallinity of TiO_2 and gold dispersion', *Journal of Catalysis*, **87**, 265-275

Simakov A, Tuzovskaya I, Pestryakov A, Bogdanchikova N, Gurin V, Avalos M, Farías, MH, 2007, 'On the nature of active gold species in zeolites in CO oxidation', *Applied Catalysis A: General*, **331**, 121-128

Skibsted L H, Bjurrum J, 1974, 'Studies on Gold Complexes. I. Robustness, Stability and Acid Dissociation of the Tetramminegold(III) ion', *Acta Chemica Scandinavica A*, **28(7)**, 740-746

Solsona BE, Garcia T, Jones C, Taylor SH, Carley AF, Hutchings GJ, 2006, 'Supported gold catalysts for the total oxidation of alkanes and carbon monoxide', *Applied Catalysis A: General*, **312**, 67-76

Thielecke N, Aytemir M, Prüße U, 2007, 'Selective oxidation of carbohydrates with gold catalysts: Continuous-flow reactor system for glucose oxidation', *Catalysis Today*, **121**, 115-120

Thielecke N, Vorlop K, Prüße U, 2007, 'Long-term stability of an Au/Al_2O_3 catalyst prepared by incipient wetness in continuous-flow glucose oxidation', *Catalysis Today*, **122**, 266-269

Thompson D, 1998, 'New Advances in Gold catalysis Part I', *Gold Bulletin*, **31**, 4, 111-118

Titus E, Cabral G, Madaleno JC, Neto VF, Shokuhfar T, Blau WJ, Ramesh Babu P, Misra DS, Gracio J, 2007, 'Synthesis of highly oriented carbon nanotube thin films by nickel functionalisation', *Diamond and Related Materials*, **16**, 1195-1199

Ueda A, Haruta M, 1999, 'Nitric Oxide Reduction with Hydrogen, Carbon Monoxide, and Hydrocarbons over Gold Catalysts', *Gold Bulletin*, **32**, 1, 3-11

Ullman's Encyclopedia of Industrial Chemistry, 6th Edition, Vol. 16, 2003, Wiley-VCH, Weinheim, 1-25

Valden M, Pak S, Lai X, Goodman DW, 1998, 'Structure sensitivity of CO oxidation over model Au/TiO_2 catalysts', *Catalysis Letters*, **56**, 7-10

Wang GY, Zhang WX, Lian HL, Jiang DZ, Wu TH, 2003, 'Effect of calcination temperatures and precipitant on the catalytic performance of Au/ZnO catalysts for CO oxidation at ambient temperature and in humid circumtances', *Applied Catalysis A: General*, **239**, 1-10

Webb PA, Orr C, 1997, 'Analytical Methods in Fine Particle Technology', 1st Edition, Micromeritics Instruments Corp., Norcross, 53-69, 155-189, 226-227

Wolf A, Schüth F, 2002, 'A systematic study of the synthesis conditions for the preparation of highly active gold catalysts', *Applied Catalysis A: General*, **226**, 1-13

Yuan Y, Kozlova AP, Asakura K, Wan H, Tsai K, Iwasawa Y, 1997, 'Supported Au Catalysts Prepared from Au Phosphine Complexes and As-Precipitated Metal Hydroxides: Characterization and Low-Temperature CO oxidation', *Journal of Catalysis*, **170**, 191-199

Zanella R, Giorgio S, Henry CR, Louis C, 2002, 'Alternative Methods for the Preparation of Gold Nanoparticles Supported on TiO_2', *Journal of Physical Chemistry B*, **106**, 7634-7642

Zanella R, Louis C, 2005, 'Influence of the conditions of thermal treatments and of storage on the size of the gold particles in Au/TiO_2 samples', *Catalysis Today*, **107-108**, 768-777

Zou X, Qi S, Suo Z, An L, Li F, 2007, Activity and deactivation of Au/Al_2O_3 catalyst for low-temperature CO oxidation', *Catalysis Communications*, **8**, 784-788

6 Appendices

Appendix A: Support treatment and characterisation

Sample calculation for nanotube wall thickness

Using the untreated nanotubes:

Number of tubes measured for outer diameter: $N_{Tubes\ outer} = 34$

Number of tubes measured for inner diameter: $N_{Tubes\ inner} = 55$

Tube Diameters:

Outer Diameter	Inner Diameter
d_{OD}	d_{ID}
nm	nm
67.43738532	31.35330296
60.07958716	36.21867882
75.78669725	40.25649203
60.61307339	117.0444191
158.9731651	37.45740319
56.65555556	27.52121771
48.71481481	24.21494465
45.20925926	27.00645756
37.03703704	27.52121771
50.95925926	27.14760148
54.46481481	25.1798893
64.68240741	28.22324723
44.54074074	19.01845018
41.37777778	33.32564576
104.7564815	30.34501845
93.81111111	15.01752768
51.92592593	22.29335793
59.28796296	26.09225092
90.34814815	18.92804428
51.86018519	28.29889299
48.52037037	17.74446494
21.11481481	19.72140221

72.06759259	19.91420664
50.11111111	23.62730627
63.9962963	38.7998155
41.77962963	31.98339483
52.05833333	24.83948339
50.39259259	27.42804428
72.60092593	23.06273063
60.32037037	21.51660517
65.375	28.29889299
49.5	29.53505535
64.2037037	25.84686347
72.73055556	25.1798893
	27.13191882
	26.25461255
	27.9197417
	23.35608856
	18.92804428
	21.61531365
	44.35701107
	33.92066421
	56.93450185
	7.935424354
	42.01199262
	48.92804428
	52.83302583
	7.380073801
	17.81642066
	14.7601476
	19.74261993
	38.22601476
	21.21771218
	29.75
	33.26199262

Finding the geometric mean diameters:

$$R_g = \sqrt[n]{(1 + d_1)(1 + d_2)\ldots(1 + d_n)} - 1$$

Where:

R_g Geometric mean diameter

n Number of tubes measured

d Diameter of a single tube

The wall thickness was calculated as the geometric mean outer diameter less the geometric mean inner diameter

	Outer Diameter	Inner Diameter	Wall Thickness
Count (n)	34	55	
Geometric mean (nm)	58.33633	26.68678	15.82478

BJH pore size distribution calculation from N_2 physisorption data

Thickness of the adsorbed layer remaining on the pore walls is given by:

$$t = \left(\frac{13.99}{0.034 - \log\left(\frac{P}{P_0}\right)} \right)^{\frac{1}{2}}$$

Where:

t Thickness of adsorbed layer

P/P_0 Relative pressure

The pore radius is calculated as follows:

$$\ln\left(\frac{P}{P_0}\right) = -\left[\frac{2 \cdot \gamma \cdot \upsilon \cdot \cos(\theta)}{R \cdot T \cdot (r - t)}\right]$$

Where:

γ Liquid surface tension

ν Molar volume of condensed adsorptive

θ Contact angle between solid and condensed phase

R Universal gas constant

T temperature

r Pore radius assuming cylindrical pores

Data for N_2 physisorption on untreated carbon nanotubes:

Average Pore Diameter		dD	Incremental Pore Volume (dV)		
Å	nm	nm	cm3/g	d(ln(V))	d(ln(V))/dD
1400.3	140.03		0.146396	-1.92144	
1106.8	110.68	29.35	0.009432	-4.6636471	0.158897687
1043.4	104.34	6.34	0.006044	-5.1086892	0.805786946
1009.5	100.95	3.39	0.004937	-5.3109974	1.566665906
934	93.4	7.55	0.010684	-4.539008	0.60119311
813.3	81.33	12.07	0.015467	-4.1690466	0.34540568
685	68.5	12.83	0.016859	-4.0828706	0.318228421
566.9	56.69	11.81	0.018404	-3.9951872	0.338288505
464.6	46.46	10.23	0.018691	-3.9797132	0.389023769
383.9	38.39	8.07	0.016254	-4.1194162	0.510460501
318.8	31.88	6.51	0.012598	-4.3742172	0.671922766
264.5	26.45	5.43	0.009431	-4.6637531	0.858886398
216.3	21.63	4.82	0.007578	-4.882506	1.012968043
171.9	17.19	4.44	0.006583	-5.0232647	1.131365926
136.7	13.67	3.52	0.005063	-5.2857961	1.501646615
110	11	2.67	0.004119	-5.4921449	2.056983095
85.9	8.59	2.41	0.004501	-5.4034557	2.242097794
64.4	6.44	2.15	0.004757	-5.3481381	2.487506075
49.1	4.91	1.53	0.003459	-5.6667757	3.703774999
38.7	3.87	1.04	0.002922	-5.835487	5.611045159
31.2	3.12	0.75	0.004179	-5.4776833	7.303577727
27.5	2.75	0.37	0.002511	-5.9870742	16.18128162
26	2.6	0.15	0.001007	-6.9007797	46.00519777
24.1	2.41	0.19	0.003151	-5.7600354	30.31597587
21.8	2.18	0.23	0.001431	-6.5493818	28.47557295
19.9	1.99	0.19	0.000426	-7.7610712	40.84774322

Mercury pycnometry calculations

The pore diameters are calculated as follows:

$$D = \frac{-4 \cdot \gamma \cdot \cos(\theta)}{P}$$

Where:

D	Pore diameter
γ	Surface tension of mercury (485dyn/cm)
θ	Contact angle (130°)
P	Applied pressure

The bulk density of the sample was calculated as follows:

$$\rho_{bulk} = \frac{W_s}{V_p - V_{Hg}}$$

Where:

ρ_{bulk}	Bulk density
W_s	Mass sample
V_p	Volume of empty penetrometer
V_{Hg}	Volume of mercury

The skeletal density of the sample is given by:

$$\rho_{skeletal} = \frac{W_s}{V_{se} - V}$$

Where:

$P_{skeletal}$	Skeletal density

W_s Mass sample

V_{se} Volume of penetrometer less the volume of the mercury

V Total volume of mercury filling the pores

And the porosity of defined as follows:

$$\text{Porosity} = \left(1 - \frac{\rho_{bulk}}{\rho_{skeletal}}\right) \cdot 100$$

The total pore area is calculated as follows:

$$A = \frac{4 \cdot V}{D_m}$$

Where D_m is the mean pore diameter.

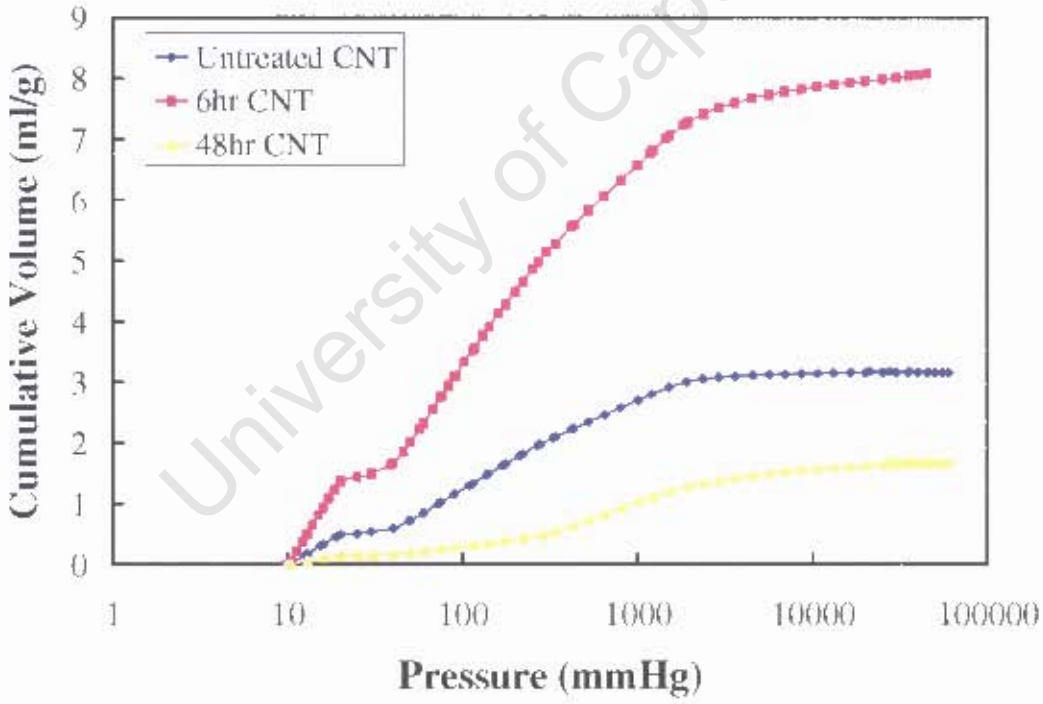

Figure 6.1: Cumulative mercury intrusion vs. pressure

Infrared spectra of the supports

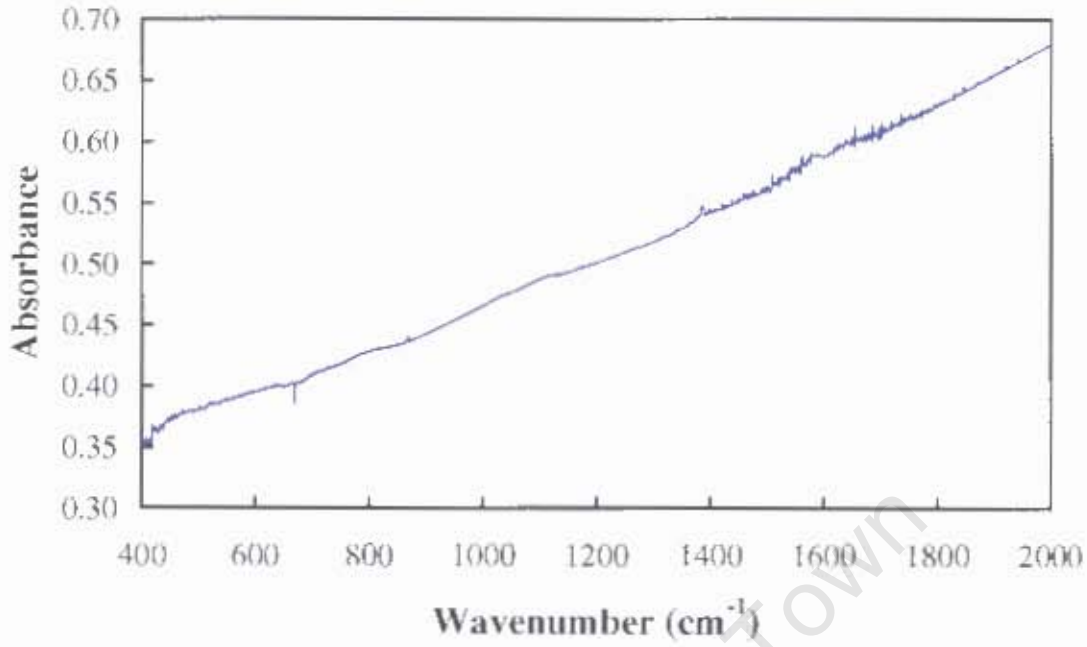

Figure 6.2: Infrared spectra of untreated carbon nanotubes

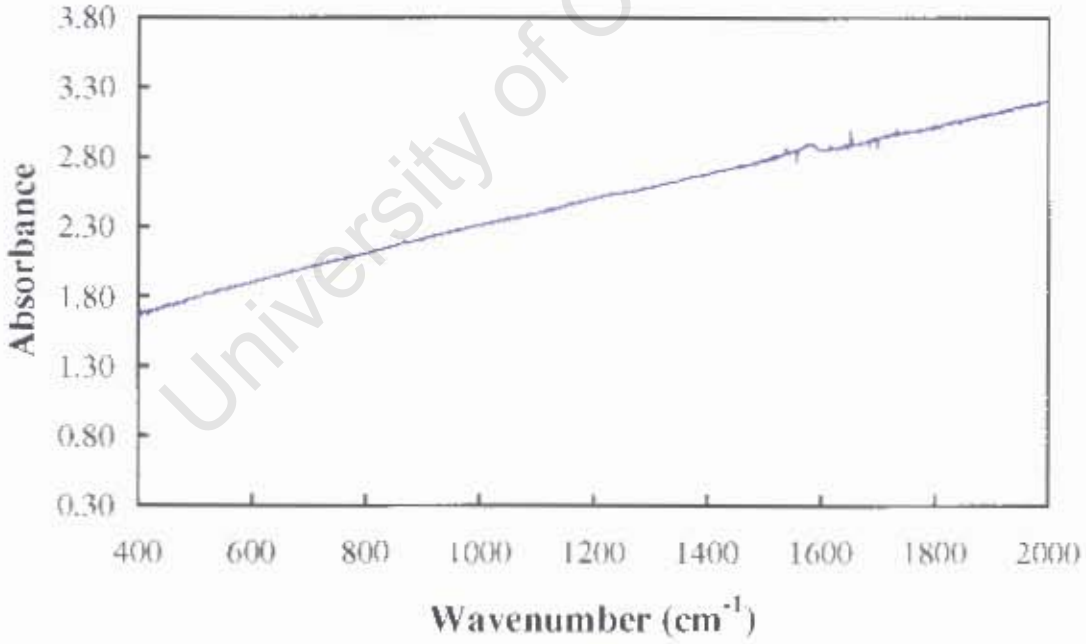

Figure 6.3: Infrared spectra of 6 hour treated carbon nanotubes

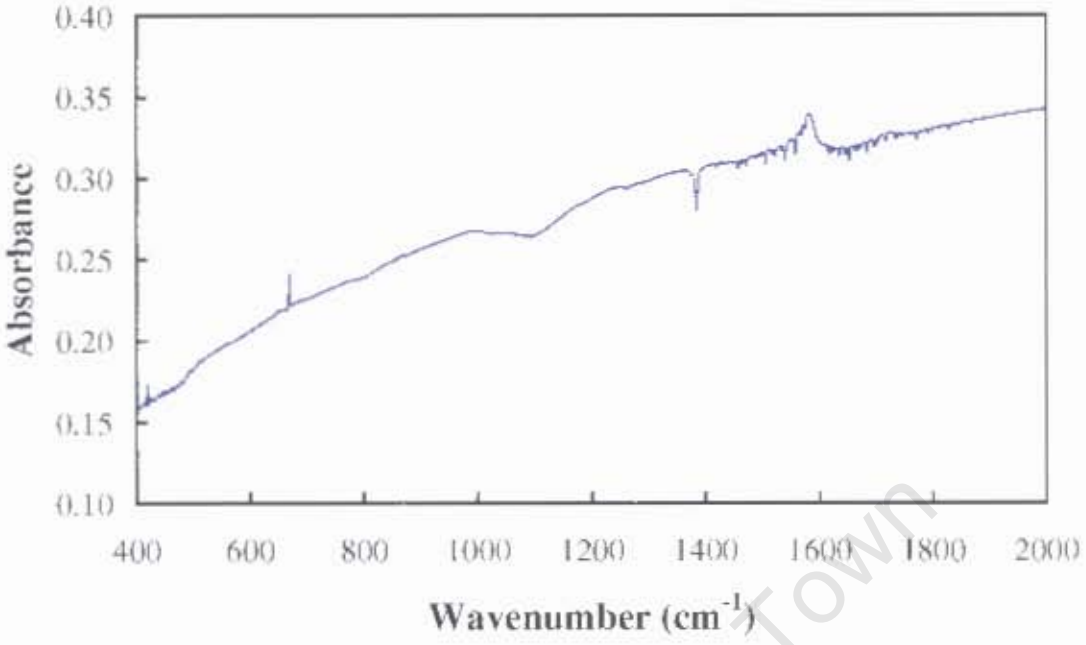

Figure 6.4: Infrared spectra of 48 hour treated carbon nanotubes

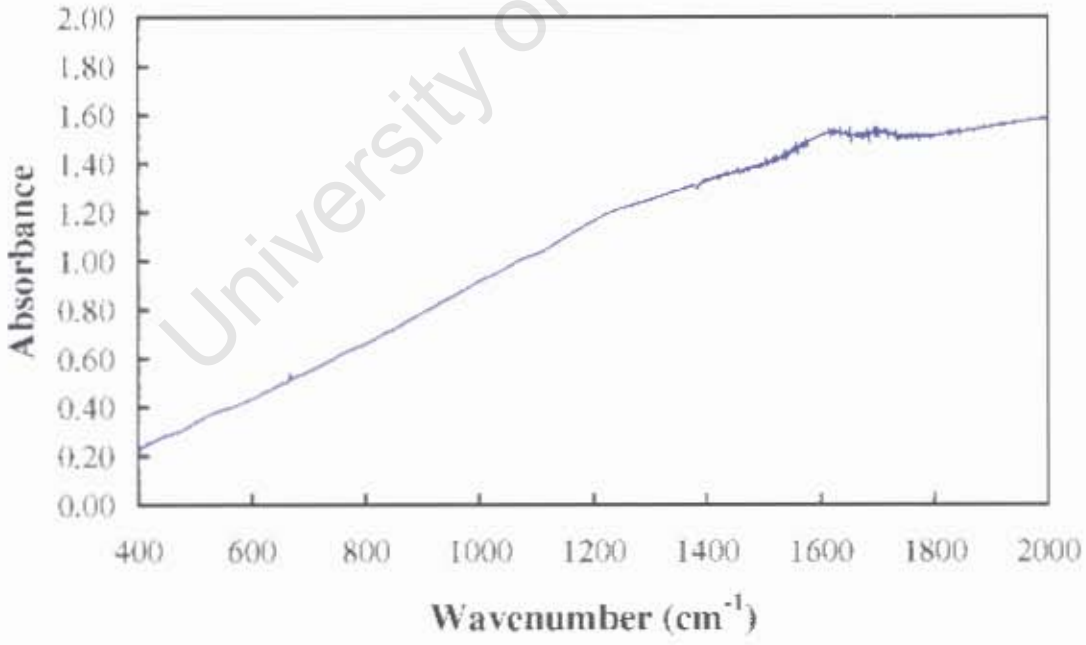

Figure 6.5: Infrared spectra of activated carbon

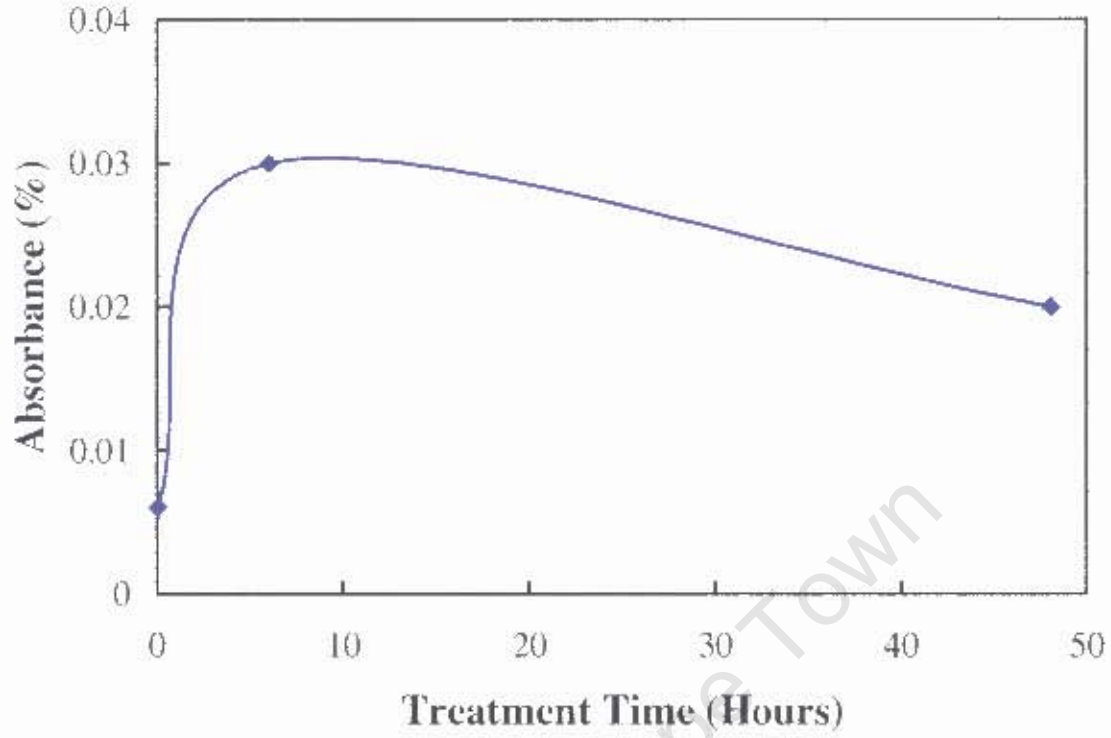

Figure 6.6: Absorbances for the stretching mode of carboxyl groups on the surface of the carbon nanotubes

Raman Spectra of the Carbon Nanotubes

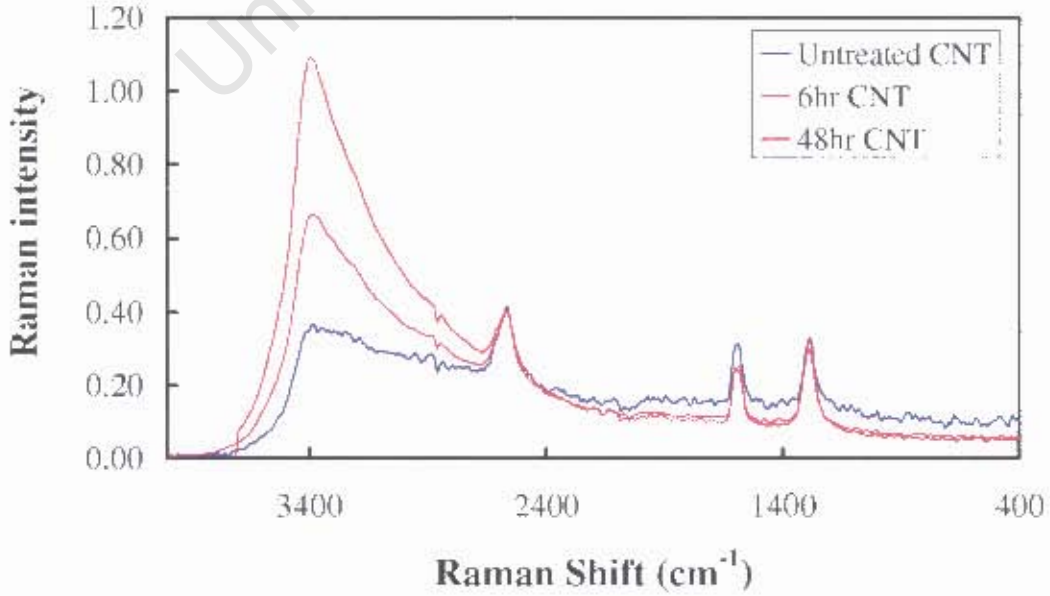

Figure 6.7: The Raman spectra for the untreated and boiled carbon nanotubes

Appendix B: Preparation of tetramminegold (III) nitrate

TAGN preparation 1 - Gold balance

GOLD IN:	Liquid volume: HAuCl4	10
	Au conc: HAuCl4 (g/l)	50
	Total Au in (g)	**0.50**
GOLD OUT:	Mass TAGN in AAS sample (g)	0.0552
	Liquid volume of AAS sample (ml)	70.0
	AAS result: Au conc in liquid sample (mg/l)	197.0
	Au content of TAGN (wt%)	24.98
	Mass TAGN produced(g)	1.355
	Total Au in TAGN produced (g)	0.3384
	Liquid volume filtrate (ml)	145
	AAS result: Au conc in liquid sample (mg/l)	578
	Total Au in filtrate (g)	0.08381
	Total Au out (g)	**0.422**

TAGN preparation 2 - Gold balance

GOLD IN:	Liquid volume: HAuCl4	10
	Au conc: HAuCl4 (g/l)	50
	Total Au in (g)	**0.50**
GOLD OUT:	Mass TAGN in AAS sample (g)	0.0542
	Liquid volume of AAS sample (ml)	70.0
	AAS result: Au conc in liquid sample (mg/l)	190.89
	wt% Au in TAGN	24.65
	Mass TAGN (g)	1.432
	Total Au in TAGN produced (g)	0.3529
	Liquid volume filtrate (ml)	143
	AAS result: Au conc in liquid sample (mg/l)	1209.98
	Total Au in filtrate (g)	0.17303
	Total Au out (g)	**0.526**

TAGN preparation 3 - Gold balance

GOLD IN:	Liquid volume: HAuCl4	10
	Au conc: HAuCl4 (g/l)	50
	Total Au in (g)	**0.50**
GOLD OUT:	Mass TAGN in AAS sample (g)	0.0474
	Liquid volume of AAS sample (ml)	70.0
	AAS result: Au conc in liquid sample (mg/l)	99.80
	wt% Au in TAGN	14.74
	Mass TAGN (g)	2.193
	Total Au in TAGN produced (g)	0.3232
	Liquid volume filtrate (ml)	140
	AAS result: Au conc in liquid sample (mg/l)	889.81
	Total Au in filtrate (g)	0.12457
	Total Au out (g)	**0.448**

Appendix C: Preparation of gold on carbon catalysts

Catalyst 1 preparation - Gold balance.

Loading aim:	5 wt%	**Preparation pH:**	4
Precursor:	TAGN		

GOLD IN:	Mass TAGN	0.5999
	wt% Au in TAGN	24.98
	Total Au in (g)	**0.150**
GOLD OUT:	**Filtrate**	
	Liquid volume of filtrate (ml)	1500
	AAS result: Au conc in liquid sample (mg/l)	98.9
	Total Au in filtrate (g)	0.1484
	Ethanol wash	
	Liquid volume of ethanol wash (ml)	28.5
	AAS result: Au conc in liquid sample (mg/l)	6.84
	Total Au in ethanol wash (g)	1.95E-04
	Catalyst	
	Mass catalyst in AAS sample (g)	0.104
	Liquid volume of AAS sample (ml)	45
	AAS result: Au conc in liquid sample (mg/l)	11.84
	Au content of catalyst (wt%)	0.514
	Mass catalyst produced (g)	1.421
	Total Au in catalyst (g)	0.007
	Total Au out (g)	**0.156**

Catalyst 2 preparation - Gold balance.

Loading aim:	5 wt%	**Preparation pH:**	2
Precursor:	TAGN	**Support:**	6h nanotubes

GOLD IN:	Mass TAGN	0.4862
	wt% Au in TAGN	24.98
	Total Au in (g)	**0.1215**

GOLD OUT:	**Filtrate**	
	Liquid volume of filtrate (ml)	985
	AAS result: Au conc in liquid sample (mg/l)	123.0
	Total Au in filtrate (g)	0.1212
	Ethanol wash	
	Liquid volume of ethanol wash (ml)	25.4
	AAS result: Au conc in liquid sample (mg/l)	9.34
	Total Au in ethanol wash (g)	2.37E-04
	Catalyst	
	Mass catalyst in AAS sample (g)	0.0998
	Liquid volume of AAS sample (ml)	45
	AAS result: Au conc in liquid sample (mg/l)	14.94
	Au content of catalyst (wt%)	0.674
	Mass catalyst produced (g)	1.762
	Total Au in catalyst (g)	0.012
	Total Au out (g)	**0.133**

Catalyst 3 preparation - Gold balance.

Loading aim:	5 wt%	**Preparation pH:**	1
Precursor:	HAuCl4	**Support:**	6h nanotubes

GOLD IN:	Vol HAuCl4 (ml)	5
	Au content of HAuCl4 (g/l)	50.0
	Total Au in (g)	**0.25**

GOLD OUT:	**Filtrate**	
	Liquid volume of filtrate (ml)	385
	AAS result: Au conc in liquid sample (mg/l)	538.0
	Total Au in filtrate (g)	0.2071
	Ethanol wash	
	Liquid volume of ethanol wash (ml)	12.6
	AAS result: Au conc in liquid sample (mg/l)	354
	Total Au in ethanol wash (g)	4.46E-03
	Catalyst	
	Mass catalyst in AAS sample (g)	0.0798
	Liquid volume of AAS sample (ml)	45
	AAS result: Au conc in liquid sample (mg/l)	17.05
	Au content of catalyst (wt%)	0.961
	Mass catalyst produced (g)	3.813
	Total Au in catalyst (g)	0.037
	Total Au out (g)	**0.248**

Catalyst 4 preparation - Gold balance.

Loading aim:	5 wt%	**Preparation pH:**	4	
Precursor:	TAGN	**Support:**	48h nanotubes	
GOLD IN:	Mass TAGN			0.4004
	wt% Au in TAGN			24.65
	Total Au in (g)			**0.099**

GOLD OUT:	**Filtrate**	
	Liquid volume of filtrate (ml)	893
	AAS result: Au conc in liquid sample (mg/l)	65.4
	Total Au in filtrate (g)	0.0584
	Ethanol wash	
	Liquid volume of ethanol wash (ml)	9.6
	AAS result: Au conc in liquid sample (mg/l)	24.5
	Total Au in ethanol wash (g)	2.35E-04
	Catalyst	
	Mass catalyst in AAS sample (g)	0.085
	Liquid volume of AAS sample (ml)	45
	AAS result: Au conc in liquid sample (mg/l)	14.23
	Au content of catalyst (wt%)	0.752
	Mass catalyst produced (g)	1.963
	Total Au in catalyst (g)	0.015
	Total Au out (g)	**0.073**

Catalyst 5 preparation - Gold balance.

Loading aim:	5 wt%	**Preparation pH:**	2	
Precursor:	TAGN	**Support:**	48h nanotubes	
GOLD IN:	Mass TAGN			0.4199
	wt% Au in TAGN			24.65
	Total Au in (g)			**0.104**

GOLD OUT:	**Filtrate**	
	Liquid volume of filtrate (ml)	877
	AAS result: Au conc in liquid sample (mg/l)	71.0
	Total Au in filtrate (g)	0.0623
	Ethanol wash	
	Liquid volume of ethanol wash (ml)	17.5
	AAS result: Au conc in liquid sample (mg/l)	20.9
	Total Au in ethanol wash (g)	3.66E-04
	Catalyst	
	Mass catalyst in AAS sample (g)	0.062
	Liquid volume of AAS sample (ml)	45
	AAS result: Au conc in liquid sample (mg/l)	20.7
	Au content of catalyst (wt%)	1.498
	Mass catalyst produced (g)	1.826
	Total Au in catalyst (g)	0.027
	Total Au out (g)	**0.090**

Catalyst 6 preparation - Gold balance.					
Loading aim:	5 wt%	**Preparation pH:**	1		
Precursor:	HAuCl4	**Support:**		48h nanotubes	
GOLD IN:	Vol HAuCl4 (ml)				5
	Au content of HAuCl4 (g/l)				50.0
	Total Au in (g)				**0.25**
GOLD OUT:	**Filtrate**				
	Liquid volume of filtrate (ml)				380
	AAS result: Au conc in liquid sample (mg/l)				471.3
	Total Au in filtrate (g)				0.1791
	Ethanol wash				
	Liquid volume of ethanol wash (ml)				9.8
	AAS result: Au conc in liquid sample (mg/l)				13.9
	Total Au in ethanol wash (g)				1.36E-04
	Catalyst				
	Mass catalyst in AAS sample (g)				0.1009
	Liquid volume of AAS sample (ml)				45
	AAS result: Au conc in liquid sample (mg/l)				52.5
	Au content of catalyst (wt%)				2.341
	Mass catalyst produced (g)				2.743
	Total Au in catalyst (g)				0.064
	Total Au out (g)				**0.243**

Catalyst 7 preparation - Gold balance.					
Loading aim:	5 wt%	**Preparation pH:**	1		
Precursor:	HAuCl4	**Support:**		AC	
GOLD IN:	Vol HAuCl4 (ml)				385
	Au content of HAuCl4 (mg/l)				538.0
	Total Au in (g)				**0.21**
GOLD OUT:	**Filtrate**				
	Liquid volume of filtrate (ml)				387
	AAS result: Au conc in liquid sample (mg/l)				33.8
	Total Au in filtrate (g)				0.0131
	Ethanol wash				
	Liquid volume of ethanol wash (ml)				13.0
	AAS result: Au conc in liquid sample (mg/l)				4.65
	Total Au in ethanol wash (g)				6.05E-05
	Catalyst				
	Mass catalyst in AAS sample (g)				0.0602
	Liquid volume of AAS sample (ml)				45
	AAS result: Au conc in liquid sample (mg/l)				32.91
	Au content of catalyst (wt%)				2.460
	Mass catalyst produced (g)				3.671
	Total Au in catalyst (g)				0.090
	Total Au out (g)				**0.103**

Catalyst 8 preparation - Gold balance.

Loading aim:	5 wt%	**Preparation pH:**	4
Precursor:	TAGN	**Support:**	Activated Carbon

GOLD IN:	Mass TAGN	0.4056
	wt% Au in TAGN	14.70
	Total Au in (g)	**0.060**

GOLD OUT:	**Filtrate**	
	Liquid volume of filtrate (ml)	895
	AAS result: Au conc in liquid sample (mg/l)	0.12
	Total Au in filtrate (g)	0.0001
	Ethanol wash	
	Liquid volume of ethanol wash (ml)	13.4
	AAS result: Au conc in liquid sample (mg/l)	0.71
	Total Au in ethanol wash (g)	9.51E-06
	Catalyst	
	Mass catalyst in AAS sample (g)	0.118
	Liquid volume of AAS sample (ml)	45
	AAS result: Au conc in liquid sample (mg/l)	25.98
	Au content of catalyst (wt%)	0.989
	Mass catalyst produced (g)	1.546
	Total Au in catalyst (g)	0.015
	Total Au out (g)	**0.015**

Catalyst 9 preparation - Gold balance.

Loading aim:	5 wt%	**Preparation pH:**	2
Precursor:	TAGN	**Support:**	Activated Carbon

GOLD IN:	Mass TAGN	0.4092
	wt% Au in TAGN	14.70
	Total Au in (g)	**0.060**

GOLD OUT:	**Filtrate**	
	Liquid volume of filtrate (ml)	888
	AAS result: Au conc in liquid sample (mg/l)	2.6
	Total Au in filtrate (g)	0.0023
	Ethanol wash	
	Liquid volume of ethanol wash (ml)	20.3
	AAS result: Au conc in liquid sample (mg/l)	0.08
	Total Au in ethanol wash (g)	1.62E-06
	Catalyst	
	Mass catalyst in AAS sample (g)	0.0995
	Liquid volume of AAS sample (ml)	45
	AAS result: Au conc in liquid sample (mg/l)	26.66
	Au content of catalyst (wt%)	1.206
	Mass catalyst produced (g)	1.643
	Total Au in catalyst (g)	0.020
	Total Au out (g)	**0.022**

Sample TEM images of the catalysts

Catalyst 1:

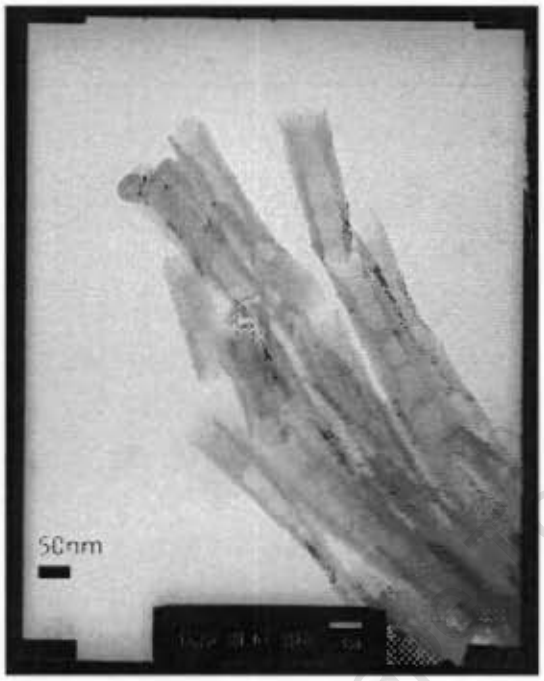

Catalyst 2:

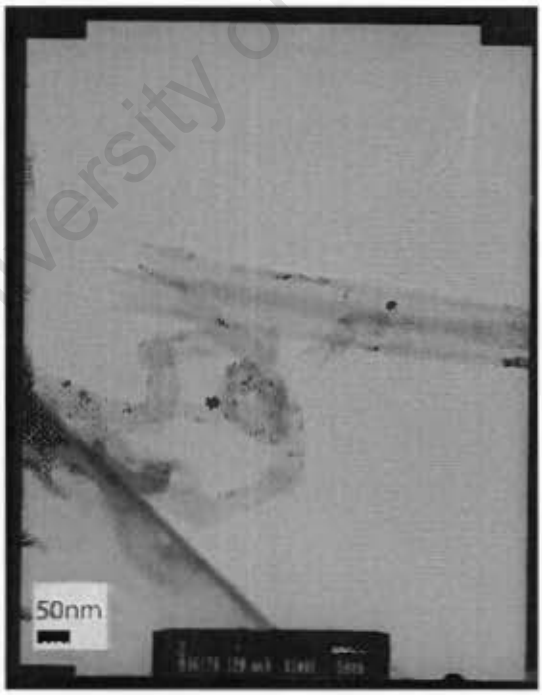

Catalyst 3:

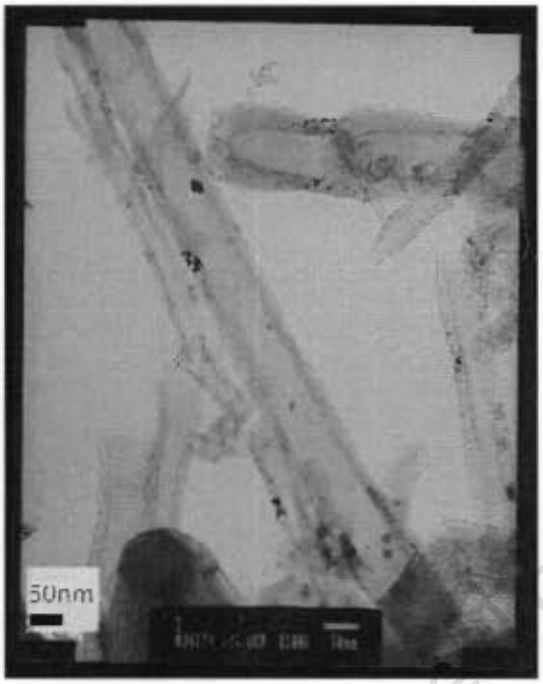

Catalyst 4:

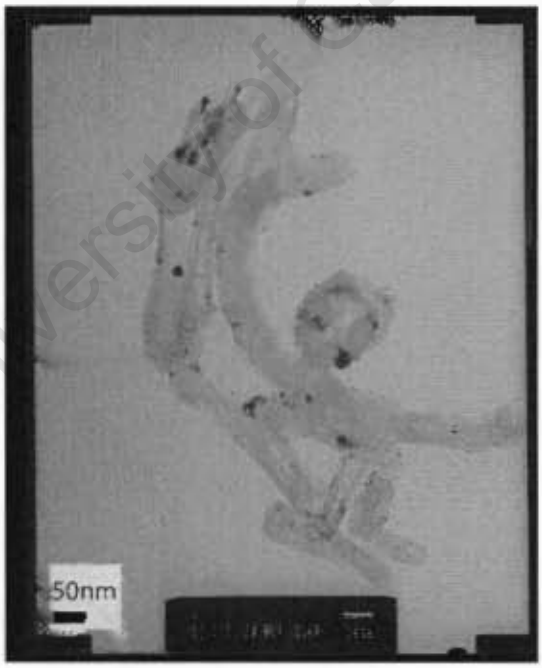

Catalyst 5:

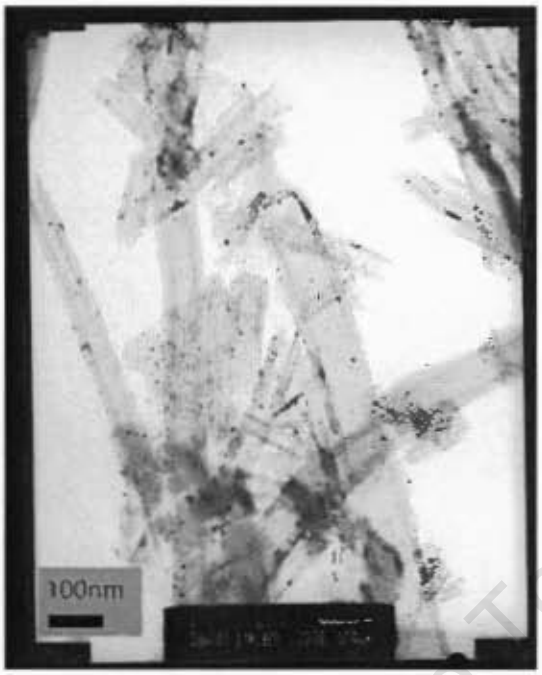

Catalyst 6:

Catalyst 7:

Catalyst 8:

Catalyst 9:

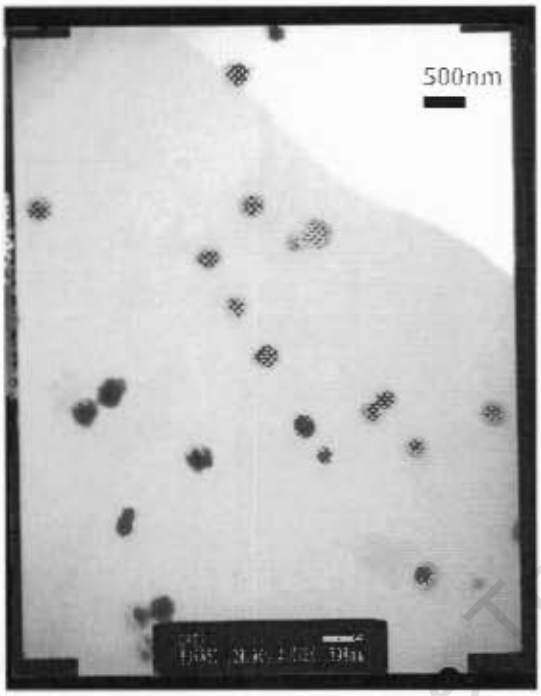

Gold crystallite size distribution calculations

No. ($N_{Particles}$)		245
Mean	**nm**	4.57035
σ	**nm**	3.09859

Number of particles in 2 nm bin $N_{Bin} = 30$

Calculating the frequency:

$$F(x) = \frac{N_{Bin}}{N_{Particles}} \cdot 100 = \frac{20}{245} \cdot 100 = 8.16\%$$

Log Normal Distribution Calculations

The log normal probability density is given by:

$$f(x) = \frac{1}{\sqrt{2 \cdot \pi} \cdot x} \cdot e^{\frac{-(\ln(x) - \alpha)^2}{2 \cdot \beta^2}}$$

where:
α – scale parameter
β shape parameter
x particle size

The parameters α and β were estimated by comparing to the measured data, and minimising the error using Microsoft Excel© Solver using Newton's method.

Oxygen chemisorption calculations

The following dual isotherms were fitted to the data as discussed in the results section:

$$V_{O_2} = V_{m,1} + V_{m,2} \cdot \frac{K_2 \cdot p_{O_2}}{1 + K_2 \cdot p_{O_2}} \qquad (1)$$

$$V_{O_2} = V_{m,1} \cdot \frac{K_1 \cdot p_{O_2}^n}{1 + K_1 \cdot p_{O_2}^n} + V_{m,2} \cdot \frac{K_2 \cdot p_{O_2}^m}{1 + K_2 \cdot p_{O_2}^m} \qquad (2)$$

The parameters K_1 and K_2 were estimated by comparing to the measured data, and minimising the error using Microsoft Excel© Solver using Newton's method.

From the volume of the monolayer obtain on the metal surface ($V_{m,1}$) dispersion was calculated using the following equation:

$$\text{Dispersion} = \frac{V_m \cdot n \cdot MM_{Au}}{V_{std} \cdot L_{cat}} \cdot 100$$

Where:

V_m	Monolayer volume on metal surface
n	n=1 for associative chemisorption and n=2 for dissociative chemisorption
MM_{Au}	Molecular mass of gold
V_{std}	Standard molar volume of the gas
L_{cat}	Catalyst loading

The diameter in nm was then calculated using the following equation:

$$\text{Diameter} = \frac{6 \cdot L_{cat} \cdot V_{std} \cdot X}{N_A \cdot V_m \cdot n \cdot \rho_{Au}}$$

Where

X	Gold surface atoms per unit area
N_A	Avogadro's number
ρ_{Au}	Density of gold

Appendix D: Catalytic testing with glucose oxidation

Evaluation of the rate constants

First order kinetics was assumed in order to evaluate the rate constants:

$r_G(t) = k \cdot C_G(t)$

Where

r_G Rate of consumption of glucose at time t

k First order rate constant

C_G Concentration of glucose at time t

The rate constants were calculated in Polymath© using non-linear regression using the Levenberg-Marquardt method and the concentration data was fitted to the following equation:

$C_G(t) = C_{G0} \cdot e^{(-k \cdot t)}$

Where

C_{G0} Initial concentration

t Time

Analysis of Reaction products with HPLC

For the analysis of the HPLC data, the peak areas were analysed in order to determine the concentration of the reaction products. Standards of possible reaction products were produced and tested. A sample calculation is given below:

Substance	Mass	Volume	Concentration		Retention Time	Channel	Area	
	g	l	g/l	M	min		UV	RI
Glucose (monohydrate)	0.0118	0.05	0.236	0.0012	10.91	RI	-	69070
Glucose (monohydrate)	0.1036	0.05	2.072	0.0105	10.91	RI	-	546483
Glucose (monohydrate)	0.2088	0.05	4.176	0.0211	10.91	RI	-	1137176

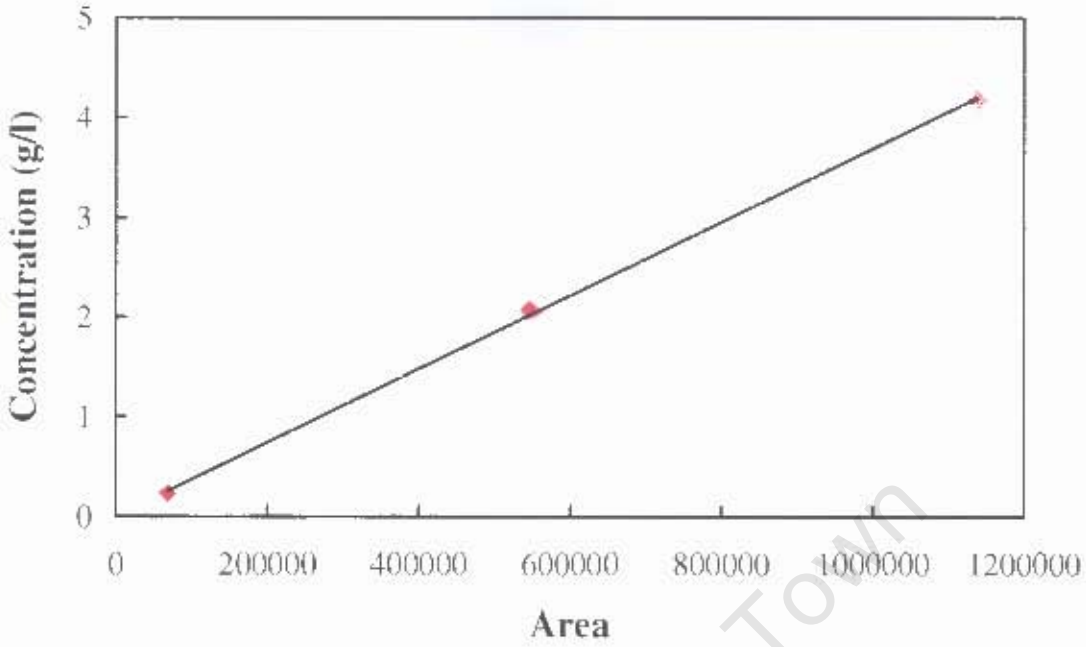

Figure 6.8: HPLC calibration curve for glucose standards

A straight line was fitted to the data. From the peak area and the slope of the line, the concentration can be calculated:

$$C_{Glucose} = 3.69 \times 10^{-6} \times A_{RI}$$

where $C_{Glucose}$ is the concentration of glucose and A_{RI} is the area of the glucose peak in RI. This method was also used for the other possible reaction products such as gluconic acid and fructose.

Appendix E: Ethics Form

EBE Faculty: Assessment of Ethics in Research Projects

Any person planning to undertake research in the Faculty of Engineering and the Built Environment at the University of Cape Town is required to complete this form before collecting or analysing data. When completed it should be submitted to the supervisor (where applicable) and from there to the Head of Department. If any of the questions below have been answered YES, and the applicant is NOT a fourth year student, the Head should forward this form for approval by the Faculty EIR committee: submit to Ms Zulpha Geyer (Zulpha.Geyer@uct.ac.za; Chem Eng Building, Ph 021 650 4791). Students must include a copy of the completed form with the thesis when it is submitted for examination.

Name of Principal Researcher/Student: B.A. BEEMING Department: CHEMICAL ENGINEERING

If a Student: Degree: MSc(Eng) Supervisor: E. VAN STEEN
J. CASE

If a Research Contract indicate source of funding/sponsorship:

Research Project Title: SYNTHESIS AND CHARACTERISATION OF CARBON SUPPORTED GOLD CATALYSTS PREPARED BY ION-EXCHANGE

Overview of ethics issues in your research project:

Question 1: Is there a possibility that your research could cause harm to a third party (i.e. a person not involved in your project)?	YES	(NO)
Question 2: Is your research making use of human subjects as sources of data? If your answer is YES, please complete Addendum 2.	YES	(NO)
Question 3: Does your research involve the participation of or provision of services to communities? If your answer is YES, please complete Addendum 3.	YES	(NO)
Question 4: If your research is sponsored, is there any potential for conflicts of interest? If your answer is YES, please complete Addendum 4.	YES	(NO)

If you have answered YES to any of the above questions, please append a copy of your research proposal, as well as any interview schedules or questionnaires (Addendum 1) and please complete further addenda as appropriate.

I hereby undertake to carry out my research in such a way that

- there is no apparent legal objection to the nature or the method of research; and
- the research will not compromise staff or students or the other responsibilities of the University;
- the stated objective will be achieved, and the findings will have a high degree of validity;
- limitations and alternative interpretations will be considered;
- the findings could be subject to peer review and publicly available; and
- I will comply with the conventions of copyright and avoid any practice that would constitute plagiarism.

Signed by:

	Full name and signature	Date
Principal Researcher/Student:	B.A. BEEMING	24/11/2008

This application is approved by:

Supervisor (if applicable):		
HOD (or delegated nominee): Final authority for all assessments with NO to all questions and for all undergraduate research.		
Chair : Faculty EIR Committee For applicants other than undergraduate students who have answered YES to any of the above questions.		